

WEATHERSAFE

SAFETY ENHANCEMENT UNDER ADVERSE WEATHER CONDITIONS THROUGH IMPROVED ADAS/AD ROBUSTNESS

Deliverable D2.1

Phenomena characterization

Project Name	WeatherSafe	
Dissemination level	Consortium	
Written by	Michael Graf	Technische Hochschule Ingolstadt CARISSMA ISAFE
	Alex Kiendl	MESSRING
	Bryan Moross	Mitsubishi Heavy Industries
	Gustav Sandren	UTAC / APTIV
Issue date	27.08.2024	
Reviewer		
Keywords	Adverse Weather, Fog, Glare, Rain, Road weather, Spray	
Version	1.1	

ABSTRACT

Adverse weather conditions have not negligible impact on safe driving and accident mitigation systems. A comprehensive analysis of accident data and sensor degradation has enabled the identification of key weather phenomena, particularly rain, fog, spray, glare and wet road conditions. The most pertinent meteorological parameters for rain include precipitation intensity, droplet shape, size distribution, and fall velocity. For fog, the Meteorological Optical Range (MOR) and fog droplet size distribution are of paramount importance when characterizing these phenomena. A market analysis was conducted to ascertain the most appropriate instrument for the given variables. In Europe, liquid precipitation is moderate, with extreme intensities exceeding 100 mm/h occurring infrequently. However, some regions, such as the Alps, experience higher rain rates regarding high temporal resolution intensity measurements. The occurrence of fog events has decreased since 1980 due to improvements in air quality in Europe. However, low visibility situations appear in a regular pattern, mainly in Central, Eastern and Northern Europe. The presence of a wet road conditions, which is an even more widespread appearing condition, results in the formation of spray. Additionally, changes in weather conditions reduce road friction, prolonging braking distances and contributing to accidents. This report identifies the most relevant characterization parameters and the probability of occurrence for the most relevant adverse weather phenomena to enhance the resilience of active safety functions and the robustness of driver assistance systems through additional safety tests.

REVISION HISTORY

Revision	Date	Description, updates and changes	Status
0.1	27.08.2024	Version 0.1 ready for review	Draft
1.1	16.06.2026	Minor update before publication	Approved

ABBREVIATIONS

DSD	Droplet size distribution
DWD	Deutscher Wetterdienst
ICAO	International Civil Aviation Organization
MOR	Meteorological optical range
WMO	World Meteorological Organization

TABLE OF CONTENTS

ABSTRACT 2
REVISION HISTORY 2
ABBREVIATIONS 2
TABLE OF CONTENTS 3
1. INTRODUCTION 4
2. ENVIRONMENTAL INDICATORS 4
3. RAIN 6
4. FOG 41
5. GLARE 64
6. ROAD CONDITIONS DUE TO ADVERSE WEATHER CONDITIONS 70
7. CONCLUSION 72
8. ACKNOWLEDGEMENTS 73
9. TABLE OF ILLUSTRATIONS 74
10. REFERENCES 75

1. Introduction

Adverse conditions, such as heavy rain, fog, glare or other external factors, can impede the safe operation of vehicles and contribute to accidents. Studies have shown that the occurrence of adverse weather conditions can increase the probability of accidents [1–3], but also change human driving behaviour [4–6] and the volume of road traffic [7] at the same time. Similarly, environmental sensors installed in automated vehicles are also susceptible to these adverse conditions [8–10]. To ensure that automated driving functions and active safety systems can safely protect human car occupants from accidents in the future, these systems must be robust against external influences. In order to define test cases that contribute to the development, testing and validation of today's vehicles to increase their robustness under adverse conditions, it is essential to identify the most relevant phenomena, defining their characteristics and quantifying their frequency of occurrence.

While an overview of all phenomena, including their characteristic properties, is provided at the beginning, only the most relevant phenomena will be addressed in more detail in the subsequent report. It offers a summary of the characteristics of the most relevant effects, as well as background knowledge, a summary of current scientific studies, and an analysis of the occurrence of the respective effects. This provides a deep insight into the respective phenomena.

2. Environmental Indicators

Table 1 provides an overview of the environmental conditions together with associated parameters for a characterization of these phenomena. A distinction is made between primary weather phenomena (such as rain, fog, snow, ...) and secondary weather phenomena (change in road surface state resulting from primary weather event).

Table 1: Overview about environmental conditions with corresponding indicators [11]

Item		Environmental Indicator					
Primary weather phenomena: Weather	**Temperature**	Temperature					
	Humidity	Humidity					
	Rain	Rainfall Intensity	Droplet Size Distribution	Raindrop Velocity	Distribution	Direction / Wind	pH
	Fog	Visibility	Fog Water Content	Droplet Size Distribution	Distribution	pH	
	Snow	Snowfall Amount	Snow Type	State	Droplet Size Distribution	Water Content	Visibility
		Snowfall Velocity	Direction / Wind	pH			
	Sunlight / Solar Radiation	Illuminance	Color Temperature	Irradiance (Heat Value)	Color Temperature	Spectrum	
	Glare	Angle	Light Source Diameter	Illuminance	Color Temperature	Luminance	
Secondary weather phenomena: Road condition	**Dry**	Road Surface Type	Temperature	Friction			
	Wet	Road Surface Type	Temperature	Water Amount	Area	Flow Velocity	Friction Coefficient
	Spray / Splash	Water Amount	Droplet Size Distribution	Extending area	Water volume distribution		
	Snow Cover	Snow Depth	Snow-Ice Ratio	Density	Water Content	Friction Coefficient	
	Icy Surface	Ice Thickness	Surface Temperature	Internal Temperature	Density	Moisture Content	Hardness
		Water Amount	Dirt	Friction Coefficient			
	Other	Manhole	Puddle	Crack	Shadow	Soil / Sand	Road Marking
		Crosswalk	Guardrail	Traffic Light			

3. Rain

According to the World Meteorological Organization (WMO) rain is defined as liquid precipitation of drops of water that falls from a cloud [12]. Thereby rain can have different characteristics, depending on its origin and the surrounding boundary conditions.

3.1 General Characteristics

3.1.1 Meteorological background

The occurrence of rain can have various origins. Principally, rain is formed within the earth's atmosphere. While everything up to a height of approx. 500-600 km is considered to be the atmosphere, only the effects in the troposphere are relevant for the occurring weather on earth [13]. The troposphere is lowest layer of the earth's atmosphere and reaches up to an height of approx. 8 (at the geographical poles) to 18 km (at the equator) [14].
Rain and clouds usually form when relatively warm and humid air masses rise and are cooled. This results in the condensation of tiny water droplets, causing clouds to form. Air movements within a cloud lead to a collision of the resulting water droplets. When small droplets merge (so called coalescence), it results in a droplet growth [15].

Precipitation can be divided into three groups based on the reasons that generate these rising streams:

1. Orographic rain:
   When wind brings warm and moist air from the sea or lowlands towards the mainland with mountains, orographic rain occurs [16]. Due to a mountain in the path of the wind, the air masses are forced to rise and cool down as a result. When condensation occurs in the saturated air, water droplets or clouds are formed. These can lead to heavy rainfall on the windward side of the mountains and in the promontory. Depending on the weather condition, the intensity and duration of the rainfall can vary significantly. This effect is especially apparent in the warm sector of a large depression. As a result, the leeward side of the mountain is usually quite dry, and the downward flow leads to a strong warming air stream. Orographic rain occurs mainly in the tropics, subtropics and moderate climate regions [17].
   With a focus on Europe, this has a particularly noticeable effect around the Alps, which reach up to 4800 m above sea level at their peak [13]. Moist air masses are pushed from the Atlantic and the Mediterranean by southerly and westerly winds to and over the Alps, resulting in increased precipitation in the affected regions.

2. Cyclonic rain:
   The formation of large-scale air movements occur when pressure differences in the atmosphere arise [15]. This can result from a variety of reasons, but the sun's radiation being one of the most significant. As a result, contact zones between cold and warm, humid air masses are formed. Depending on the front, this results in:
   - Warm front: Warm air glides above the colder areas. Formation of a large precipitation zone with strong precipitation thanks to the constant supply of moist, warm air.
   - Cold front: Cold air moves below the warm air and pushes the warm air upwards, which leads in the end to rainfall.

   Most of the precipitation in areas with a moderate climate is due to cyclonic precipitation, although the effect also occurs in the subtropics.

3. Convective rain:

   Convective rain mainly occurs when large amounts of water in the ground or on water surfaces vaporize. Low, moist air masses are transported upwards by air streams due to the warming from the sun. During this process air masses are cooled down again, which leads to a condensation of water. The size and type of the created clouds depend on the duration and the intensity of the convective flow, but the horizontal dimension of such an air mass is 15 km or less in general [15]. This usually leads to a short but heavy shower, which often occurs in the late afternoon. Frequently, convective rain also occurs in combination with thunder. It mainly affects the tropics and subtropics, but also occurs in summer in moderate climate regions such as Europe.

It should be noted that very often the causes of precipitation are also combinations of the above mechanisms [13].

3.1.2 Formation of liquid precipitation

Within a cloud, various effects can occur that lead to the formation of the actual rain drops. Starting point is always the condensation of water. Condensation usually occurs around small particles, the so-called condensation nuclei [18]. In addition, ice crystals on crystallization nuclei are possible through resublimation. These particles remain in the cloud as long as they are hovering due to air friction or upwinds. If this equilibrium can no longer be maintained due to droplet growth, the droplets will fall to the ground due to gravity. For example, in clouds with updraughts of less than 50 $cm*s^{-1}$ droplets with the diameter of 0.2 mm and more will fall out. A distinction can be made between drizzle and rain in this process:

1. Drizzle:
   Drizzle is mainly caused by the spontaneous collision and fusion of small cloud droplets, also known as coalescence [19]. This usually occurs in stratus clouds when they have to rise at geographical peaks. If a cloud rises in altitude, the droplets in the cloud also move upwards. Due to their size, it causes that small droplets rise faster than larger droplets, resulting in collisions and thus droplet growth. Drizzle is often formed from shield of low and flat clouds [15].

2. Rain:
   The formation process of rain can be divided into droplet growth in warm clouds and cold clouds.

   a) If a cloud contains only liquid water, it is referred to as a warm cloud. The drop formation effect is similar to that of drizzle. Large droplets fall earlier downwards. They collide and, in most cases, merge with other droplets inside the cloud. However, the process requires the presence of a large amount of water vapor, which is rarely existent in moderate climate regions and thus only drizzle occurs in the most times [19]. Large raindrops have radii of 2 to 3 mm. Cloud droplets, on the other hand, are of the order of 10^{-3} cm. This means that about 10^{6} cloud droplets are needed to form a raindrop. In the tropics, however, where temperatures and humidity are higher, the process can certainly result in actual rain.

   b) If clouds consist entirely or partly of ice crystals, they are classified as cold clouds. This occurs often the area of moderate climate regions. Unlike usual, water in clouds does not freeze at 0° C, whereby there are also liquid droplets in the cloud below 0°C, the so-called supercooled drops. Between -10° C and -35° C water is present

in a mixture of supercooled water and ice crystals. Below this temperature it exists in form of ice crystals, although these clouds are then higher than 6000 - 7000 m. Due to instability of climatic phenomena, such as the Bergeron-Findeisen process [20], frozen water is released from the cloud in the form of ice crystals/snowflakes. This means that these ice crystals turn into rain when they fall through warmer layers of air [19].

3.2 ATTRIBUTES OF RAIN

3.2.1 RAIN INTENSITY

Rain intensity is measured in **millimetre per hour (mm/h)**. This characterizes the amount of rain that accumulate on an area of one square metre within one hour. If the amount of accumulated rain is measured, it can be converted like this:

$$\frac{1\,L}{1\,m^2} = \frac{0{,}001\,m^3}{m^2} = 0{,}001\,m = 1\,mm \quad \rightarrow \quad 1\,\frac{L}{m^2 * h} = 1\,\frac{mm}{h} \qquad \textit{(Eq. 1)}$$

Often, instantaneous rainfall intensity or instantaneous rain rate is given in units of mm/hr even though the measurement period was much shorter than one hour. By electrical devices usually time intervals between 1 and 10 minutes are measured and converted to mm/h, to standardise the worldwide measurements. This can be understood as the amount of rain that would have fallen per hour if the specific short-term rainfall rate had been unchanged for an hour. But as rain has a large temporal variance, an unchanged rain rate for one hour does not appear in real world.

3.2.2 DROPLET SHAPE

When a drop starts to fall from a cloud, its falling speed increases until it reaches an equilibrium between the air resistance and the gravitational forces. In the process, the droplet constantly changes its shape to achieve a fluid mechanical optimum. The shape formed depends on the drop size. This process is illustrated in Figure 1.

Droplets with a diameter smaller than 280 µm have a nearly perfect round shape [22]. Slightly deformed and looking like slightly flattened spheroids are drops up to 1 mm. When the diameter is further enlarged, the terminal falling speed also increases. This results in a further flattening of the drop on the bottom side. For even larger drops, a constriction occurs on the inside when the air pressure overcomes the surface tension. Due to the instability the droplet then splits into two smaller droplets to take on a more fluidic shape. This is also the reason why the maximum droplet diameter is normally limited to approx. 6 mm, in a maximum for a short time up to 9-10 mm [23].

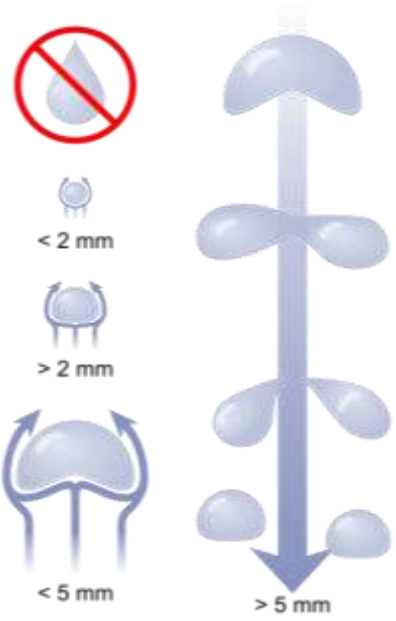

Figure 1: Droplet shape in relation to droplet diameter [21]

A mathematical description of the axial ratio of raindrops as a function of the drop diameter can be found in relevant literature. Pruppacher [24] predict the axis ratio using mathematical calculations as well as wind tunnel tests. Green [25] calculated the shape by considering only hydrostatic terms, while Beard [26, 27] used a more advanced laboratory setup than Pruppacher. Li [28] developed an simplified and optimized expression of non-axisymmetric raindrops for studies that mainly address the influence of wave attenuation.

It should be noted that the problem that a deformed drop cannot be correctly specified by its diameter is solved by the definition of the equivalent drop diameter. It represents a sphere with the same volume as that of the deformed drop.

3.2.3 DROPLET SIZE DISTRIBUTION (DSD)

The raindrop size distribution (DSD) is defined as a function that specifies the number of droplets with diameters (mm) between D and $D + dD$ per unit volume of air (cm^3) and has the unit $m^{-3}mm^{-1}$ [29]. Therefore, DSD is one of the most important parameter for the characterization of rain events, because microphysical effects can be derived on this basis.
The DSD depends on the precipitation intensity, as shown in Figure 2.

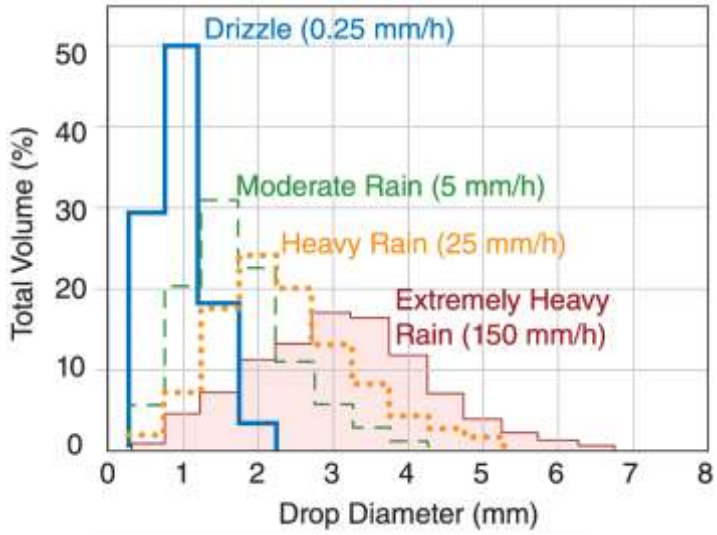

Figure 2: Typical distribution of droplet sizes during different rain rates [30]

It should be noted that the y-axis of this diagram is plotted against the total volume of drops and not against the number of drops, which means that the peak of the number of drops would not be at the same point as in this diagram. Nevertheless, it is clearly shown that the mean droplet diameter grows with increasing rainfall intensity. The DSD can vary from rain event to rain event and can also have local differences. For this reason, there are countless worldwide measurements of different DSDs in the literature [31–34].
The number of total drops can be calculated using following formula:

$$N = \int N(D)dD \qquad \textit{(Eq. 2)}$$

Nevertheless, there are numerous approaches to model a raindrop distribution in which the distribution depends on only a few parameters. It should be noted that these model distributions only describe a long-term averaging of a DSD. Each model has different advantages and disadvantages, but the four most common are the following:

a) Lognormal distribution (LN)

Several researchers suggested the use of a lognormal distribution with three parameters [35–40]:

$$N(D) = \frac{N_T}{\sqrt{2\pi}\, ln(\sigma) D} exp\left(\frac{-ln^2(\frac{D}{D_m})}{2ln^2(\sigma)}\right) \quad \textit{(Eq. 3)}$$

Where N(D) (m^{-3} mm^{-1}) is the concentration of raindrops between D and D + dD, N_T (m^{-3}) the total number of droplets per unit volume, D_m (mm) is the mean droplet diameter and σ is the standard geometrical deviation of D. The three purely physical values can be approximated as a function of the rain intensity R using the following function [41]:

$$\sigma = 1.43 - 3 * 10^{-4} R \quad \textit{(Eq. 4)}$$

$$N_T = 172 * R^{0.22} \quad \textit{(Eq. 5)}$$

$$\mathrm{D_m} = 0.72 * \mathrm{R}^{0.23} \quad \text{(Eq. 6)}$$

b) Weibull distribution (W)

The Weibull distribution resulted from assumptions about the drop formation and splitting process by Langmuir [42] and Weibull [43].

$$N(D) = N_0 \frac{c}{b} \left(\frac{D}{b}\right)^{c-1} e^{-\left(\frac{D}{b}\right)^c} \quad \textit{(Eq. 7)}$$

where $\mathrm{N_0} = 1000\, m^{-3} mm^{-1}$, $c = 0{,}95 * R^{0{,}14}$ and $b = 0.26 * R^{0.44}$ [44].

c) Exponential / Marshall and Palmer distribution (MP)

The most commonly used DSD is the simple negative experimental parameterization of Marshall and Palmer [45], which was fitted on the basis of DSD measurements of intensities from 1 to 23 mm/h [46].

$$N(D) = N_0 e^{-\Lambda D} \quad \textit{(Eq. 8)}$$

N_0 stands for the intercept and Λ a scaling parameter. According to [45] the parameters can be calculated with $N_0 = 8000\, m^{-3} cm^{-1}$ and Λ with respect to the rain intensity R: $\Lambda = 4.1 * R^{-0.21}$.
Special values for different types of rain, such as drizzle widespread rain and thunderstorm, are suggested by [47].

Type of rainfall	$N_0\ (m^{-3}cm^{-1})$	$\Lambda - R\ relation$
Marshall and Palmer	8000	$\Lambda = 4.1 * R^{0.21}$
Drizzle	30000	$\Lambda = 5.7 * R^{0.21}$
Widespread	7000	$\Lambda = 4.1 * R^{0.21}$
Thunderstorm	1400	$\Lambda = 3.0 * R^{0.21}$

It can be seen as a problem that the MP distribution is not accurate for small drops (<1 mm) and overestimates their number [48–50]. Also, very big droplets are overrepresented in this distribution [50, 51]. This can lead to inaccuracies in further calculations.
Although the MP distribution is still considered a good approximation of the DSD by many researchers, according to [52] it is mainly representative of low or moderate precipitation. For heavy rain (>10-20 mm/h) or rain in tropical regions, the MP-distribution offers only a limited DSD characterization [29].

d) Gamma / Ulbrich distribution (U)

The gamma distribution originally presented by Ulbrich [53] was adopted by many researchers and adapted to their DSD measurements [51, 54–60].

$$N(D) = N_0 D^{\mu} e^{-\Lambda D} \qquad \text{(Eq. 9)}$$

If $\mu = 0$, the gamma distribution is equal to the MP-DSD.

All in all, the Weibull (W) and Ulrich (U)-DSD models tend to represent the most realistic DSD for rain, especially for heavier rain events [61]. In particular, these two represent a drop peak that realistically moves to larger droplet diameters with increasing rainfall intensity. For low rain intensities (<10 mm/h), however, the (MP)-DSD provides a good fit [29].

If wind occurs in addition to rain, studies by [62] show that more larger drops tend to occur, which leads to a shift of the DSD.

Moreover, a variety of parameters exist to simplify the comparison of different droplet size distributions [63–65]. While variables such as the mean droplet diameter provide a fundamental understanding of the droplet size distribution, specific parameters offer different weightings for individual aspects of the distribution. The most important ones are:

- Arithmetic Mean Diameter D[1,0]:

$$D_{1,0} = \frac{\sum_i N_i * D_i}{\sum_i N_i} \qquad \textit{(Eq. 10)}$$

D[1,0] is the mean drop size. N_i is the number of droplets in size class i, and D_i is the diameter of the droplets in the class.

- Volumetric Mean Diameter D[3,0]:

$$D_{3,0} = \frac{\sum_i N_i * {D_i}^3}{\sum_i N_i} \qquad \textit{(Eq. 11)}$$

The volumetric mean diameter is calculated as the ratio of the third moment of the droplet size distribution to the total number of droplets. It is particularly useful when the liquid water content is a relevant factor.

- Sauter Mean Diameter D[3,2]:

$$D_{3,2} = \frac{\sum_i N_i * {D_i}^3}{\sum_i N_i * {D_i}^2} \qquad \textit{(Eq. 12)}$$

The Sauter diameter is defined as the ratio of the volume of the droplets to the surface area.

- De Brouckere mean diameter D[4,3]:

$$D_{4,3} = \frac{\sum_i N_i * {D_i}^4}{\sum_i N_i * {D_i}^3} \qquad \textit{(Eq. 13)}$$

When the existence of large drops needs to be determined explicitly, the De Brouckere mean diameter can be used. This factor describes the volume-weighted mean.

Furthermore, the volume of the droplets can be used for characterization. Thus $Dv[0{,}1]$ indicates the diameter at which 10 % of the droplets are smaller than $Dv[0{,}1]$ and 90 % have a larger diameter. Equivalently, $Dv[0{,}5]$ and $Dv[0{,}9]$ are also frequently used [66].

3.2.4 DROPLET FALLING SPEED

Depending on the size of a droplet, its terminal velocity is affected by the equilibrium between air resistance and gravity. For this, the laboratory measurements of Gunn and Kinzer [67] with the pressure corrections of Beard [27] are still regarded as the general standard. This has been confirmed by recent measurements with modern and highly accurate measuring devices [68]. There are also some analytical approaches in the literature for determining the terminal fall velocity, such as [69, 70]. However, these often overestimate the velocity of larger droplets (>3 mm), as the flattening of the droplets is not taken into account. Figure 3 shows the droplet terminal velocity under windless conditions.

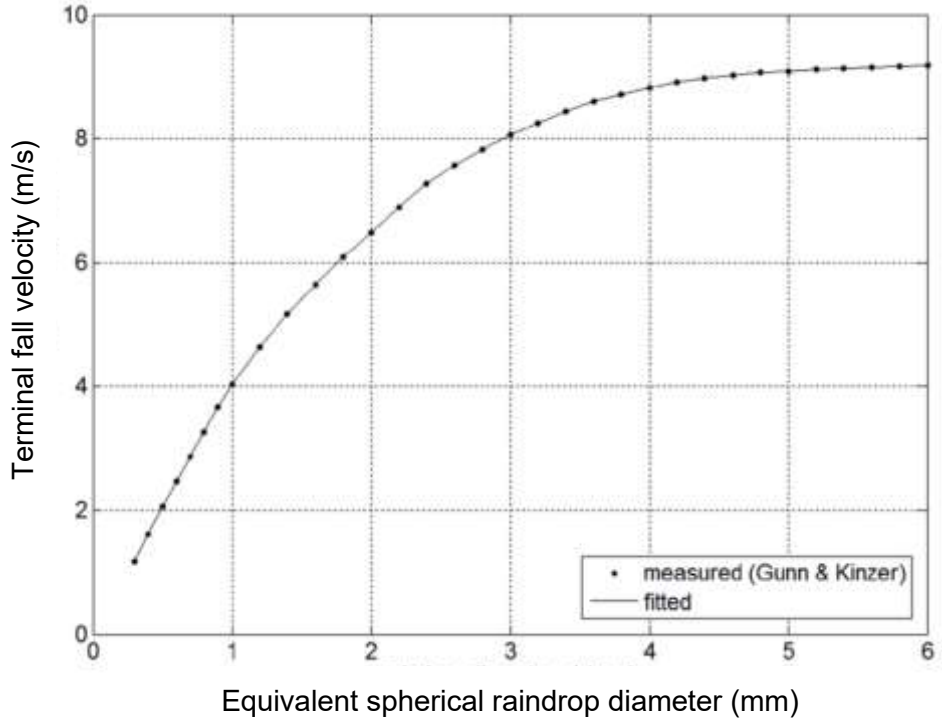

Figure 3: Terminal velocity of cloud drops as a function of droplet diameter [67]

It should be noted that the equivalent droplet diameter is used on the x-axis. The equivalent diameter is defined as the diameter of a sphere with the same volume as a deformed drop. According to [71], the curve can be described as a function using the formula Eq. 14. Up to an equivalent droplet size of 8 mm, the function provides an excellent fit.

$$v_{max}(D) = -0.1021 + 4.932 * D - 0.9551 * D^2 + 0.07934 * D^3 - 0.002362 * D^4 \qquad \textit{(Eq. 15)}$$

Variations from the mean terminal fall velocity (> ±30 %) are referred to as "sub-terminal" or "super-terminal" and, according to today's knowledge, occur due to droplet collisions or break-ups [72–76]. The frequency of drop collisions depends on the rain intensity and the occurrence is different for each drop diameter [77].

If additionally, turbulence is generated by wind, the result is that the mean falling speed will decrease almost linearly with an increasing turbulence intensity [62]. Also, the speed distribution is wider.

3.3 CLASSIFICATION OF RAIN EVENTS ACCORDING TO LITERATURE

Rain can be separated according to various characteristics, such as drop size (distribution), number of drops or droplet fall speed (distribution). Each rain event has individual characteristics for those criterions. For this reason, there are various approaches for the classification of rain, in which individual or several criteria are defined with measurable variables. A definition and explanation of the meteorological terms can be found in [78].

Precipitation intensity is the most common used parameter for characterizing rainfall events. There are various definitions in the literature specifying which measured rainfall intensity can be assigned to which theoretical rainfall level. Definitions can be found in technical standards, specialized literature and from weather services. To provide an overview of the various definitions, some of them are listed below. Drizzle is listed in Table 2, while Table 3 is focused on rain and heavy shower events.

Table 2: Overview over literature definition of drizzle intensity levels

Source	Light drizzle	Moderate drizzle	Strong drizzle
WMO [79]	< 0,1 mm/h	0,1 – 0,5 mm/h	> 0,5 mm/h
Deutscher Wetterdienst (DWD) [80]	< 0,1 mm/h	0,1 – 0,5 mm/h	> 0,5 mm/h
Met Office [15]	„Negligible runoff from roofs“	< 1 mm/h	> 1 mm/h
NF P99-320 [81]	< 0,25 mm/h	0,25 – 0,5 mm/h	> 0,5 mm/h

Table 3: Overview over literature definition of shower intensity levels

Source	Light rain/shower	Moderate rain/shower	Strong rain/shower	Violent rain/shower
WMO [79]	< 2,5 mm/h	2,5 – 10 mm/h	10 – 50 mm/h	> 50 mm/h
Deutscher Wetterdienst (DWD) [80]	< 2,5 mm/h	2,5 – 10 mm/h	10 – 50 mm/h	> 50 mm/h
American Meteoritical Society [82]	< 2,5 mm/h	2,5 – 7,6 mm/h	> 7,6 mm/h	/
U.S. Federal Meteorological handbook [83]	< 2,5 mm/h (Orig. < 0,25 mm in 6 min)	2,5 – 7,6 mm/h (Orig. 0,25 – 0,76 mm in 6 min)	> 7,6 mm/h (Orig. > 0,76 mm in 6 min)	/
MeteoSchweiz [84]	0,1 – 2 mm/h	2 – 10 mm/h	10 – 30 mm/h (strong) & 30 – 50 mm/h (very strong)	> 50 mm/h
Koppe [85]	0,1 – 2,4 mm/h	2,4 – 12 mm/h	12 – 48 mm/h	> 48 mm/h
Met Office [15]	< 2 mm/h	2 – 10 mm/h	10 – 50 mm/h	> 50 mm/h
NF P99-320 [81]	< 2,5 mm/h	2,5 – 7,5 mm/h	> 7,5 mm/h	/
Dracos [13]	0,25 mm/h	1 – 5 mm/h	15 – 20 mm/h	100 mm/h

It should be mentioned that the WMO specifies that the intensity values are based on a 3-minute measurement. In the literature violent rain is sometimes also listed to as "intense", "extreme", "very heavy", "storm" or "cloudburst". Furthermore, the intensity is sometimes differentiated between normal rain and rain showers, whereby the main difference is that the amount of precipitation is specified for showers with shorter measurement intervals (between 5 - 10 minutes). In order to maintain a structured table, the intensities were in these cases converted to the unit mm/h.
In the British "CAP 746: Requirements for meteorological observations at aerodromes" [86], shower is defined as precipitation from cumuliform clouds.

Some literature further distinguishes liquid precipitation according to the prevailing droplet diameters. In general, drizzle mainly consists of smaller drops than normal or heavy rain. Various definitions from the literature can be found in Table 4.
According to the UK Met Office the difference between drizzle and rain is purely one of drop size rather than intensity of precipitation [15].

Table 4: Overview over literature definition of rain types based on droplet diameter

Source	Drizzle	Moderate rain/shower	Strong rain/shower	Violent rain/shower
Dracos [13] *(Mean diameter is specified)*	0,25 mm	0,45 mm	1,5 mm	3 mm
Häckel [19]	0,05 – 0,25 mm	0,25 – 3 mm		
Met Office [15]	0,2 – 0,5 mm	> 0,5 mm		

As drizzle tends to consist of smaller droplets, the falling velocities of the droplets are also lower.

Raindrops are falling at different speeds depending on their diameter. The speed depends on the equilibrium between gravity and air resistance. Drizzle drops usually fall at a speed of between 0.25 and 2 m/s, while the (larger) drops of rain or showers reach terminal velocities of up to 9 m/s [13, 19]. By measuring these velocities, it is also possible to draw conclusions about the type of rain. Finally, it can be noted that slowly falling drizzle drops are often further influenced by an additional horizontal speed component due to crosswinds.

3.4 MEASUREMENT DEVICES

Rain measurement devices can be classified into two categories: Analogue rain gauges, which are used to accurately measure rainfall by hand, and electrical devices, which can independently measure and store data as well as record other characteristics in addition to the amount of liquid precipitation. Although many devices can measure other forms of precipitation, such as snow or hail, only the rain measurement capabilities are considered here.
Guidelines specifying the boundary conditions of the measurement can be found in WMO Reports No. 8 [12] and No. 168 [79], as well as regional guidelines such as for Germany in VDI Guideline 3786 Sheet 1 [87] and Sheet 8 [88] and publications of the DWD [89].

3.4.1 ANALOGUE PRECIPITATION METERS

Traditionally, precipitation is measured using a rain gauge, which collects rainfall over a defined period of time. Rain gauges typically consist of cylindrical collecting buckets with a scale that allows for the determination of the amount of rainfall. The rainfall amount is taken manually and, for example, daily. The inlet opening typically has a funnel shape to capture larger amounts of precipitation and a thin gap with a collection container underneath to prevent evaporation. Figure 4 displays a standard structure of a rainwater collector according to Prof. Hellmann, which is a common design in Europe.



Figure 4: Precipitation gauge according to Prof. Hellmann [90]

In 1886, Professor Hellmann developed this measuring device consisting of a cylindrical collecting vessel with an opening area of 200 cm^2 and a funnel that prevents water in the collecting vessel from evaporating [90]. In more than 100 countries the gauge is positioned at a range height between 0.5 – 1,5 metres horizontally above the ground [91]. In some cases, there are country-specific mounting height specifications, such as those of the DWD, e.g. to take the expected snow heights into account [89]. Sufficient lateral clearance from trees, buildings or other obstacles must be ensured [92]. The WMO recommends that the distance between objects should be at least two to four times the height of the nearest obstacle and the terrain shall not be inclined more than 19° [12, 79]. It is recommended to avoid locations with strong winds or to install a suitable windbreak. A rain gauge, like any object, can cause a change in the wind and pressure field surrounding it. This can cause small droplets to be deflected away from the gauge, leading to measurement errors. Furthermore, the system should not be used on steep slopes, as this leads to increased inaccuracies due to changes in wind characteristics. Wind is usually the main cause of inaccuracies, as the higher the wind speed, the greater the error [92]. Inaccuracies in measurements can further result from additional disturbance effects caused by site-related sources of error, such as obstruction and

congestion effects due to obstacles like houses and trees, or construction-related sources of error, such as wind, adhesive water, or evaporation effects as well as splashing water and inaccuracies in the reading of the scale [90, 92]. In general, it is assumed that there is a measurement error of between 5 – 10 %, which can increase significantly with low precipitation intensities [93]. Studies in Switzerland have revealed an underestimation of the annual average precipitation of up to 25 – 30 % if the rain gauge is mounted in unfavourable locations, such as in mountainous regions with high wind speeds [94, 95]. To compensate for these errors, average correction values are used, as shown in Figure 5.

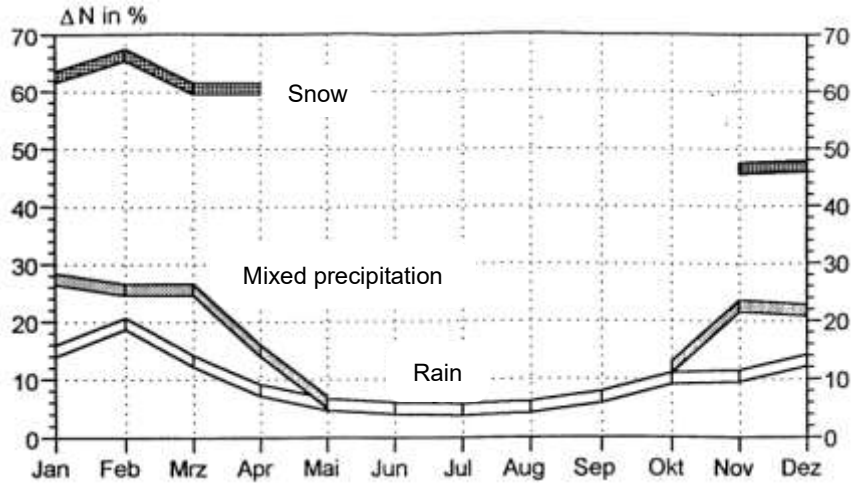

Figure 5: Percentage underestimation of the measured precipitation amount in the German lowlands due to the wetting and wind error depending on the shape of the precipitation and the month for a catchment area of 200 cm² [96]

In [96], more precise correction values can be found depending on the location, time of year, mounted wind shield and location of data collection.

3.4.2 Electrical Devices

Electrical devices are primarily used nowadays for measuring rainfall due to the limitations of manual rain gauges. They require significant effort to take daily readings and do not provide a temporal graph of rainfall intensity. Electric rain gauges are capable of accurately measuring and storing precise amounts of precipitation with a high resolution in time. A detailed comparison with real-world tests of a large number of electric rain gauges was carried out by the WMO in 2009 and can be found in [97]. An overview of the various measuring systems and principles of electrical rain gauges is shown in Figure 6.

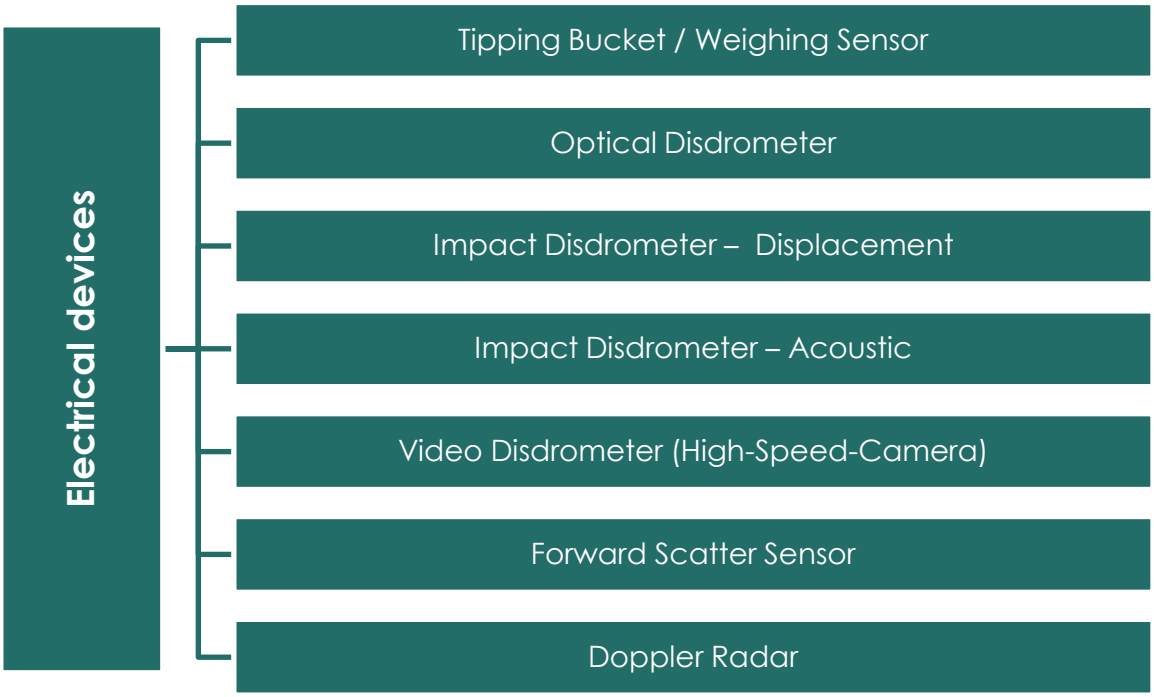

Figure 6: Types of electric rain gauges

3.4.2.1 Tipping bucket / Weighing sensor

For automatic rain gauges, measurement using a tipping bucket or weighing bucket is a widely used method. Precipitation is collected in a small bucket, and when sufficient weight has been collected, the tipping device is triggered, which is detected electronically by a reed contact, and the bucket is emptied by the movement of the bucket. The gauges are often constructed according to the design of Joss and Tognini [98]. According to WMO, the tipping bucket has be of a size that it is filled with 2 cm^3, which means that precision is typically 0.1 mm [99]. This can be expanded by integrating a scale that determines the amount of precipitation by weight. In most cases this is achieved by using a strain gauge. In this way, precipitation can be measured with a resolution up to 0.001 mm. Studies have shown that systematic deviations are rather small, with an error of 5 – 10 % to be expected for most measuring devices [97].
The advantage is a high temporal resolution of the data with respect to the quantity collected. Weighing gauges can also measure snowfall directly, i.e. without additional heating. The disadvantage is that this type of rain gauge cannot distinguish between liquid and solid precipitation, such as rain and snow, nor can it distinguish between drop sizes.

Other mechanical designs are the Drop Counter, which collects drops to a standard drop size and then counts the number of standard drops or the precipitation recorder with a swimming float. However, as these are less common today, a more detailed description will not be given here.

Table 5 and Table 6 list several examples of tipping buckets available on the market, along with their specifications.

Table 5: Specifications of selected tipping buckets commercially available

Name	Manufacturer	Intensity	Intensity resolution	Intensity accuracy
Precipitation Transmitter [100]	Thies CLIMA	0 – 660 mm/h	0.1 mm	± 3 %
ZDR010 [101]	ZATA	0 – 480 mm/h	0.1 mm	±2 %
NR4M [102]	ACS Control-System	0 – 960 mm/h	0.1 mm	±2 %
RainVUE20 [103]	Campbell Scientific	0 – 600 mm/h	0.1 mm	±3.58 %
Niederschlags-sensor nach Joss-Tognini-15189 [104]	LAMBRECHT meteo	0 – 480 mm/h	0.1 mm	±2 %
Rain Gauge RG13 [105]	VAISALA	Unlimited	0.2 mm	±2 %
RIM-7499-BOM [106]	RIMCO	0 – 380 mm/h		±2% to 200 mm/h ±3% to 380mm/h

Table 6: Specifications of selected weighting sensor devices commercially available

Name	Manufacturer	Intensity	Intensity resolution	Intensity accuracy
Precipitation Transmitter [107]	Thies CLIMA	0 – 1200 mm/h	0.001 mm	1 % (< 6 mm/min) 2 % (> 6 mm/min)
OTT Pluvio² S [108]	OTT HydroMet	0 – 3000 mm/h	0.001 mm	±1 %
OTT Pluvio² L [109]	OTT HydroMet	0 – 3000 mm/h	0.01 mm	±1 %
ZWR [110]	ZATA	0 – 1000 mm/h	0.1 mm	±0.2 mm (≤10 mm) ±2 % (>10 mm)
rain[e] [111]	LAMBRECHT meteo	0 – 1200 mm/h	0.001 mm/h	1 % (< 6 mm/min) 2 % (> 6 mm/min)

3.4.2.2 Optical Distrometer

Nowadays, disdrometers are frequently used to measure precipitation more accurately. While precipitation gauges record the amount of precipitation after a certain period of time, a disdrometer measures the entire precipitation duration. This enables precise determination of the start and end times, as well as variations in intensity over time. Additionally, conclusions can be drawn regarding the distribution of drop sizes and the speed at which they fall. The last two variables are primarily used to distinguish between solid precipitation (such as snow and hail) and liquid precipitation (such as rain) [112], as shown in Figure 7. An issue is that disdrometers are not widely used by national weather measurement services, which means that the spatial coverage of data is limited.

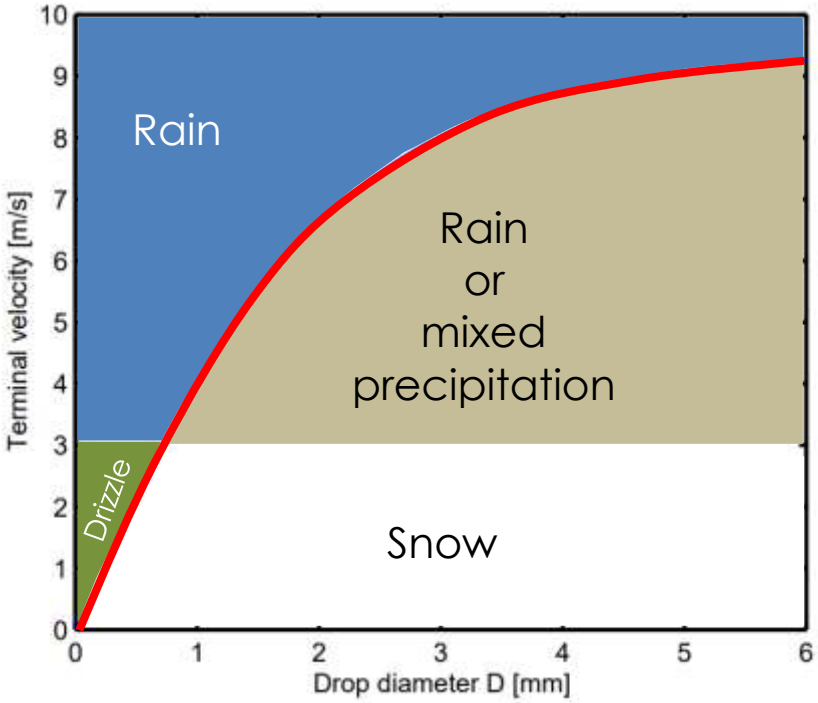

Figure 7: Exemplary classification of precipitation by drop size and velocity [113]

Various technical designs are available to accomplish this function. The most common type are optical disdrometers. A horizontal light band is generated by a laser diode and focused on a photodiode located 10 – 30 cm away, as illustrated in Figure 8. The photodiode emits the full voltage if there are no particles in the light band. However, if a drop falls through the light band, the sensor is partially obscured due to extinction effects. The size of the voltage drop, which indicates the size of the occlusion, and the duration of the obstruction are recorded. The former provides information on the drop size, while the latter provides information on the drop speed [114]. If the device counts the droplets over a period of time (usually 1 minute), the total number of droplets can be determined, and the droplet totals can then be separated into size classes. Possible sources of error during measurement are foreign particles, partial/strip crossings, coincidences, soil splashes or strong vibrations [115].



Figure 8: Functional principle of an optical disdrometer [116]

Table 7: Specifications of selected optical disdrometer commercially available

Name	Manu-facturer	Intensity	Intensity resolution	Intensity accuracy	Particle size diameter	Particle speed
Laser Precipitation Monitor [117]	Thies CLIMA	0.001 – 1000 mm/h	0.001 mm/h	± 5 %	0.16 – 8 mm (22 classes)	0.2 – 20 m/s (20 classes)
OTT Parsivel² [118]	OTT Hydro-Met	0.001 – 1200 mm/h	± 1 size class (0.2 - 2 mm) ± 0.5 size class (> 2 mm)	± 5 %	0.2 – 8 mm (32 classes)	0.2 – 20 m/s (32 classes)
ZDM100 [119]	ZATA	0.001 – 1000 mm/h		± 5 %	0.125 – 2.6 mm (32 classes)	0.1 – 22 m/s (32 classes)
ODM 470 [120]	Eigen-brodt				0.5 – 6 mm (128 classes)	/
MPS [121]	Droplet Measur-ement Techno-logies				50 µm – > 6.4 mm	

3.4.2.3 Impact Disdrometer – Displacement

Impact displacement disdrometers are used to measure the kinetic energy of individual raindrops and determine their size and quantity over time. This method is commonly referred to as the Joss and Waldvogel method. The kinetic energy is influenced by the droplet diameter and the fall velocity.

Table 8: Specifications of selected Impact Disdrometer (Displacement) commercially available

Name	Manu-facturer	Intensity	Intensity resolution	Intensity accuracy	Particle size diameter	Particle speed
Distromet RD-80 [122]	Distromet			± 5 %	0.3 – 5 mm (127 classes)	/

3.4.2.4 Impact Disdrometer – Acoustic

Acoustic disdrometers detect precipitation by using a piezoelectric sensor to generate an electrical signal when a droplet hits a special membrane. From this, the kinetic energy and therefore the droplet size can be derived for each droplet detected. This measurement principle is subject to increased inaccuracies at high rain intensities due to multiple impacts temporally close together, as well as in the detection of very small drops where the signal is difficult to distinguish from the signal noise [123].

Table 9: Specifications of selected Impact Disdrometer (Acoustic) commercially available

Name	Manu-facturer	Intensity	Intensity resolution	Intensity accuracy	Particle size diameter	Particle speed
WXT53x series [124]	VAISALA	0 – 200 mm/h	0.01 mm/h	± 4 %	/	/
RainFlow RF4 [125]	IASW	0 – 250 mm/h		± 15 %	0.5 – 7 mm (27 classes)	/
ZWS100 [126]	ZATA	0 – 600 mm/h	0.01 mm	± 4 %		

3.4.2.5 Video Disdrometer

More recently, camera technology has been increasingly used to characterise rain. Simple camera disdrometers use a stereo camera that calculates the size and number of droplets based on image occlusion [127]. More advanced, but also more expensive, measuring devices use one or more high-speed cameras, allowing each droplet to be visualised individually [128].

Table 10: Specifications of selected Video Disdrometer commercially available

Name	Manu-facturer	Intensity	Intensity resolution	Intensity accuracy	Particle size diameter	Particle speed
3D Stereo Disdrometer [127]	Thies CLIMA	0.001 – 1000 mm/h	0.001 mm/h	± 3 %	0.08 – 4 mm (22 classes)	0.2 – 20 m/s (63 classes)
1DVD [129]	Joanneum Research			< 10 %		not possible
2DVD [128]	Joanneum Research			< 10 %		possible

3.4.2.6 Forward Scatter Sensor

Forward scatter sensors are mainly used as present weather sensors to record the current weather status. However, some of these devices can also detect certain rain parameters. For example, rain intensity is measured by forward scattering of infrared light at a scattering angle of about 45°. The disadvantage is a higher inaccuracy compared to conventional disdrometers.

Table 11: Specifications of selected forward scatter sensor commercially available

Name	Manu-facturer	Intensity	Intensity resolution	Intensity accuracy	Particle size diameter	Particle speed
CS125 [130]	Campbell Scientific	0 – 999.9 mm/h	0.01 mm/h	± 15 %		
FD70 [131]	VAISALA	0.01 – 999.9 mm/h	0.01 mm/h		0.1 – 3.5 mm (41 classes)	0 – 10 m/s (26 classes)
PWD12 & PWD22 [132]	VAISALA	0 – 999.9 mm/h	0.05 mm/h			

3.4.2.7 Doppler radar

Radar-based sensors detect precipitation using the reflected signal from a Doppler radar. This allows the intensity of precipitation to be determined to the second without contact. The backscatter profile provides information on the number and distribution of droplets, while the Doppler effect indicates the velocity of the droplets.

Table 12: Specifications of selected doppler radar sensor commercially available

Name	Manu-facturer	Intensity	Intensity resolution	Intensity accuracy	Particle size diameter	Particle speed
Clima Sensor US [133]	Thies CLIMA	0.001 – 999 mm/h	0.001 mm/h	For 95% of the precipitation deviations is less than 10% compared to Laser Precipi-tation Monitor (Thies CLIMA)	0.25 – 5 mm (1 class)	/
Lufft WS100 [134]	OTT Hydro-Met	0.01 – 200 mm/h	± 0.16 mm/h	± 10 %	0.3 – 5 mm (11 classes)	0.9 – 15.5 mm (1 class)

3.4.3 WMO Measurement Standards

Certain minimum requirements and standards for the measurement of precipitation and devices are defined by the WMO. An overview of required ranges and permissible accuracy of meteorological observatories is given in Table 13.

Table 13: Requirements for precipitation measurement according to WMO [12]

Item	Unit	Range	Required measurement uncertainty
Precipitation amount	mm	0 – 500 mm	±0.1 mm (≦5mm) 2 % (>5mm)
Precipitation intensity	mm/h	0.02 – 2000 mm/h	±0.1 mm/h (0.2-2 mm/h) ±5 % (>2 mm/h)
Precipitation duration	sec to hours	0 – 24 h (Threshold value of 0.02 mm/h)	/

3.5 OCCURRENCE OF RAIN EVENTS

3.5.1 OVERVIEW OF RAINFALL EVENTS IN EUROPE

The occurrence of precipitation is influenced by various factors. Comparing the total annual precipitation globally, as shown in Figure 9, Europe can be classified as a moderate region with some exceptions in northern and eastern coastal regions.

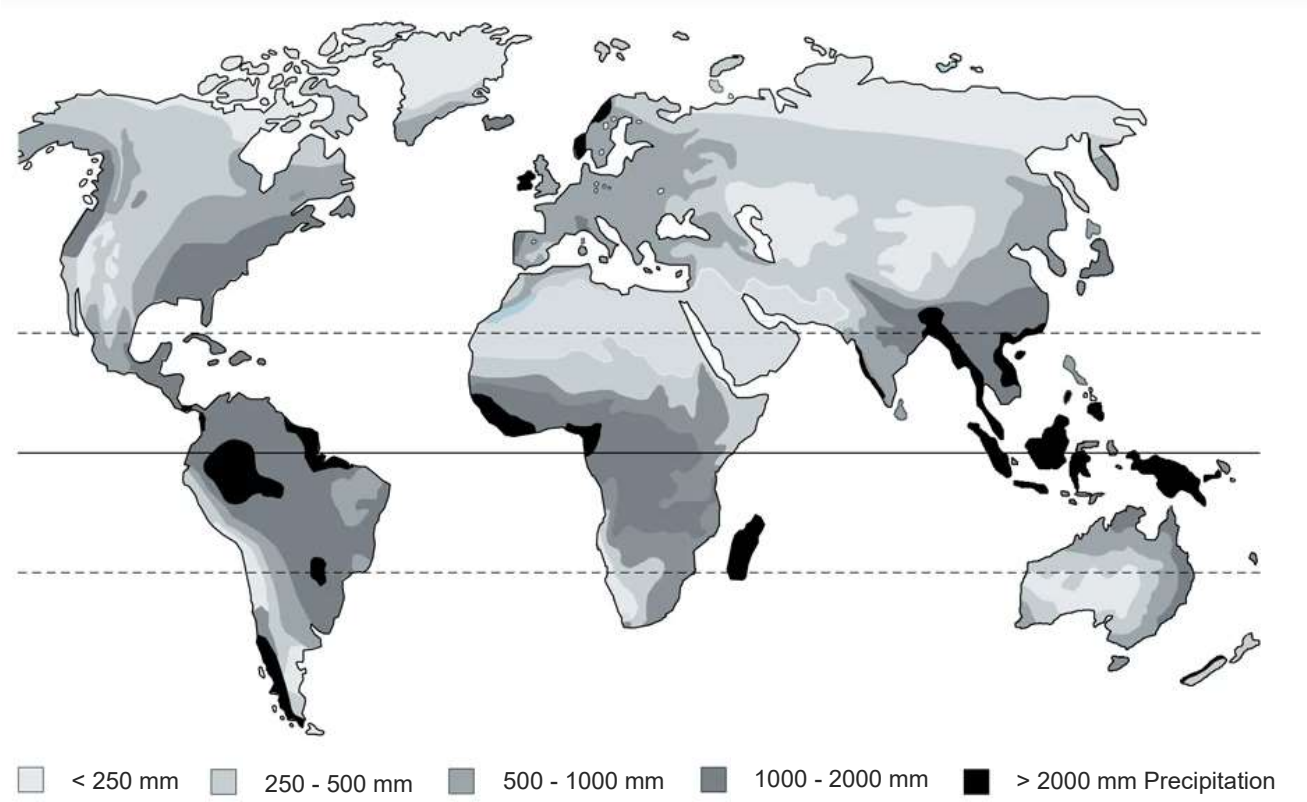

Figure 9: Global annual precipitation totals [135]

The distribution of precipitation in Europe is influenced by topography and geographical location. Most rain in (central) Europe is caused by winds from the west and north from moving depressions [19]. As the depressions usually last only a few days, there is a gradient in the distribution of precipitation from the coasts in western Europe to the inland [136]. This effect can be observed in Figure 10, for example, in the Scandinavian coastal areas or in the UK.

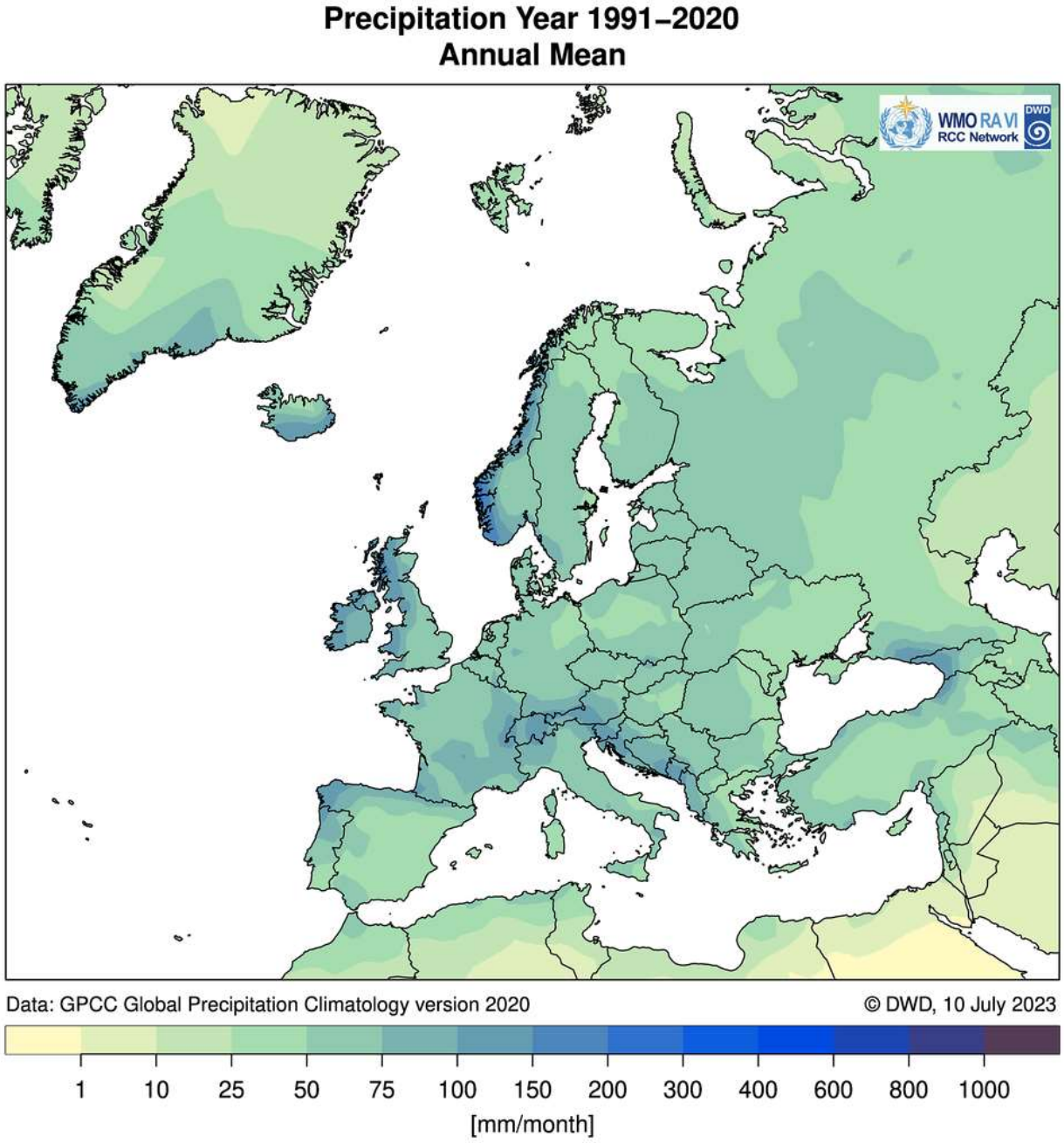

Figure 10: Average rainfall total per month in Europe for 1991-2020 [137]

A significant reason for the different amounts of precipitation is the varying geographical altitude. The higher a mountain, the more precipitation is recorded. Accumulation effects lead to precipitation as well as higher air velocities that can transport larger quantities of moist air into these areas. An example of the westward gradient of precipitation loss associated with a mountain can be seen in the Scandinavian mountains, where the rainfall in Bergen is above average, while the eastern and leeward side of the mountains is much drier due to the foehn effect. This effect can also be observed in the Alps. The increase in precipitation in coastal regions can be explained by another effect. When humid winds from the sea reach the land masses, they are slowed down. This leads to a forced rise of the air masses due to congestion, resulting in precipitation [19].

Another remarkable effect on the dependence of precipitation is the time of a year, as shown in Figure 11.

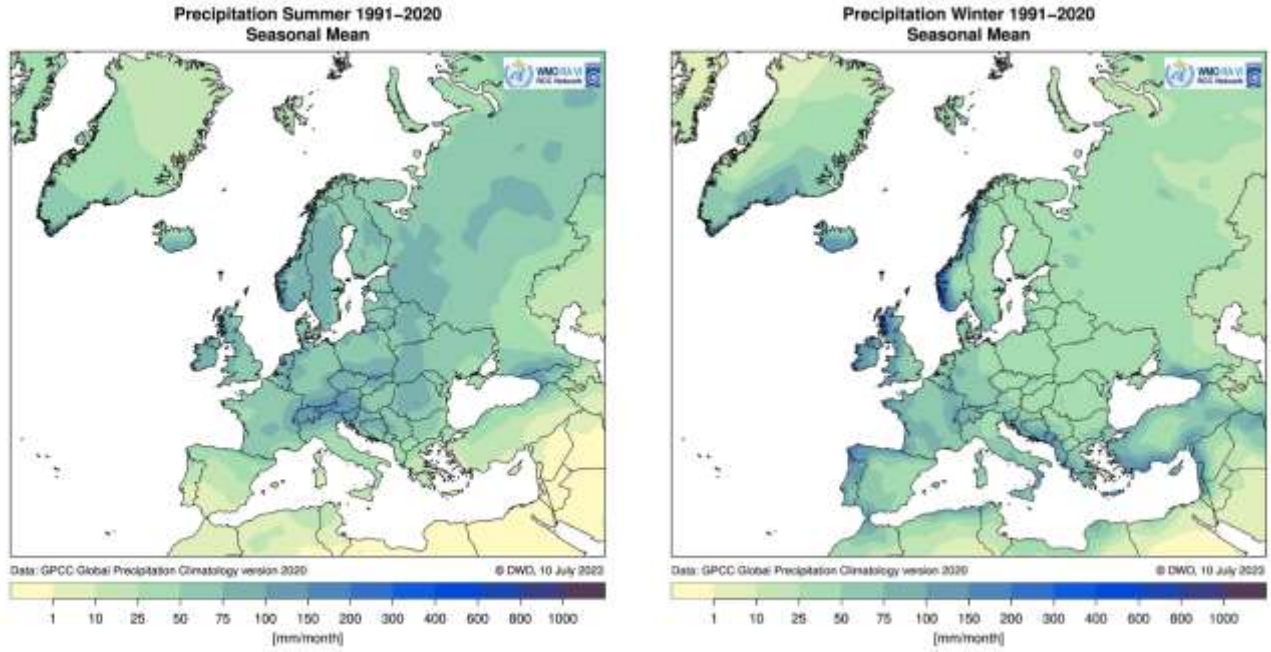

(a) (b)

Figure 11: Mean precipitation total per month in (a) summer and (b) winter [137]

In the summer months, depressions are mainly pushed to the north of Europe, keeping the Mediterranean region dry. In winter, however, the westerly wind jet shifts to more southerly regions, allowing Atlantic depressions to reach the Mediterranean. At the same time, depressions form independently in the comparatively warm Mediterranean region in winter, leading to additional rainfall.
Also in East Europe rainfall increases towards the summer of the year, as precipitation is caused by a strong warming of the land masses inland due to the hygric mainland [136]. This leads to convective precipitation.

In addition to the spatial and temporal variations in precipitation, a long-term view also reveals the influence of climate change on the amount of total precipitation. Overall, precipitation in Europe has increased by 6 – 8 % over the last 60 years [138]. While precipitation in northern Europe has increased by 10 – 40 %, southern Europe and the Mediterranean region have experienced decreases of up to 30 %. The increase in precipitation in Northern Europe is mainly due to an increase in rainfall during the winter months. Meanwhile, the decrease in southern Europe can be observed throughout the year. For the rest of the 21st century, several models with various scenarios are feasible. These range from only very moderate predicted changes to a continuing north-south shift in the amount of precipitation [139–142]. Consistently, a decrease in summer precipitation is expected across Europe. The projected evolution of total precipitation due to climate change, classified by geographical location, is shown in Table 14.

Table 14: Projected precipitation trends for different climate change models [143]

	Northern Europe			Western Europe			Central-eastern Europe			Southern Europe		
	Past	Future		Past	Future		Past	Future		Past	Future	
		Low	High		Low	High		Low	High		Low	High
Total precipitation	↑	↗	↑	↗	→	↘	↗	↗	→	↓	↘	↓
Heavy precipitation	↑	↗	↑	↑	↗	↑	↑	↗	↑	↑	↗	↑

It should be noted that future total precipitation varies by region, but heavy rainfall events are increasing across all regions.

3.5.2 RAIN EXTREMES

Rainfall frequency, amount, and duration are dependent upon several factors. A look at the long-term weather records reveals the absolute maximum weather extremes that can occur on earth. The frequency, quantity and yield of rainfall depends on a number of factors. Particularly high levels of precipitation are observed where warm, humid air is forced to rise along orographic obstacles [19]. Table 1 therefore provides an overview of international records, while Table 2 only shows records within some selected European countries. Data is taken from [19, 79, 144–148].

Table 15: Rain records worldwide

Greatest rainfall in…	Value	Corresponding intensity	Location	Year
1 minutes	31.2 mm	1872 mm/h	Unionville, USA	1956
1 hour	305 mm	305 mm/h	Holt, USA	1947
12 hours	1.144 m	95 mm/h	Foc-Foc, La Réunion	1966
24 hours	1.825 m	76 mm/h	Foc-Foc, La Réunion	1966
48 hours	2.493 m	52 mm/h	Cherrapunji, India	1995
72 hours	3.930 m	55 mm/h	Cratère Commerson, La Réunion	2007
96 hours	4.936 m	51 mm/h	Cratère Commerson, La Réunion	2007
12 months	24.47 m	2,8 mm/h	Cherrapunji, India	1861

It should be mentioned that these conditions are absolute exceptions and do not represent an average weather situation in Europe. Nevertheless, they can be a good indicator of the absolute upper limits regarding the functionality of certain instruments, sensors or measurement devices.

Table 16: European Rain records in selected European countries

Greatest rainfall in…	Value	Corresponding intensity	Location	Year
UK:				
1 minute	5.1 mm	306 mm/h	Croydon	1935
2 minutes	8.4 mm	252 mm/h	Chepstow	1912
5 minutes	31.7 mm	380 mm/h	Preston	1983
10 minutes	45 mm	270 mm/h	Carlton-in-Cleveland	2003
15 minutes	56 mm	224 mm/h	Bolton	1964
30 minutes	80 mm	160 mm/h	Eskdalemuir	1953
1 hour	92 mm	92 mm/h	Maidenhead	1901
2 hours	193 mm	97 mm/h	Walshaw Dean Lodge	1989
24 hours	279 mm	12 mm/h	Martinstown	1955
France (only Metropolitan France):				
6 minutes	36 mm	360 mm/h	France	1982
15 minutes	84 mm	336 mm/h	France	1982
30 minutes	100 mm	200 mm/h	France	1982
1 hour	136 mm	136 mm/h	France	2010
2 hours	203 mm	102 mm/h	France	2010
Germany:				
8 minutes	126 mm	945 mm/h	Füssen	1920
2 hours	245 mm	123 mm/h	Münster	2014
24 hours	354 mm	15 mm/h	Zinnwald-Georgenfeld	2002
Switzerland:				
10 minutes	41 mm	246 mm/h	Lausanne	2018
1 hour	91,2 mm	91 mm/h	Locarno-Monti	1997
24 hours	455 mm	455 mm/h	Camedo	1935

It can be observed that the observation period has a significant impact on the resulting precipitation intensity. The difference between the observation intervals is shown as an example in Figure 12.

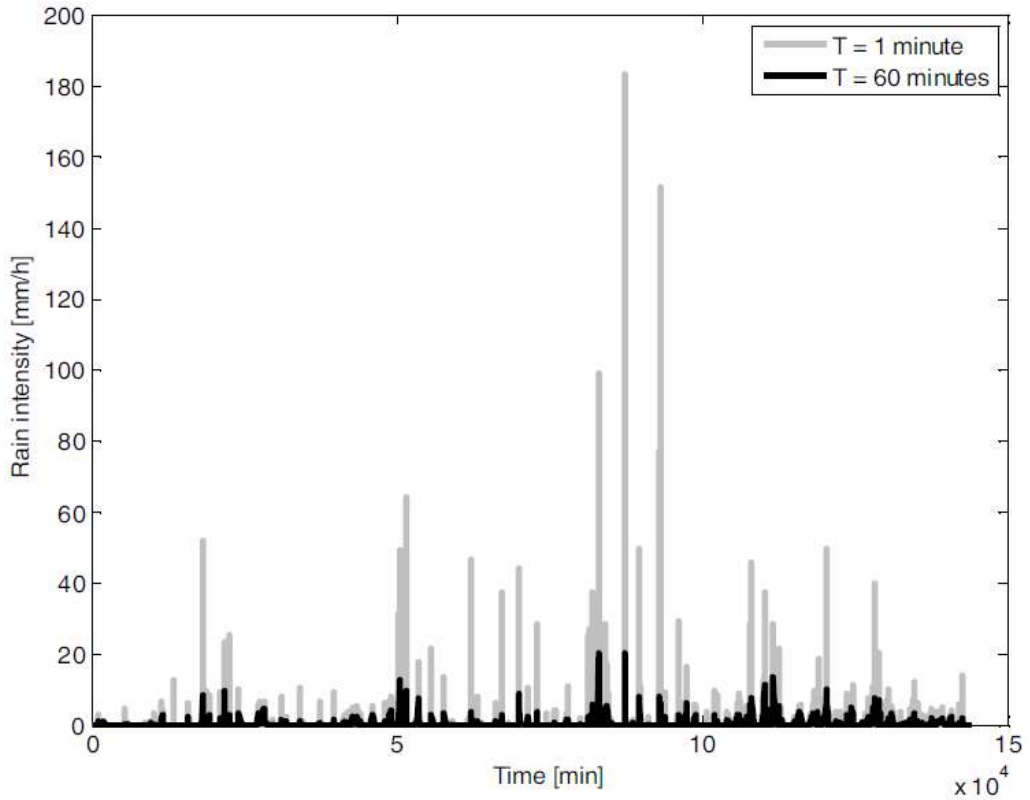

Figure 12: Influence of observation interval on rain intensity [149]

Given the high degree of variability in rainfall intensity over time within a single shower, it is recommended that the shortest possible time interval be selected for the analysis of precipitation intensity.
Unfortunately, 1-minute precipitation data are not commonly available worldwide. To account this issue, the ITU-R published the recommendation "P.837-7 - Characteristics of precipitation for propagation modelling" [150]. The method provides a prediction of precipitation rate statistics with an integration time of one minute. Additionally, it offers a conversion method for measurements with an observation interval of between five and sixty minutes into an observation interval of one minute. It should be noted that more detailed and accurate conversion models, most of which are based on or compare with the ITU-R model, can also be found in the literature, e.g. in [151–155].

3.5.3 Occurrence and intensity of short-term, extreme rainfall in Europe

For a more detailed analysis, weather data from the last few decades has to be studied. The following main objectives were addressed:

- To determine the frequency of very heavy rain showers.
- Their distribution within a year (dependency on the seasons)
- Their distribution within a day (dependency of the time of the day)
- To determine the most representing DSD for heavy rainfall events in Europe

Given the relevance of information on heavy rainfall occurrences to a number of different fields, including radio transmission, wastewater management, flood forecasting, and others, there is a wide variety of approaches and analyses employed.

3.5.3.1 Global: ITU-R 837

ITU-R 837-7 [150] provides a worldwide map showing the precipitation frequency that is statistically exceeded by 0.01 % of the time per year, as illustrated in Figure 13.

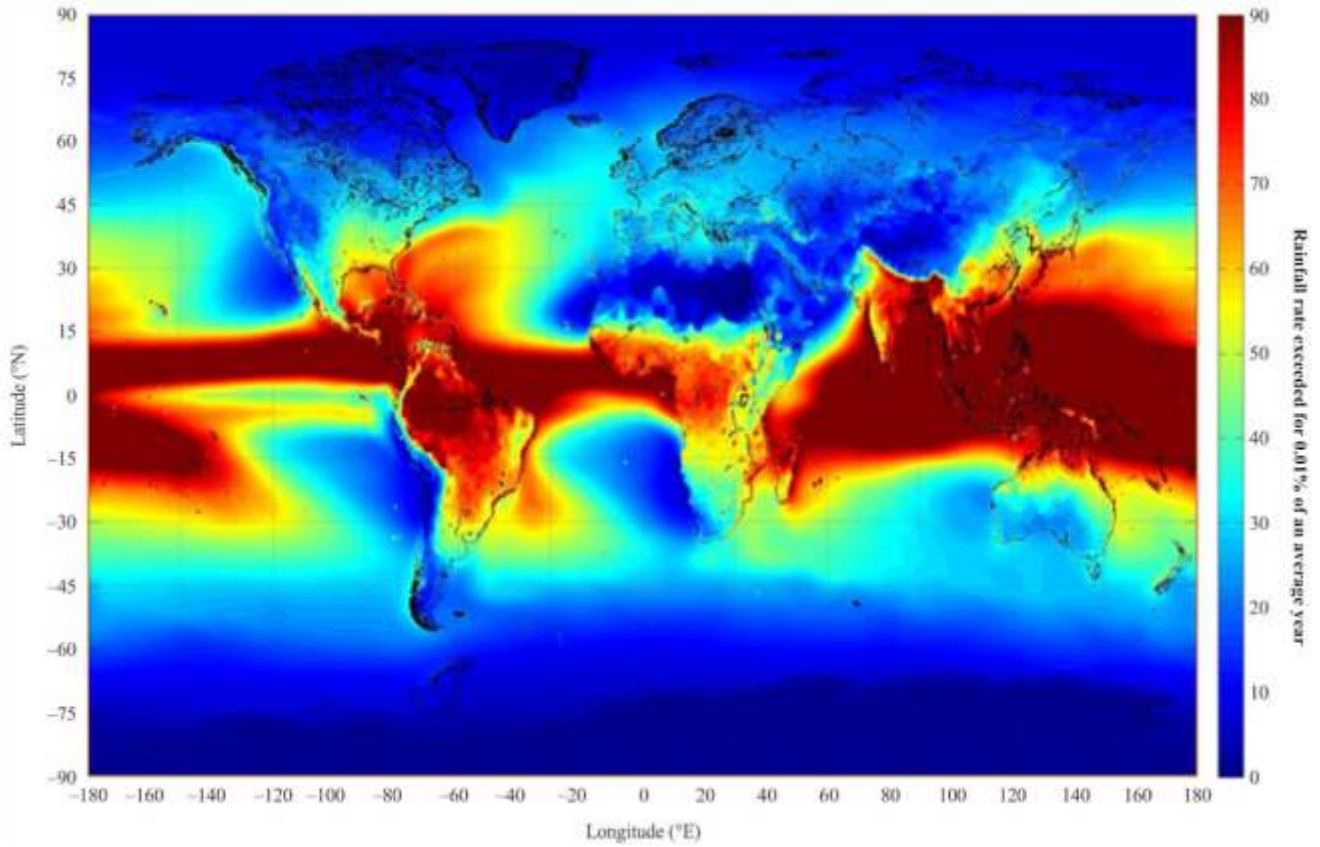

Figure 13: Average rainfall rate exceeded for 0.01% of an average year [150]
Reproduced with the kind permission of the ITU from Recommendation P.837

It can be observed that the minimum level of precipitation intensity in Europe, which occurs 0.01% of the time in an average year, is between approximately 20 and 45 mm/h. A more detailed version can be found in a previous version of this report by the ITU from 1994, which is shown in Figure 14.

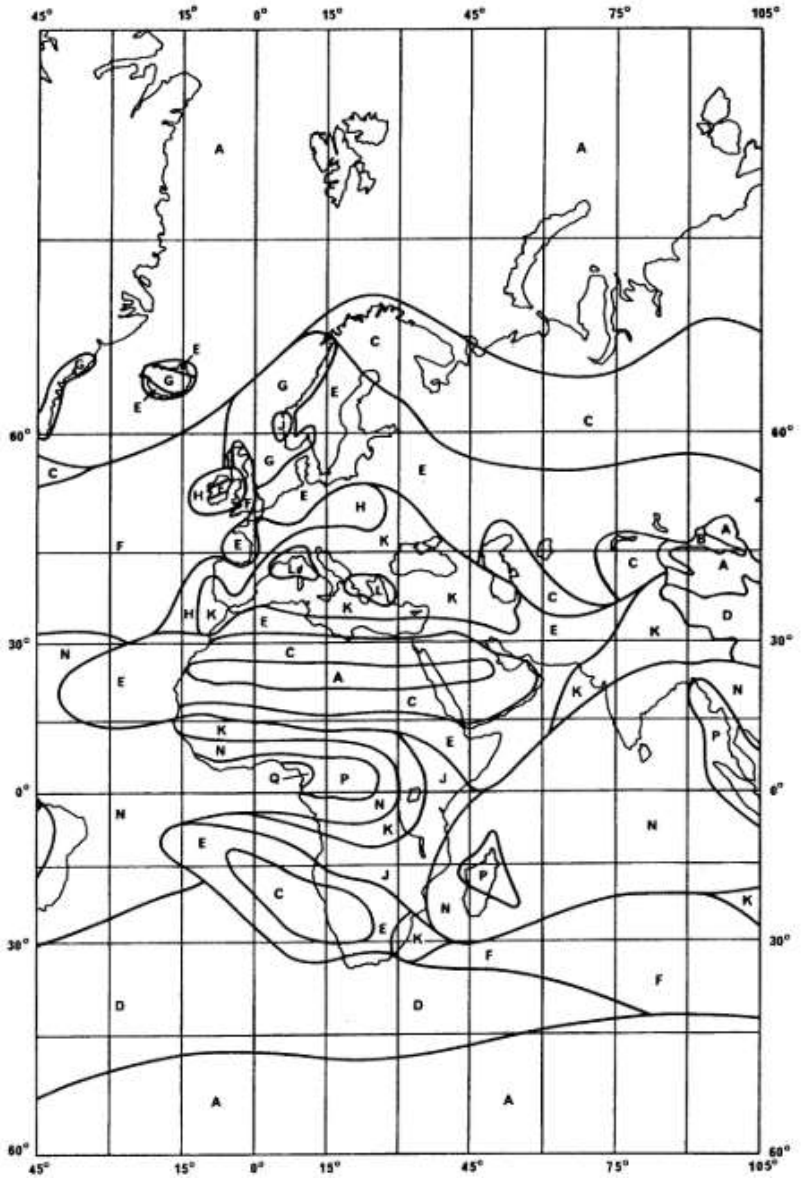

Rainfall intensity exceeded (mm/h)

Percentage of time (%)	A	B	C	D	E	F	G	H	J	K	L	M	N	P	Q
1.0	<0.1	0.5	0.7	2.1	0.6	1.7	3	2	8	15	2	4	5	12	24
0.3	0.8	2	2.8	4.5	2.4	4.5	7	4	13	42	7	11	15	34	49
0.1	2	3	5	8	6	8	12	10	20	12	15	22	35	65	72
0.03	5	6	9	13	12	15	20	18	28	23	33	40	65	105	96
0.01	8	12	15	19	22	28	30	32	35	42	60	63	95	145	115
0.003	14	21	26	29	41	54	45	55	45	70	105	95	140	200	142
0.001	22	32	42	42	70	78	65	83	55	100	150	120	180	250	170

Figure 14: Statistic precipitation intensity [156]
Reproduced with the kind permission of the ITU from Recommendation P.837

The figure clearly illustrates that the frequency of rainfall in Europe is particularly dependent on the geographical location. The majority of Europe is situated within areas E and K. In these areas, heavy rainfall of at least 12 mm/h and more occurs 0.03 % and 0.1 % of the time, respectively. Smaller European zones are within zones H, C and L.

3.5.3.2 Europe

Due to the limited availability of high time resolution rainfall data in Europe, Vajda [157] has focused its heavy rainfall research on daily total amount of rainfall where more data is available. Figure 15 shows the probability of a day having more than 30 mm precipitation, while Figure 16 summarizes the number of days with more than (A) 100 mm and (B) 150 mm of total rainfall per day.

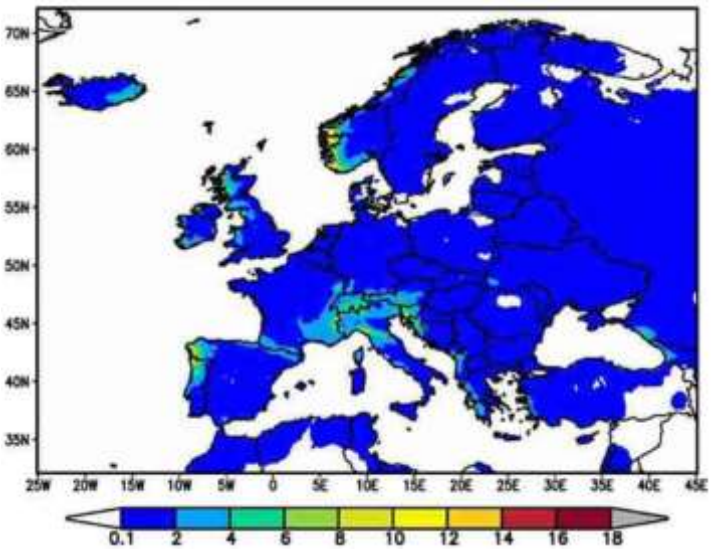

Figure 15: Frequency-based probability of daily rainfall exceeding 30 mm (in percent) during the period 1971-2000 based on E-OBS data [157]

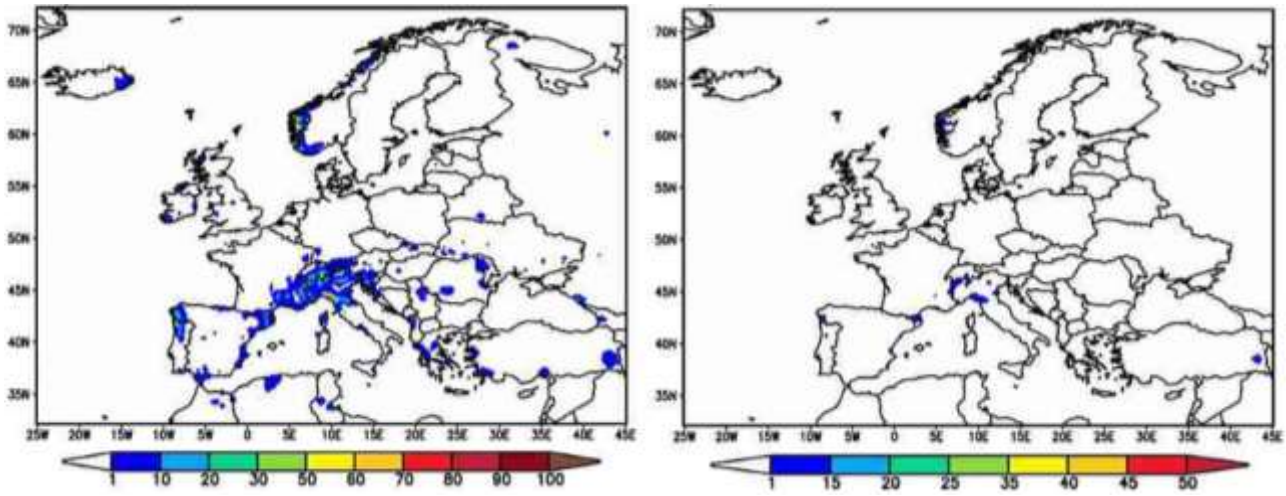

Figure 16: Total numbers of days with rainfall exceeding (A) 100 mm and (B) 150 mm during the period 1971-2000 based on E-OBS data

In most parts of Europe, the probability of having more than 30 mm of rain per rain event is about 2%. The Alpine region, the west coast of the United Kingdom, and the west coast of Scandinavia are more likely. In contrast, the eastern part of Scandinavia has particularly low precipitation, with less than 5 days per year exceeding 30 mm/day. Very large amounts of precipitation in excess of 150 mm/day are very rare according to these data. However, Vajda points out that these very high values are mostly levelled off in the E-OBS gridded data [157]. The data also show that heavy rainfall events (30 mm/day) occur mainly in winter.
Groenemeijer [158] analysed more recent radar data (1981-2010) from the E-OBS dataset. Figure 17 shows the 3-hour precipitation amounts that occur on average every 10 years.

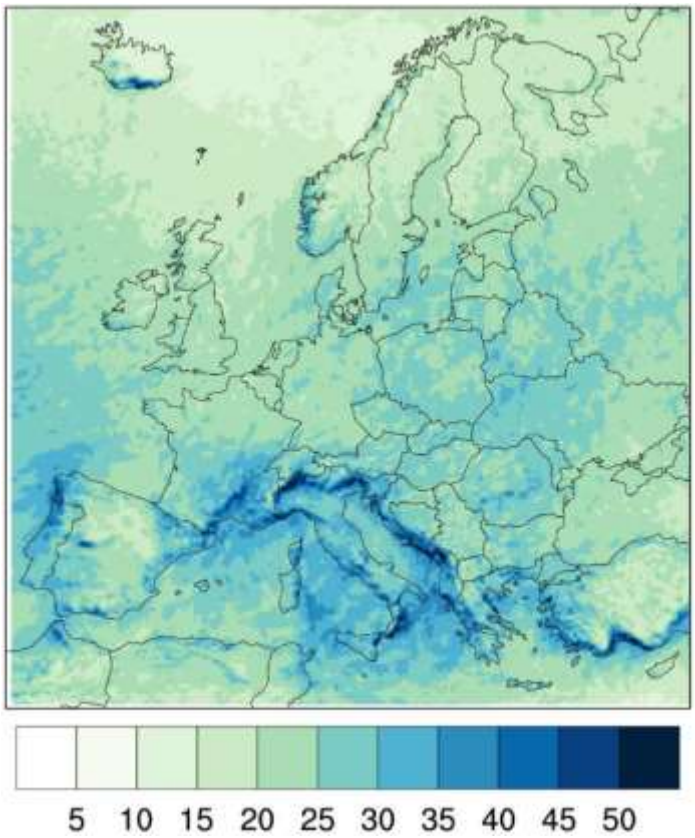

Figure 17: 10-year return level of 3-hourly precipitation. Data 1981-2010. [mm/3 hr] [158]

It is important to note that this is a 3-hour period. Since the intensity of the precipitation is highly variable, the intensity peaks are not visible in this figure.

Ryu [159] investigated the frequency of occurrence of certain droplet size distributions in heavy rainfall events (>10 mm/h). He identified three typical global droplet size distributions as shown in Figure 18. Type 1, the most continental type, is especially common in Europe. The strong convection typical over land creates clouds that produce particularly large drops during heavy rainfall. The fact that the largest drops are produced here is therefore consistent with the general rain characteristics found over land [159].

Type 1 is also most common in the United States, South America, and the western Pacific Ocean. Southeast Asian and East Asian monsoon regions and the North Atlantic Ocean are particularly common with Type 2. Type 3 is generally found alternating with type 2.

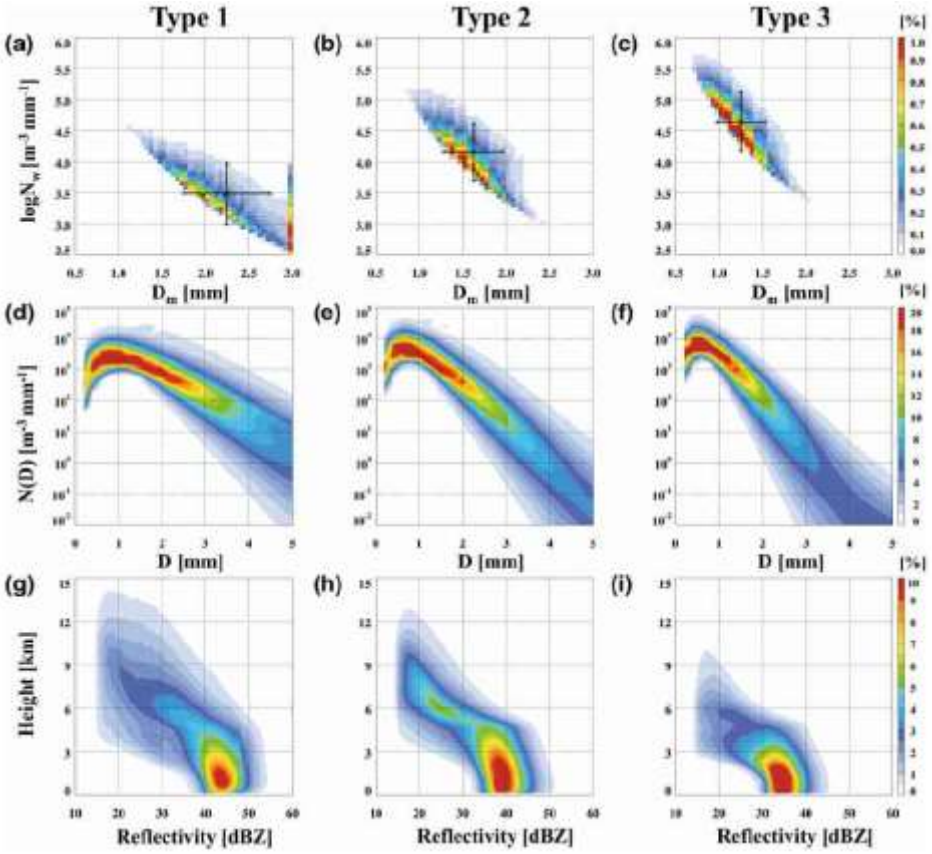

Figure 18: (a, b, c) Joint histograms of D_m and $\log N_w$, and (d, e, f) histogram of calculated number concentration for the three DSD types of heavy rainfall. Black cross in the upper panel represents mean ± one standard deviation of D_m and $\log N_w$. (g, h, i) Contoured frequency by altitude diagrams of Ku-band reflectivity for the three DSD types. D_m, mean diameter; DSD, drop size distribution; N_w, normalized intercept parameter.

3.5.3.3 In-depth analysis of German weather data

While each European country records data separately through its national weather service, there is no central European database providing high-resolution temporal and spatial data with all the necessary information. As high-resolution data is required to analyse short-term and heavy precipitation, national databases have to be used. However, the national databases differ significantly in terms of which data is recorded and in which intervals. Each national database records different data and intervals, which makes it difficult and effortful to analyse them. The DWD in Germany operates one of the narrowest and most widespread climate data network in Europe. The recorded data is made publicly accessible to everyone by the Climate Data Center [160]. Precipitation data is collected at approximately 1200 measuring stations located throughout Germany. Rainfall totals are available in monthly, daily, hourly, 10-minute, 5-minute and 1-minute time intervals. For the following analysis, the 1-minute precipitation totals were evaluated.

A selection of 10 stations was chosen for further analysis due to the large amount of data. These stations are shown in Figure 19 and Table 17. Care was taken to select stations in various locations, including near the coast, in the mountains, and in the lowlands, in order to account for different influences. The selection also includes both urban and rural areas.

A 15-year observation period between 2009 and 2023 was chosen because minute-by-minute data is available for most stations starting from a period between 2004 and 2008. For the selected period data was available in average for 99.8 % of the time. It is important to mention that this analysis considers all forms of precipitation, without distinguishing between liquid and solid precipitation. As this analysis focuses mainly on high precipitation intensities, solid

precipitation, which often occurs at lower intensities over a longer period of time, is assumed to have only a very small influence on the analysis.

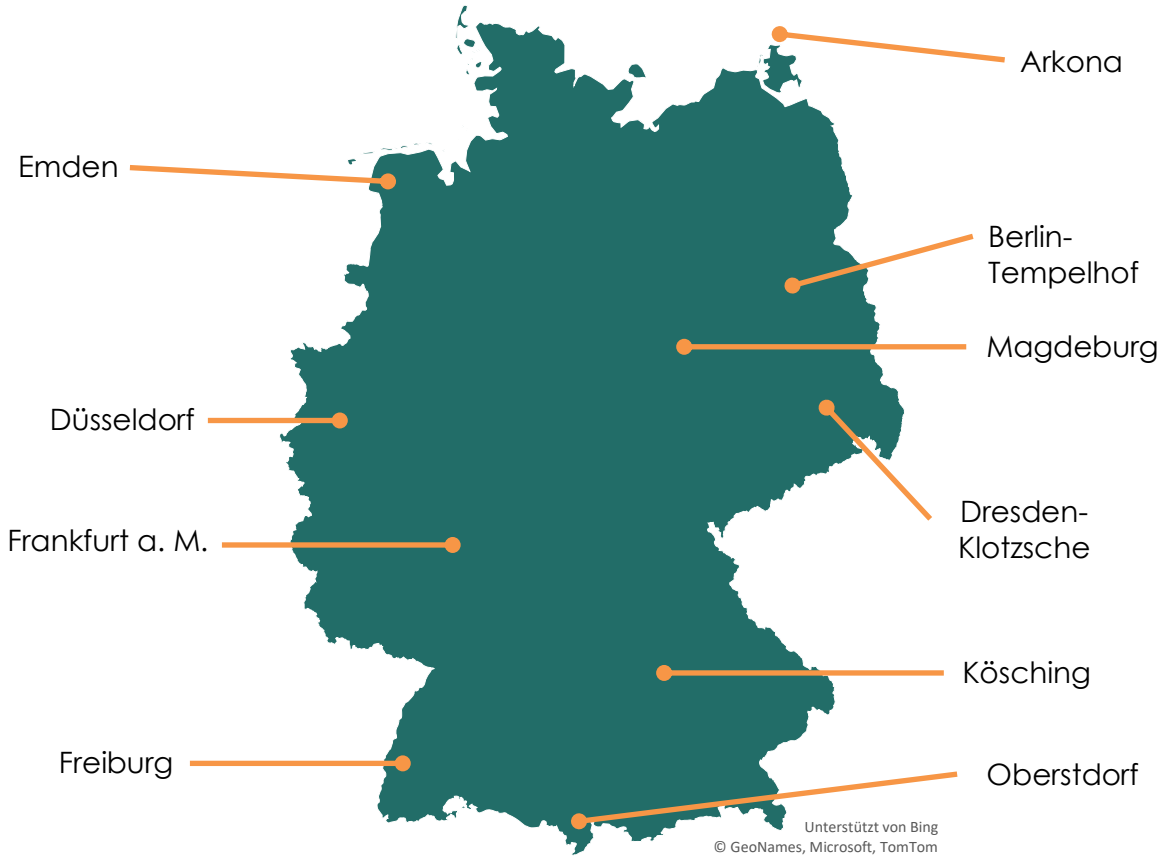

Figure 19: Selected weather stations

Table 17: Location data of the selected weather stations

Station name	Station ID	Station altitude	Latitude	Longitude
Arkona	00183	42 m	54.6791	13.4344
Berlin-Tempelhof	00433	48 m	52.4676	13.4020
Dresden-Klotzsche	01048	228 m	51.1278	13.7543
Düsseldorf	01078	37 m	51.2960	6.7686
Emden	05839	0 m	53.3881	7.228
Frankfurt a. M.	01420	100 m	50.0259	8.5213
Freiburg	01443	237 m	48.0232	7.8343
Kösching	02700	416 m	48.8302	11.4872
Magdeburg	03126	79 m	52.1029	11.5827
Oberstdorf	03730	806 m	47.3984	10.2759

Regarding the average precipitation in Germany, as shown in Figure 20, this covers both stations in rather dry areas as well as in areas with high precipitation.

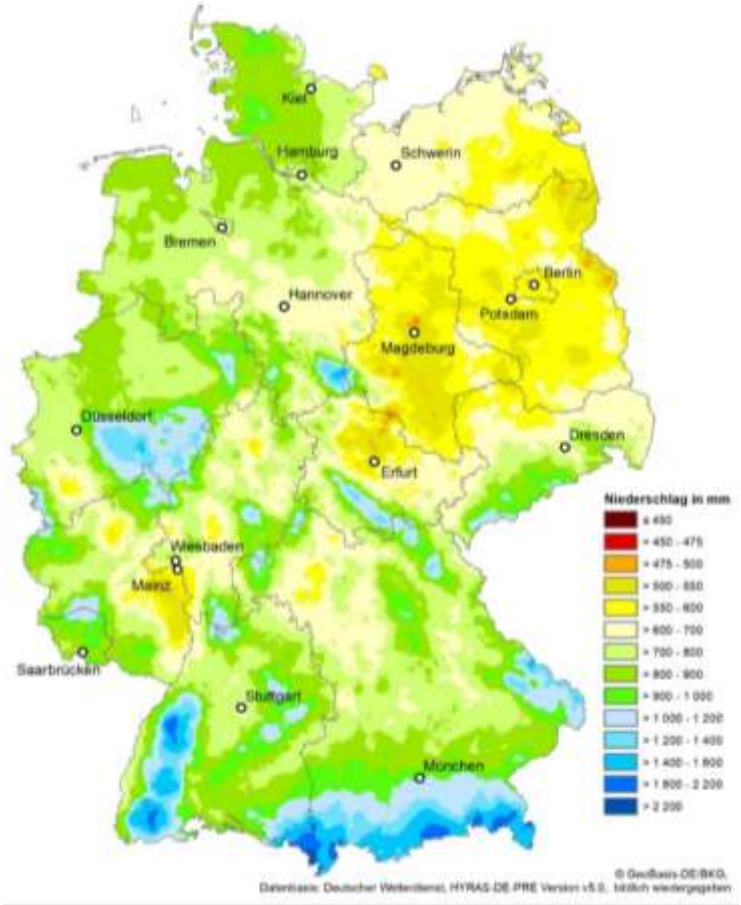

Figure 20: Mean rainfall distribution for 1991-2020 in Germany [161]

Depending on the location, this results in a different frequency of precipitation, as shown in Figure 21.

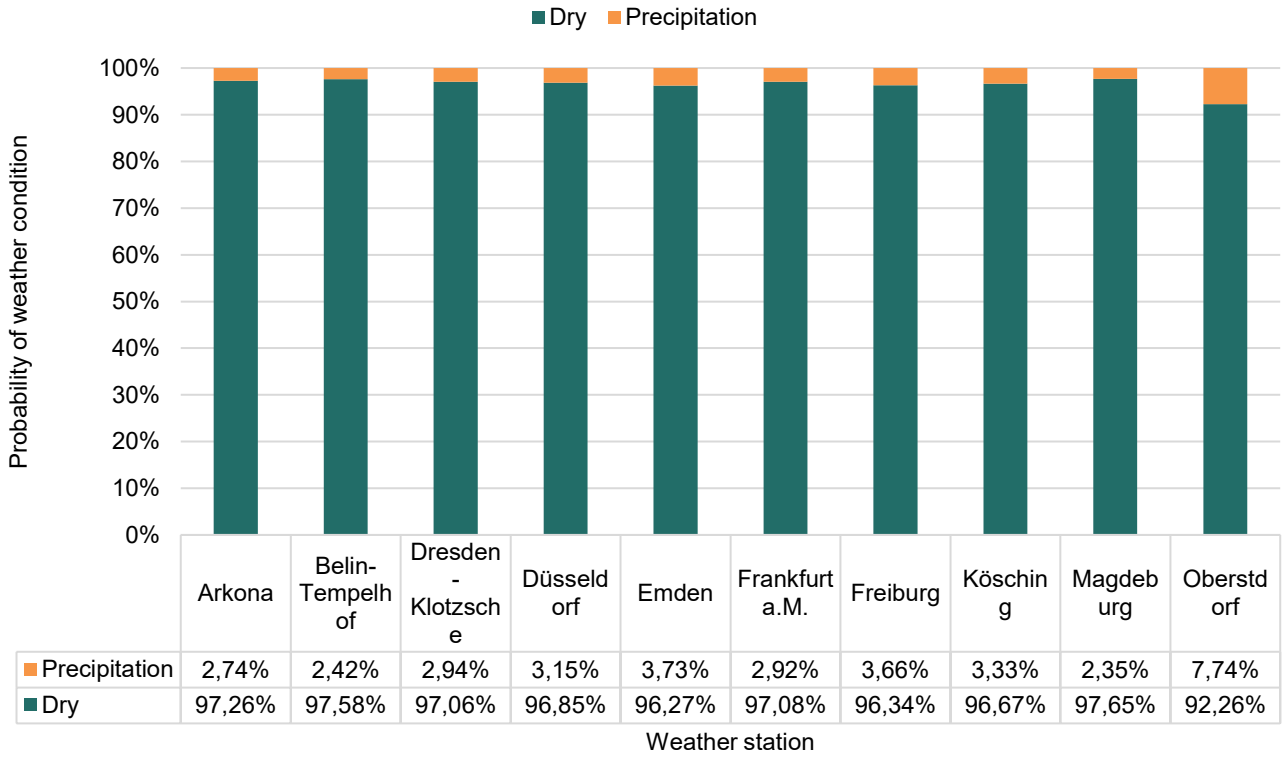

	Arkona	Belin-Tempelhof	Dresden-Klotzsche	Düsseldorf	Emden	Frankfurt a.M.	Freiburg	Köschin g	Magdeburg	Oberstdorf
Precipitation	2,74%	2,42%	2,94%	3,15%	3,73%	2,92%	3,66%	3,33%	2,35%	7,74%
Dry	97,26%	97,58%	97,06%	96,85%	96,27%	97,08%	96,34%	96,67%	97,65%	92,26%

Figure 21: Probability of precipitation during the analysed period (2009-2023)

During the analysed period, precipitation was not observed for 92.26% to 97.65% of the time. The frequency of rainfall varies depending on the geographical location of the weather station. Precipitation was particularly frequent at the Oberstdorf weather station, which can be explained by its location in the Alps, as shown in Figure 20. The areas with low total precipitation around Berlin, Brandenburg, and Saxony-Anhalt, represented in this analysis by the Berlin-Tempelhof and Magdeburg stations, also have the lowest precipitation frequencies in this analysis. However, apart from Oberstdorf, the stations show similar frequency ranges.

Furthermore, knowledge of the frequency and maximum intensity of precipitation events is more decisive. This enables safety functions to be designed for the maximum events that occur at least once within a defined time interval. Therefore, the existing database was analysed for each weather station according to the occurrence frequency of a precipitation event with a defined intensity in the last 15 years.
Figure 22 and Figure 23 shows the frequency of rain events with a minimum intensity of x mm/h occurring for one minute. The y axis (left) shows the total number of minutes in which a rain event with at least this intensity of the x axis was detected each year in average.

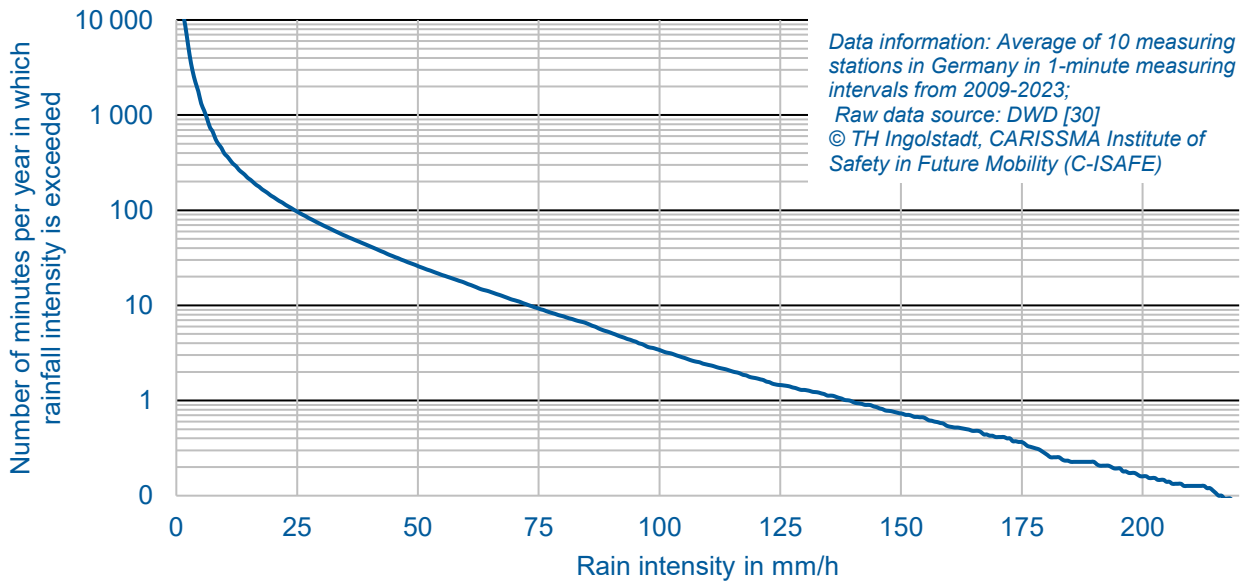

Figure 22: Number of minutes per year in which different rainfall intensities are exceeded

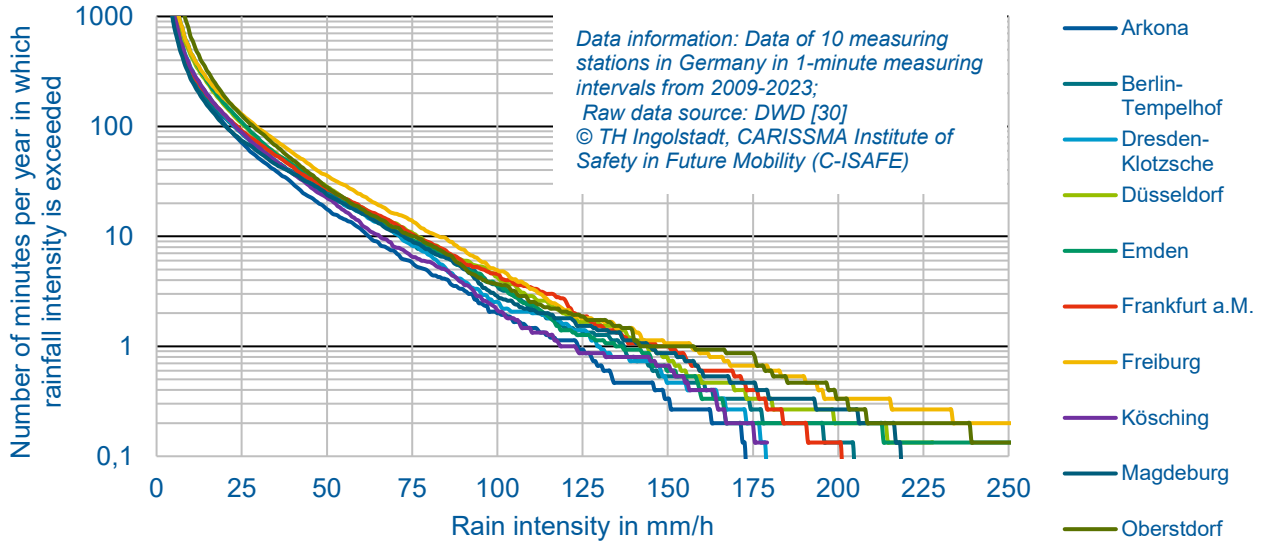

Figure 23: Occurrence frequency of precipitation events in Arkona, Berlin-Tempelhof, Dresden-Klotzsche, Düsseldorf, Emden, Frankfurt, Freiburg, Kösching, Magdeburg, Oberstdorf

Figure 24 shows the average frequency of a precipitation event for the different months over all stations considered.

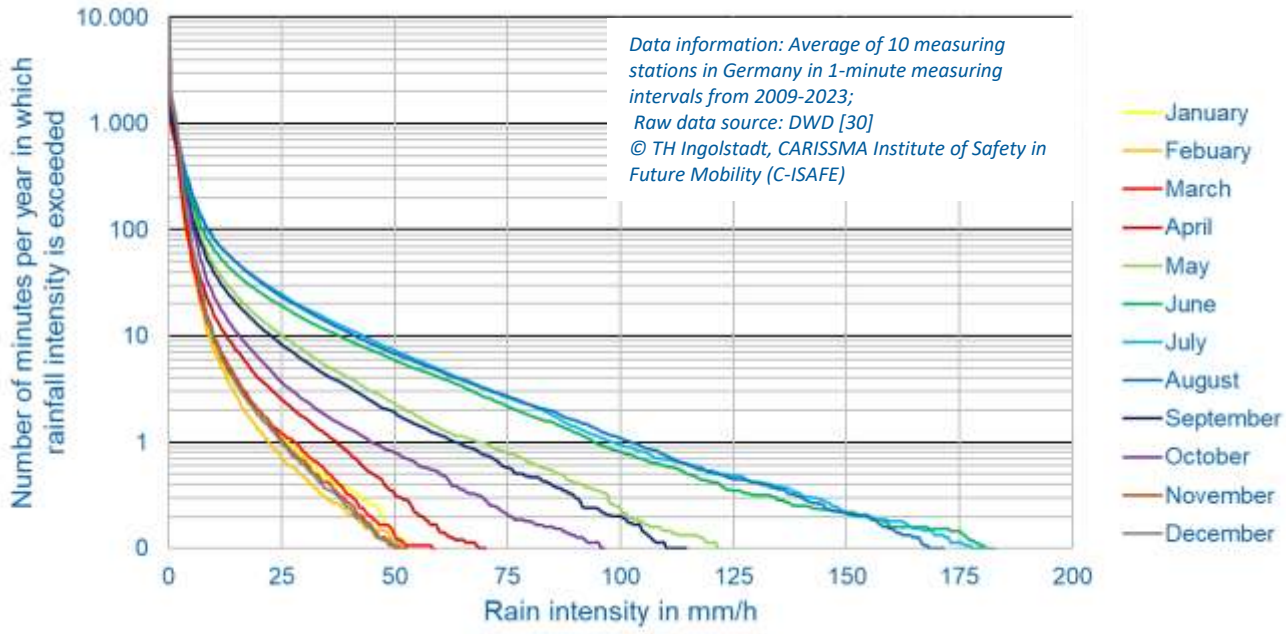

Figure 24: Average occurrence frequency of precipitation events depending on the month

The most frequent heavy rainfall events in Germany occur in the summer months, especially in June, July, and August. The months with the least frequent heavy rainfall events are all in winter: November, December, January, and February. When comparing this result to the total precipitation sum in summer and winter from Figure 11, it is noticeable that the total precipitation sums are minimal lower for winter. However, this difference is significantly more relevant for heavy precipitation events, as severe rain intensities occur disproportionately in summer.

Next, the frequency of precipitation at different times is shown in Figure 25.

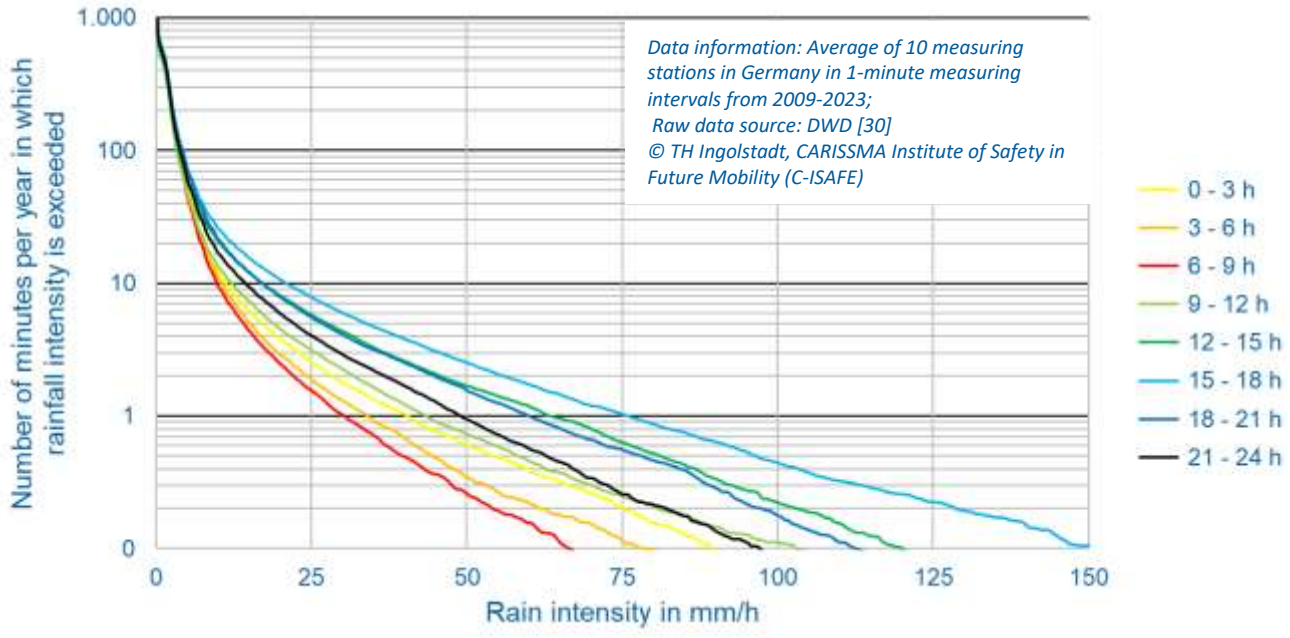

Figure 25: Average occurrence frequency of precipitation events divided by daytime

The accumulation of heavy precipitation in the afternoon and evening is clearly noticeable. As convective heavy precipitation events are characterised by strong evaporation, heavy rain events are mainly expected towards the end of the day. Together with the previous finding that heavy rainfall events mainly occur in summer, this analysis is in line with the expectations from the literature.

3.6 RAIN CLASSIFICATION

Based on the above findings, the following classification of precipitation events based on intensity is proposed.

Table 18: Rain classification

Type	Range
No rain	0 mm/h
Drizzle	Precipitation rate < 1 mm/h (with very fine droplets)
Light rain	Precipitation rate < 2,5 mm/h
Moderate rain	Precipitation rate between 2,5 mm/h and 10 mm/h
Heavy rain	Precipitation rate between 10 mm/h and 50 mm/h
Violent rain	Precipitation rate between 50 mm/h and 100 mm/h
Cloudburst	Precipitation rate > 100 mm/h

The intensity values refer to highly local (e.g. rain gauge) and short-term (e.g. 1 minute) precipitation measurements. These measured values are not directly transferable to measurements with a high spatial resolution (e.g. precipitation radar measurements) or longer time intervals (e.g. 1 hour).

Based on the frequency of occurrence, the range of heavy rain and violent rain in particular should be used for tests to investigate the robustness of environmental sensors in intelligent and automated vehicles. To encompass a range of intensity levels, tests may be conducted with varying intensities in this range of heavy and violent rain.

At higher precipitation intensities, increasingly large droplets are present. Therefore, it is recommended to use the droplet size distribution according to Weibull or Ulrich, which both model the shift in mean droplet sizes with increasing precipitation intensity more closely.

Ideally, a disdrometer should be used to determine the characteristics, as this can determine the amount of precipitation, drop size distribution and velocity distribution at the same time.

4. Fog

4.1 General Characteristics

When water vapor condenses or resublimes in moisture-saturated air, and not on solid surfaces, fog is formed [162]. Thereby fog is defined according to international definitions as a suspension of very small droplets in the air, which reduce the horizontal visibility to less than 1 km [163–165]. With greater visibility, the phenomenon is often colloquially referred as mist, haze or "light fog" [166]. Mist is defined as a obscurity that still have a visibility above 1 km [167, 168]. As mist also consists of fine water droplets, humidity is still close to 100 %. The droplet concentration is just less than with fog. From a physical point of view, a further distinction is made between fog and mist, when the air is completely saturated with moisture, and haze, smoke, snow as well as rain, when it is not (yet) saturated [19]. Haze results in a horizontal visibility reduction due to non-aqueous particles. When the visibility is low and the humidity is below about 80 %, it is assumed to be haze [12]. However, according to the WMO-No. 8 all occasions of visibility of less than 1 km are regarded climatological summaries as fog, so the lowest horizontal visibility for haze is assumed with 1 km [12].

Table 19: Distinction between fog, mist and haze

	Fog	Mist	Haze
Visibility	Occasions with horizontal visibility < 1 km	Occasions with horizontal visibility > 1 km	Occasions with horizontal visibility > 1 km
Humidity	Relative humidity near 100 %	Very high relative humidity (> 95 %)	Relative humidity below about < 80 %
Particles	Fine water droplets	Fine water droplets	Non-aqueous particles: e.g. dust, sand, salt, aerosols, or photochemical smog

Fog causes a strong scattering of the incident light and thus a reduction in visibility of up to 10 m in heavy fog [14]. The reduction in visibility has a strong dependency on the structure of fog, like number density and size distribution of the fog droplets, which is highly dependent on time and space [164]. Its general occurrence of fog is especially frequent where and when night-time temperatures drop particularly low.
Basically, fog forms when air near the earth's surface gets supersaturated or nearly saturated air is cooled down by several effects. Thereby of the main causes is the effect that warm air can contain more water vapor than cold air. However, there are also other effects for the formation of fog, as shown in Table 20.

Table 20: Types of fog formation according to [19]

Cooling of moisture air	
Radiation losses from the ground, an aerosol or fog layer	Radiation fog
Cooling of the air when passing over a cold surface or air layer	Advection fog
Adiabatic cooling of the air as it rises over an obstacle	Orographic fog / Upslope fog
Supply of water vapor	
into heated unsaturated air, which then cools below the dew point by mixing with cold air	Mixed fog / Steam fog / Frontal fog
Supply of condensation nuclei	
from industrial, domestic and vehicle exhaust gases into humid air:	Urban fog / smog

It should be noted that even if fog normally consists of numerous very small and liquid water particles, freezing fog can occur at outside temperatures below 0° C, known as icy fog [169]. While this type still consists of liquid droplets in the air, it freezes when it comes into contact with surfaces [170].

4.1.1 Radiation fog

As the temperature of the ground decreases at night, a heat transfer from the air layers above to the ground occurs. This heat transfer causes a cooling of air layers close to the ground. Consequently, the temperature drops below the dew point and water vapor condenses. This process can be observed especially frequently on clear, windless nights or mornings before sunrise in valley basins, depressions or along rivers [163, 171]. Although it should not be too calm, as this would prevent heat transfer and dew would form on the surface instead [172].

A characteristic aspect of radiation fog is that it consists primarily as a ground-level fog layer that rarely grow higher than 300 meters, whereby the thickness of the fog layer depends on the moisture content of the air as well as on the temperature [14]. Furthermore, as a result of the formation process, the water content is quite low, which leads to rather small, mostly non-wetting drops. Its occurrence is more frequent in winter, as the nights are longer which allows more time for the ground to cool down [169].

Even if fog itself has a high self-preserving effect, as it reflects up to 90% of the solar radiation, radiation fog is usually dissipated during the morning of a day as the sun warms up the environment and air masses are vigorous mixed [19].

Due to his occurrence radiation fog is often also referred to as "continental fog" [173].

4.1.2 Advection fog

In contrast to radiation fog, advection fog is a more permanent and humid type of fog [13]. This type is often also called "maritime fog" [173]. It occurs when warm and moist air is pushed over a cold layer or surface and the air cools below its dew point [174].
In moderate regions, this type of fog occurs on the one hand in the winter months when warm air from the south is pushed into more northern regions and reaches cold ground there [19]. In the other hand in spring the opposite effect occurs with a cold sea or lakes and warm land air. Then, for example, maritime or sea fog occurs in coastal regions [169]. In the same way,

the collision of warm and cold ocean streams can lead to the formation of advection fog [175].
The resulting fog can extend to altitudes of far above 1000 m. This has the consequence that the sun alone is not sufficient for dissolution, rather a massive change of air masses is required [14].

4.1.3 Further fog formation processes

In addition to the two most common types of fog formation described above, there are also further types, which are only briefly described here.

Orographic fog formation process is similar to orographic rain. The rise of moist and warm air on a mountain cools it adiabatically [176]. In order to form fog and no clouds, a low level for condensation must be prevalent. This type of fog also regularly occurs in moderate European regions, such as the Alps or the central German uplands [19].

If warm air mixes with cold air and fog is created by cooling the air below the dew point, it is called mixed fog. This can occur, for example, when two precipitation fronts collide (= often also called frontal fog or precipitation fog) [177–179]. Steam fog is the opposite of advection fog. Cold air is pushed above a warm ground, which leads to the occurrence of vapor, for example over lakes, roofs or car roofs (= often also called evaporation fog or sea smoke) [180].

Moreover, fog can also occur due to the lowering of the cloud base, resulting from radiative cooling and large-scale subsidence of air-masses [178].

Smog, a symbiosis of the terms smoke and fog, describes the reduction in visibility caused by heavy air pollution. A chemical reaction between the mist droplets and the dirt particles present in the air can be leading to thicker fog and negative effects on humans [164, 181–185].

Tardif [179] developed a method with which a classification between the different types of fog is possible based on meteorological parameters such as visibility, air temperature, wind direction and speed, precipitation, cloud cover height and coverage. Developed from fog data from New York, their method has been adapted worldwide multiple times [186–191]. A different approach based on a decision from a modified Richardson number is described by Lin [192].

4.1.4 Fog life cycle

While fog is present, its characteristics changes constantly. The supply and removal of the water content depends on environmental conditions that may underly changes. Furthermore, the DSD is affected during a fog life cycle, as droplets can grow due to water vapor condensation, collision coalescence or the so called "Ostwald ripening", when the smallest droplets evaporate in favour of vapor diffusion on the largest ones [193–195].

According to literature, the life cycle of fog can be subdivided into four phases [194, 196]:

1. Formation
2. Development
3. Maturity
4. Dissipation

Even if there are a few studies, like [194, 196–198], on the physical processes within the individual stages, exact microphysical fog parameters for each phase have hardly been researched until now [199]. However, it can be noted for ground near fog particles that with increasing fog duration, the droplet spectrum shifts from small to increasingly larger fog droplets. In measurements of various radiation fog events, Prince [198] measured for several fog events a mean droplet size of 3 - 4 µm at the beginning and a mean modal diameter of approximately 16 - 18 µm after 3 - 4 hours. Similarly, a reduction in visibility correlates with larger effective mean droplet diameters and droplet numbers [199]. Further measurements on different fog stages and different fog severity cases were carried out by Liu [196] in China.
Dissipation of fog occurs due to different effect. The most common ones can be subdivided into:

- Insufficient supply of moisture to maintain saturation or additionally evaporation due to heating or drying, which leads to a decrease of the supersaturation of the air masses, contribute to a dissolution of fog [200, 201]. The lowest layer, which is closest to the ground, dissolves first, which leads sometimes to status clouds [202, 203].
- Turbulence, e.g. caused by radiative cooling at the top of the cloud, can lead to a mixing of the fog with adjacent drier air layers and thus to a dissolution of the fog [178, 202]. Downdrafts as well as the gravity itself can also be responsible for the transport of water droplets towards the ground, where droplets start to settle [204–207].
- Even though fog scatters most of the incident solar radiation, a certain amount is still absorbed. This contributes to a warming and subsequent dissolution of the fog [208]. Due to that (radiation) fog often forms during night and dissipate in the morning.
- In addition to creating turbulence, wind can also transport fog from one place of origin to another [198].
- Occurrence of precipitation [209].

4.2 ATTRIBUTES OF FOG

To characterize fog, both macroscopical, such as visibility, and microphysical parameters, such as droplet size distribution, liquid water content, average particle size, and number of particles per air volume or relationships between the mentioned parameters can be used. The most important ones are discussed in the following chapters.

4.2.1 METEOROLOGICAL OPTICAL RANGE (MOR)

At first glance, the visual range may appear to be simply defined as the maximum visual range of a human observer. Physically, visibility refers to transparency of air. However, visibility is influenced by numerous physical and subjective factors. Due to that visibility can be estimated from human eye observation or calculated from atmospheric light attenuation using an optical-based instrument. The latter one is defined as the Meteorological optical range (MOR) and is mainly used for the sake of comparability:

- **Meteorological optical range** *(MOR)*: The length of path in the atmosphere required to reduce the luminous flux in a collimated beam from an incandescent lamp, at a colour temperature of 2700 K, to 5 % of its original value. The luminous flux is evaluated by means of the photometric luminosity function of CIE, which describes the average spectral sensitivity of human visual perception of brightness [12].

The visual range of the human eye, which can also be described as visibility by contrast, can be defined as follows:

- **Visual range** *(meteorological)*: Distance at which the contrast of a given object with respect to its background is just equal to the contrast threshold of an observer [210].

- **Visibility** *(meteorological visibility, meteorological visibility at night)*: Greatest distance at which a black object of suitable dimensions can be seen and recognized against the horizon sky during daylight or could be seen and recognized during the night if the general illumination were raised to the normal daylight level [210].

The contrast threshold **ε** that is needed for the human eye to distinguish between two objects is generally assumed to be **ε** = 0.02 [211] or **ε** = 0.05 [12]. Using the Beer-Lambert law [212–214], a link between the light attenuation, due to gaseous and particulate matters in the ambient air, and the visual range can be made. This results in Koschmieder's visibility formula [215]:

$$V_N = \frac{-ln(0.02)}{\gamma_{ext}} = \frac{3{,}91}{\gamma_{ext}} \qquad [km] \qquad \textit{(Eq. 16)}$$

Here V represents the visibility in km and γ_{ext} the extinction coefficient. The definition of **ε** = 0.02 originates from the highly known publication by Koschmieder [215] from 1924. Today, the WMO [12] and International Commission on Illumination (CIE) [216] use **ε** = 0.05 for the calculation of the visibility, to take requirements from the aeronautics into account, whereas in daylight a black object should be reliably distinguished against the horizon at a wavelength of 550 nm, which is close to the peak of the optical transfer function for human vision.

$$V_{MOR} = \frac{-ln(0.05)}{\gamma_{ext}} = \frac{3}{\gamma_{ext}} \qquad [km] \qquad \textit{(Eq. 17)}$$

The colour also has an influence on the contrast, as not all objects have perfect black and white contrast, which means that the actual visibility can sometimes be less than the MOR. The visual range can be measured by a human observer, although there are difficulties with regard to objectivity, reproducibility, and recordability [217]. Alternatively, camera images are used with evaluation algorithms that consider, for example contrast, edge detection, Sobel operator, fast Fourier transform, and RGB colour information [218–222]. The comparison between humas visibility measurements by observers and camera visual-range demonstrate that these techniques can achieve accurate results during daytime [217, 223].
The most common and recommend devices by the WMO and International Civil Aviation Organisation (ICAO) to measure the MOR are devices that measure either the extinction coefficient or the scattering coefficient. Advantage is the good measurement consistency and high measurement accuracy under low visibility conditions, while the usually comparatively short and punctual measuring distance must be considered [224, 225].
In addition to the official fog definition, there are some national standards for visibility in relation to road traffic, such as the French NF P99-320:1998-04-01 [81], in which fog with visibility of less than 400 m is divided into four subcategories.

4.2.2 DSD

The DSD of fog is calculated in a similar way to that of rain, which is described in chapter 3.2.3. However, it is more challenging to separate fog at the lower end from cloud and haze particles and at the upper end from drizzle drops. Roughly speaking, the lower limit is usually set between 1–3 µm, as smaller particles are inactivated aerosols or cloud particles. Droplets from approx. 0.2 mm are counted as drizzle or raindrops, whereby this value defines the upper maximum for fog droplets [173, 226].

Generally, fog droplets are in the range between a few tenths of a micron to a few tens of microns [19, 163]. Slightly wetting fog has smaller droplets between 5 and 10 µm, while heavily wetting fog has droplets between 10 and 20 µm, with the largest droplets up to or more than 50 µm [14]. Each type of fog has a specific droplet size distribution. While in radiation fog the particle diameter varies slightly around 4 µm, in advection fog it is mainly particles close to 20 µm [173, 226]. Of course, the DSD depends very strong and random in place and time, and changes during a fog-life cycle as well as it is varying spatially [203, 227]. An extensive study of fog classifications according to their DSD has been done by [228].
Exemplary DSDs of different fogs are shown in Figure 26.

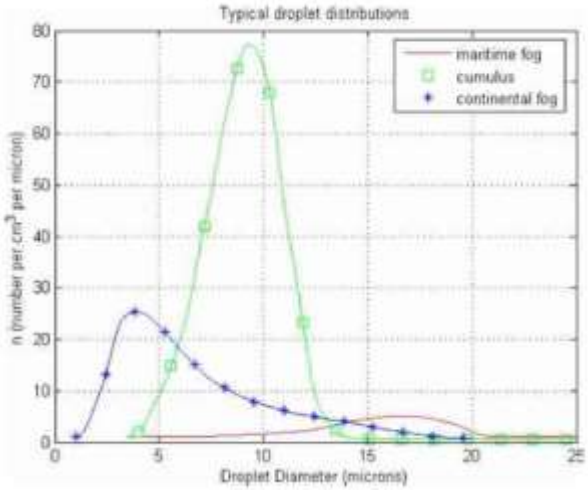

Figure 26: Typical droplet distribution for different kinds of fog according to [173]

Unlike rain, fog drops are always ideally spherical due to their small diameter [173]. Therefore, the effective diameter is used here to specify a representative diameter for a chosen fog, assuming that all droplets would have the same size, which has the same surface area and the same liquid water content, but not the same total number of droplets [229]. This can be calculated as followed:

$$D_{eff} = \frac{\int_{D_{min}}^{\infty} n(D) * D^3 dD}{\int_{D_{min}}^{\infty} n(D) * D^2 dD} = \frac{6 * LWC}{\rho_{water} * S} \qquad \textit{(Eq. 18)}$$

Thereby ρ_{water} represents the density of liquid water, LWC the liquid water content of fog and S the total surface area. It should be noted that normally the effective diameter is bigger than the mean droplet diameter.

For the droplet size distribution of fog there are also some mathematical representation models:

a) Modified Gamma Distribution

The modified gamma distribution is an often-used model to replicate a particle size distribution of fog as a function of radius r.

$$N(r) = a * r^{\alpha} * exp[-b * r^{\gamma}] \quad (Eq.\ 19)$$

Here α, b and γ indicate the shape and width of the distribution and a normalizes the total number N of droplets per unit volume [60]. According to Shettle [230] it can be parameterized with following values:

Table 21: Modified gamma distribution parameterization by Shettle [230]

Type of fog	Model	a	α	b	γ
Advection fog (heavy)	1	0.06592	3	0.3	1
Advection fog (moderate)	2	0.027	3	0.375	1
Radiation fog (heavy)	3	2.37305	6	1.5	1
Advection fog (moderate)	4	607.5	6	3.0	1

However, it should be noted that the measuring devices used to calibrate these models in 1979 had difficulties with detecting the smallest droplets (<1 µm). As a result, Shettle's model tends to underestimate the total number of droplets and overestimate the average size of the droplets. Further properties of the function are specified by Deirmendjian [60], whereby his model seems to overestimate the droplet size [228].
If $\gamma = 1$, the expression is the same as Levin's gamma distribution proposal [231]. With $\gamma = 1$ and $\alpha = 2$, the formula proposed by Khrgian and Mazin [232] is obtained. Garland [233] determined parameters for small water droplets with a visibility ranging around 1 km, which are particularly suitable for haze and have an r_c between 0.038 and 0.734 µm. Tampieri and Tomasi [234] parameterize the modified gamma distribution for a visibility of 0.2 km for different fog types with r_c values between 2.13 and 12.22 µm. Further considerations regarding this topic were published by Harris [235]. Bernardin [236] provides values for a shifted modified gamma distribution, which represents radiation fog with visibility around 50 m that was recorded during measurement campaigns near Paris [172, 203].

b) Log-normal Distribution

The log-normal distribution is defined by:

$$N(r) = \frac{N}{r\sigma\sqrt{2\pi}} * exp\left(-\frac{(ln\,(r) - ln\,(\tilde{r}))^2}{2\sigma^2}\right) \quad (Eq.\ 20)$$

Thereby σ represents the standard deviation of $\ln(r)$ and $\tilde{r}$ is such that of $\ln(\tilde{r})$ is the mean of this distribution [236]. Originally it was proposed by Levin [237] based on Kolmogorov's log-normal distribution [238].

c) Best's formula

In 1951 Best [239] provided, based on four different researchers fog data sources, with following formula:

$$1 - F = exp\,[-(\frac{x}{a})^n] \qquad (Eq.\ 21)$$

F is the fraction of liquid water in the air that contains droplets with a diameter smaller than$x$. a and n are constants that depend on the fog being considered. Parameters for different fogs with different mean diameters can be found in his publication [239].

The same characteristic values as for rain, such as D[1,0] or D[3,2], can be used for a comparison of the fog drop size distribution. Please refer to chapter 3.2.3 for further details.

4.2.3 LIQUID WATER CONTENT (LWC)

The amount of water in a fog is expressed by the Liquid Water Content (LWC) and expressed with the following equation according to [240]:

$$LWC = \int \frac{\pi * \rho_{water}}{6} * n(D) * D^3 dD \qquad [g/m^3] \qquad (Eq.\ 22)$$

The LWC is relevant for the fog density, this means that the higher the LWC, the lower the resulting visibility [226, 229]. According to literature, values between 0.01 and 0.1 g/m³ are typical for radiation fog and more than 0.2 g/m³ for advection fog [163, 173].

The literature offers several models that relate the LWC to the visual range. The VIS-LWC scheme, which is based on Koschmieder's law [215], can be expressed by the following equation:

$$VIS = \frac{ln\,(0.02)}{\beta_{ext}} = b * LWC^a \qquad (Eq.\ 23)$$

Here β_{ext} represents the extinction coefficient, while a and b are empirical constants. The empirical constants are highly dependent on the region and ambient temperatures [234, 241, 242]. According to Long [243], the K84 program is at present the most frequent used for VIS-LWC correlation. Muhammad [244] stated that as a general form for the relationship the following equation can be used:

$$VIS = b * LWC^{-2/3} \qquad (Eq.\ 24)$$

Thereby only the empirical parameter b is dependent for different fog conditions, which are listed in Table 22.

Table 22: Fog types and the values of coefficient b to estimate visibility range from LWC [244]

Fog type	b	Reference
Dense haze	0.013	Tampieri et. al [234]
Continental fog (dry and cold)	0.034	Tampieri et. al [234]
Maritime fog (wet and warm)	0.060	Tampieri et. al [234]
Dense haze and selective fog	0.017	Eldridge et. al [242]
Stable and evolving fog	0.024	Eldridge et. al [242]
Advection fog	0.02381	Koester et. al [245]

It should be noted that there are a number of alternative parameterisations for the parameters a and b, including those proposed by Gultepe [246] and Kunkel [247]. Furthermore, there are additional correlations between droplet concentration (N(d)) and the LWC, as well as between the LWC and the DSD or humidity. For further details, please refer to the summaries in [243] and [244].

4.2.4 Further attributes

In addition to the fog characterization parameters mentioned so far, the absolute number of drops N_{tot} can also be determined for each fog event.

$$N_{tot} = \int n(D) dD \qquad (Eq. 25)$$

Based on this, the mean droplet diameter D_{mean} can be calculated.

$$D_{mean} = \frac{\int n(d) * d \, dD}{N_{tot}} \qquad (Eq. 26)$$

Sometimes the ratio between N_{tot} and LWC [248, 249] or between humidity and LWC [250] is also used. Further rare used parameters as well as an own multi-factor approach are presented in [228].

4.3 MEASUREMENT DEVICES

Visibility can be determined either visually (estimation) or instrumentally (measurement). As the visual measurement is always a subjective assessment by a human observer and depends on the lighting conditions, the optical properties of the object, the background and the properties of the observer's eye, the visual measurement is not a reliable technique [99]. As visibility cannot be assessed directly from instruments, MOR is usually measured using visibility meters. Basically, the measuring devices can be divided into two groups of physical measured variables:

A) Transmission or extinction, the loss of light to turbidity particles in the air:

A transmitter and receiver are placed at a certain distance from each other, usually between 15 and 150 metres. Alternatively, the transmitter and receiver can be placed side by side if the light is deflected by a suitable mirror. The transmitter emits a light pulse, which is then detected by the receiver. Reflection, diffusion, and absorption effects on the particles in the air results in a partly extinction of the light pulse. The WMO recommends a (white) light source with a wide spectrum, as light sources with a narrow spectrum can lead to measurement errors [12]. By emitting modulated or pulsed light, the light is distinguished from daylight. The transmission is defined according to:

$$T = \frac{I}{I_0} \qquad \textit{(Eq. 27)}$$

Here T is the transmission, I_0 the light emitted and I the light received.

B) Scattering, the forward and backward scattering of turbidity particles in the air:

Similar to A), a light pulse is emitted by a transmitter. However, the receiver measures the scattered light, which is scattered by particles in a defined measurement volume. The lower the visibility, the more light is scattered, from which the MOR can be calculated. There are forwards, sideways and backwards scatterers, but they all work in the same way in principle. Forward and sideways scatter devices are usually summarised using the term forward scattering. A common scatter angle is 42° [251].

4.3.1 TRANSMISSOMETER

Transmissometers are often used in airports. Their advantage is a high accuracy [225]. Due to the large measurement distance, good spatial averaging is achieved, as there are smaller fluctuations in the measurement signal compared to visibility measurements based on scattering. Furthermore, the measuring principle is closest to the definition of MOR. Transmissometers are therefore still considered to be the highest quality of data source for visibility. One example of this is that up to this day, according to DIN CEN/TS 155518-4 [252] reference measurements with transmissometers are required for the approval of measuring or information devices for traffic and road condition monitoring systems. The downside of transmissometers is the high purchase price, often in excess of €50,000. Also a regular cleaning and maintenance is required which also increases the costs [12].

Table 23: Specifications of selected Transmissometer commercially available

Name	Manufacturer	MOR measurement range	MOR accuracy
TR30LED [253]	Degreane Horizon	10 m – 10 km (for 30 m base length; optimum)	Compliant with ICAO and WMO specifications
LT31 [254]	VAISALA	10 m – 10 km (for 30 m base length; optimum)	Exceeds the ICAO (Annex 3) recommendations

The accuracy of the devices is stated as better than the International Civil Aviation Organization (ICAO) regulation "Annex 3 to the Convention on International Civil Aviation - Meteorological Service for International Air Navigation" [255]. Here the visibility measurement requirement is specified as follows:

- ±50 m up to 600 m
- ±10 % between 600 – 1500 m
- ±20 % over 1500 m

Similarly, the WMO [12] and the British "CAP 746: Requirements for meteorological observations at aerodromes" [86] require the equal accuracy for visibility measurement systems.

4.3.2 Scatter sensors

Scatter sensors are available in different designs depending on the position of the receiver. Advantages are the lower price compared to transmissometers, the small size, ease of installation, little maintenance and relative calibration at any time [256]. A negative aspect is the lower accuracy due to the smaller sampling area, which can lead to fluctuations in the measurement. However, comparative measurements have shown that scattering sensors provide good agreement with transmissometers in terms of the accuracy of the measurement result, especially at low visibilities [99]. As a result, forward scatter meters are increasingly replacing transmissometers [256].
The following table shows a qualitative comparison between the different technologies.

Table 24: Ranking of different MOR measurement techniques. (1 = Best, 3 = Worst) [251]

	Transmission	Forward scatter	Backscatter
Sensitivity	1	1	3
Correctness	1	2	3
Compactness	3	2	1
Price	3	2	1

Due to their characteristics, only transmissometers and forward scatter meters are approved by the ICAO to measure runway visibility at airports [257].

Table 25: Specifications of selected Scatter Sensors commercially available

Name	Manufacturer	MOR measurement range	MOR accuracy
DF320 [258]	Degreane Horizon	5 m – 70 km	±10 % for 90 % of measurements up to 5 km ±15 % for 90 % of measurements from 5 – 20 km ±25 % above
TP320 [259]	Degreane Horizon	5 m – 70 km	±10 % for 90 % of measurements up to 5 km ±15 % for 90 % of measurements from 5 – 20 km ±25 % above
ONES 250 [260]	Eigenbrodt	20 m – 10 km	
MiniOFS [261]	OpticalSensors	20 m – 4 km	
SWSxxx-N-AC [262]	Orga	10 m – 75 km	MOR ~10 km: Better than 10 % MOR ~20 km: Better than 15 % MOR ~30 km: Better than 20 %
VISIC620 [263]	Sick	10 m – 16 km	±5 m for visibilities below 50 m ±10 % for visibilities below 5 km ±20 % for visibilities below 16 km
FS11 [264]	VAISALA	5 m – 75 km	±10 % for range 5 m – 10 km ±20 % for range 10 km – 75 km
FD70 [131]	VAISALA	1 m – 100 km	±10 % or ±1 m for range 1 m – 10 km ±20 % for range 10 km – 100 km
PWD1x & PWD2x [132]	VAISALA	PWD1x: 10 m – 2 km PWD2x: 10 m – 20 km	±10 % for range 1 m – 10 km ±20 % for range 10 km – 20 km

It should be noted for all devices that the measurement results are usually averaged over a certain period of time in order to compensate for variations. The visibility is usually averaged between 30 seconds and 10 minutes, preferably over a period of 1 minute [12, 86].

4.3.3 DSD

To measure the droplet size distribution of fog, special instruments are required to detect the small and numerous particles. The systems measure by analysing the forward scattered light. Due to the wide size range of fog droplets, some instruments have special filters to detect only certain sub-ranges, making them more accurate than instruments that measure across the entire size spectrum. A selection of available measuring devices is shown in Table 26.

Table 26: Specifications of selected fog DSD measurement devices commercially available

Name	Manufacturer	Measuring range (number of particles)	Measuring range (size)	Sample flow volume
Aerosol sensors welas® 2000 System [265]	Palas	Type 2070: up to 1,000,000 particles / cm^3 Type 2100: up to 500,000 particles / cm^3 Type 2300: up to 40,000 particles / cm^3	Available: 0,2 – 10 µm 0,3 – 17 µm 0,6 – 40 µm.	0,005 m^3/min
FM-120 [266]	Droplet Measurement Technologies		2 – 50 µm	1 m^3/min

4.4 OCCURRENCE OF FOG EVENTS

The occurrence of fog events will be analysed in the following section. In addition to studies from the literature, visibility data from the DWD measurement network will be analysed. This is intended to answer the following questions:

- To determine the frequency of dense fog and low visibilities.
- Their distribution of dense fog events within a year (dependency on the seasons)
- Their distribution of dense fog events within a day (dependency of the time of the day)

4.4.1.1 Europe

An overview of the annual frequency of days with low visibility (< 5 km) at various European measurement sites can be found in a study from Vautard [267] and is shown in Figure 27. For this purpose, data from 342 measuring stations from 1978-2006 were analysed at four discrete time points per day (03, 09, 15, and 21 h). Furthermore, the annual number of days with completely cloudy skies is presented.

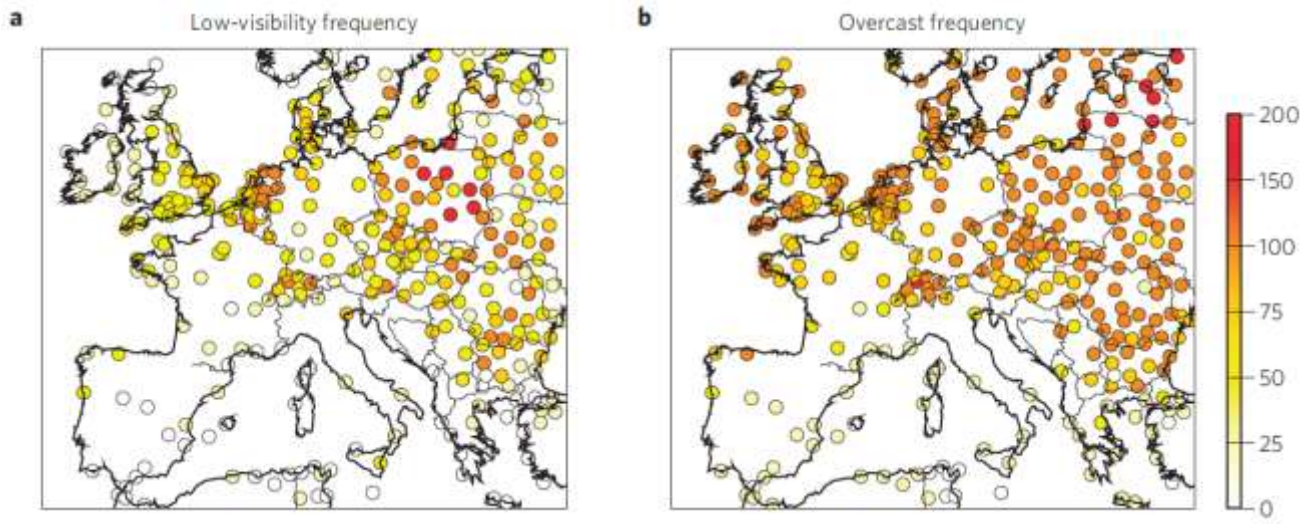

Figure 27: Annual frequency of (a)days with low visibility (<5 km)and (b) overcast days [267]

In general, low visibilities are most prevalent in the northern and eastern regions of Europe. Additionally, they occur with greater frequency in certain coastal areas, including the English Channel, the North Sea, and the Baltic Sea. Furthermore, they are observed with greater regularity in mountainous regions, such as the Alps. A similar pattern is revealed by the analysis of Vajda [157] performed an analysis of hourly visibility on 24 European airports in the timespan from 2000 till 2009 and displayed in Figure 28.

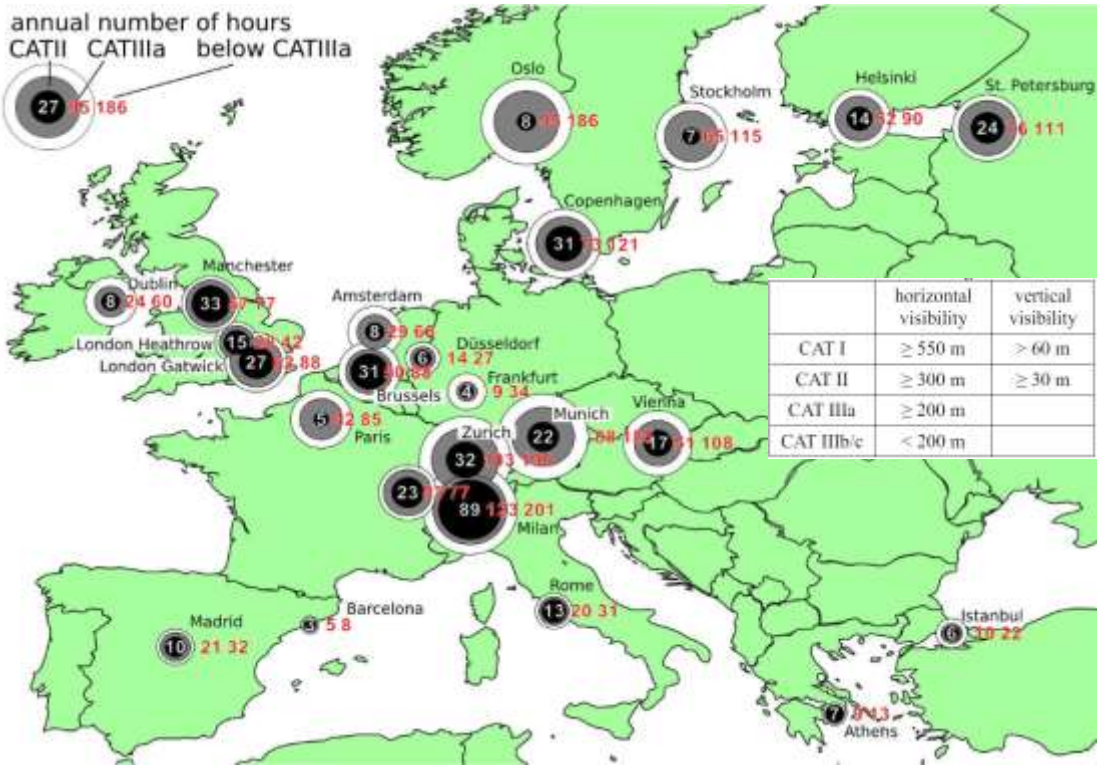

Figure 28: Annual number of hours that CATII (a.), CATIIIa (b.) and CATIIIb/c (c.) conditions occurred at selected major European airports during the period 2000-2009 [157]

A further analysis from van Oldenborgh [268] on the same data base from [267], specifically for very low visibility (less than 200 meters and less than 2 kilometres), is presented in Figure 29.

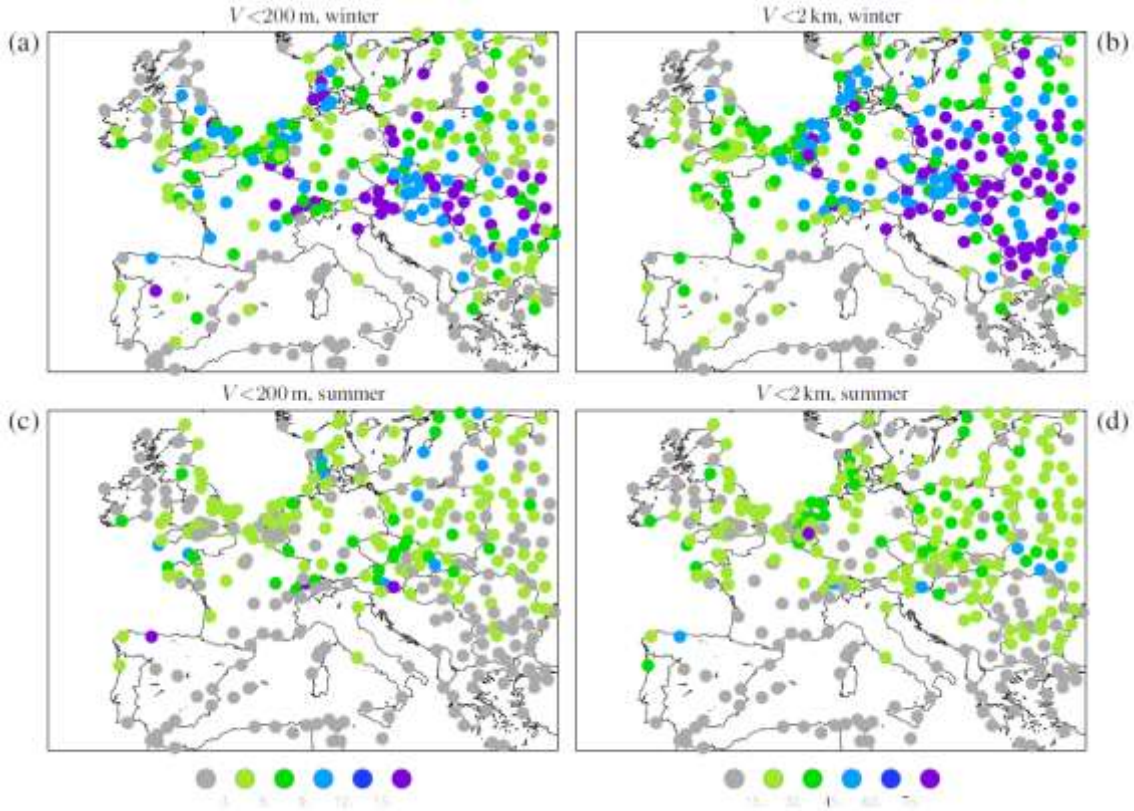

Figure 29: Mean number of days per half year with low visibility over 1976–2006 in winter (a) and (b) October–March, and summer (c) and (d) April–September. In (a) and (c) the number of days with dense fog (visibility less than 200 m) is shown, in (b) and (d) the number of days with visibility less than 2 km [268]

The bi-annual analysis indicates that fog events occur with greater frequency during the winter months. The observation that fog events are relatively uncommon in southern Europe and the north of the UK is consistent regardless of the time of year. There are numerous further country and location-specific studies regarding the occurrence fog. Since their tendency is largely similar to the results already presented here, we will only refer to these publications [203, 269–280]. Egli [281] analysed satellite data from Europe on the occurrence of fog (Vis < 1 km) in order to identify a trend in the occurrence of fog with regard to the month and time of day, as shown in Figure 30.

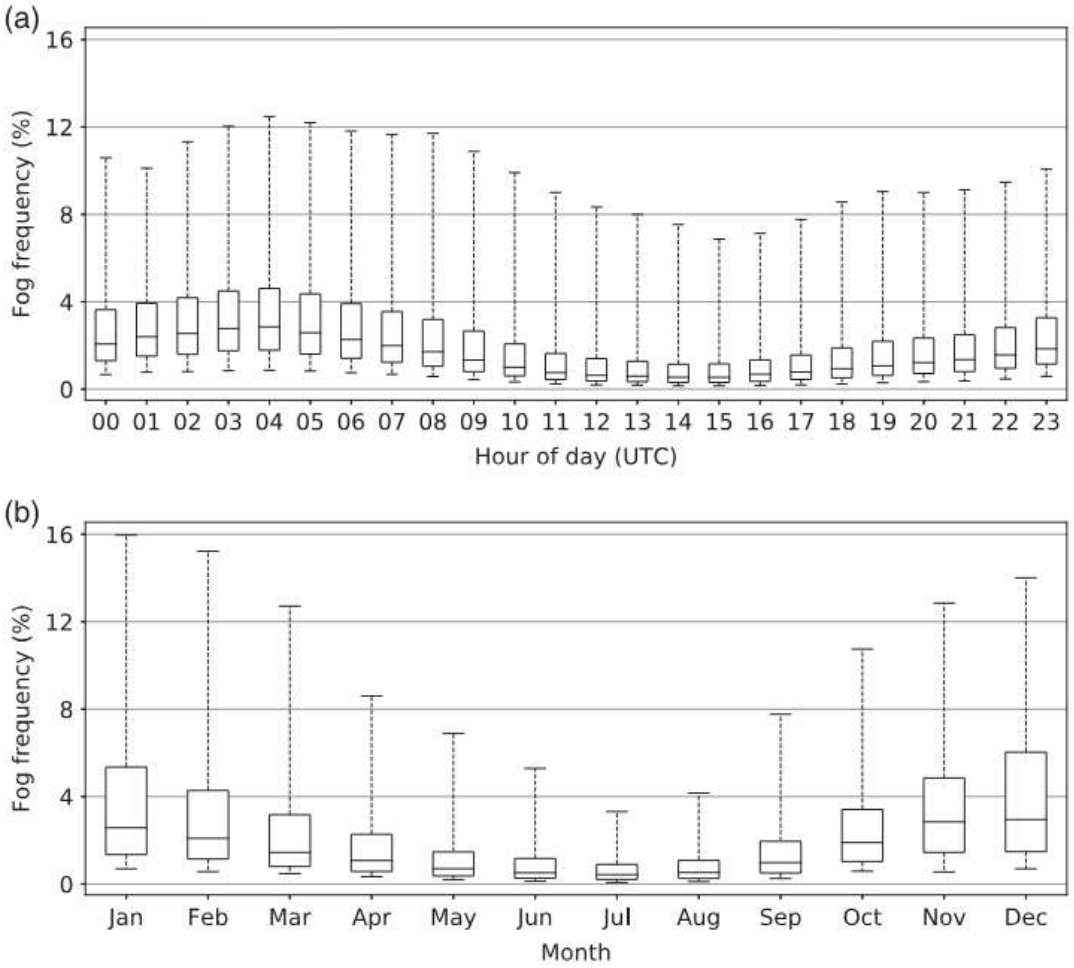

Figure 30: Fog frequency changes over (a) a day and (b) a year. Values are taken from each land pixel in the fog dataset averaged over the complete ten-year [281]

The figure illustrates that fog is most prevalent at night and in the early hours of the morning. It also demonstrates the frequency of foggy days in winter.
Furthermore, other studies show that fog occurs less frequently in inner-city areas than in non-urban regions, which is due to the higher average temperature in cities [179, 282]. Hůnová [283] used measurement data in Romania to investigate a higher incidence of fog near freshwater in the winter half-year and near seawater mainly in the summer half-year. He also determined that the frequency of fog depends on the altitude of the location above sea level [284, 285]. The higher the altitude, the greater the probability of fog. Furthermore, he describes the decrease of the effect that fog occurs mainly in the winter months with increasing altitude above sea level. From an altitude of 1400 m, the occurrence was evenly distributed over all seasons in visibility measurement data from Romania (1981-2017). With further increase of the altitude, there is even a slight reversal of the behaviour.

Some studies have also documented a change in the frequency of fog days over several years or decades. Figure 31 illustrates a temporal trend in the number of annual fog days over a 30-year period, based on the dataset from Vautard [267] von Oldenborgh and [268]. Figure 32 and is from the analysis of Vajda [157], who analysed the sum of hours with dense fog conditions (V < 200 m).

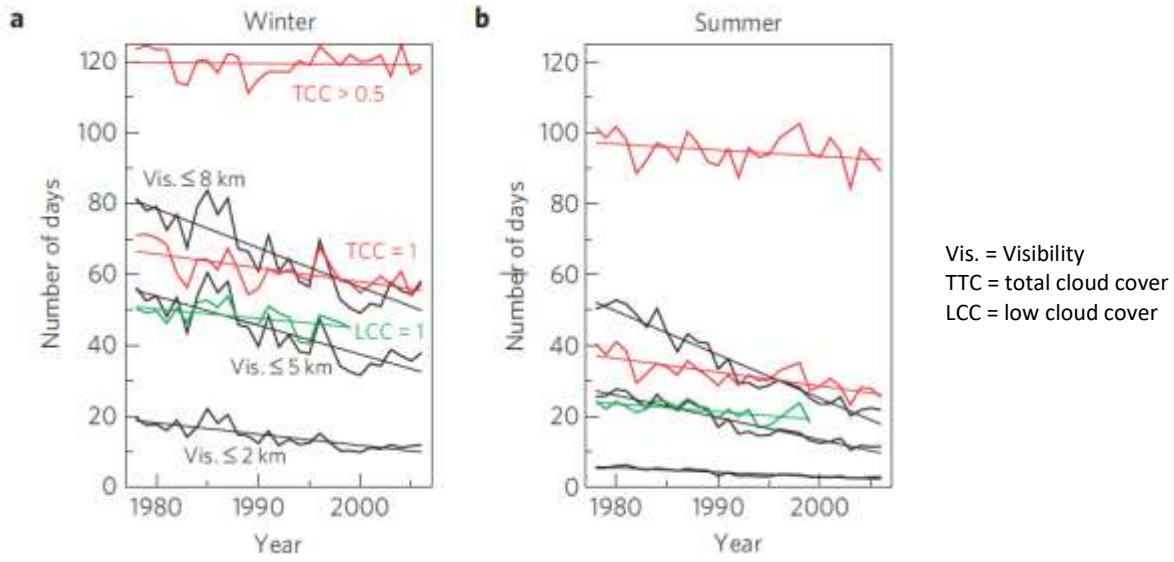

Figure 31: Annual number of days with low visibility in (a) winter and (b) summer [267]

A clear decline in the number of days with low visibility has been observed between 1978 and 2006. Since the 2000s, a flattening of this trend can be observed. The noted decrease in fog days correlates with an improvement in air quality in Europe during this period. As the air quality in Europe has already reached a high level, the authors predict a further flattening and no further sharp decrease in the number of days with low visibility [267]. Also the land-use changes and urbanization might also have played a role, due to the fact that fog appears rarer in cities [268, 282].

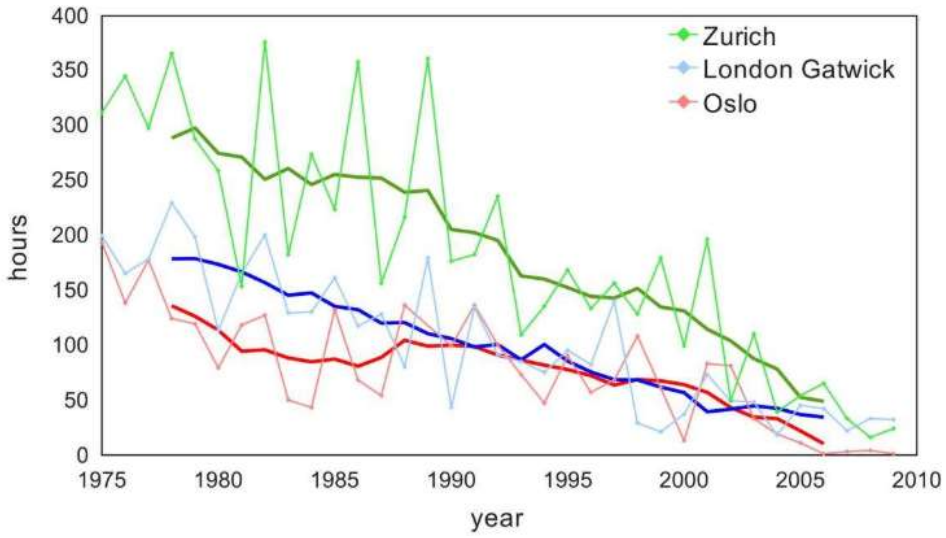

Figure 32: Annual numbers of hours with visibility <200 m at the airports of Zurich (green), London Gatwick (blue) and Oslo (red). Thin lines represent annual totals; thick lines are 7-year moving averages [157]

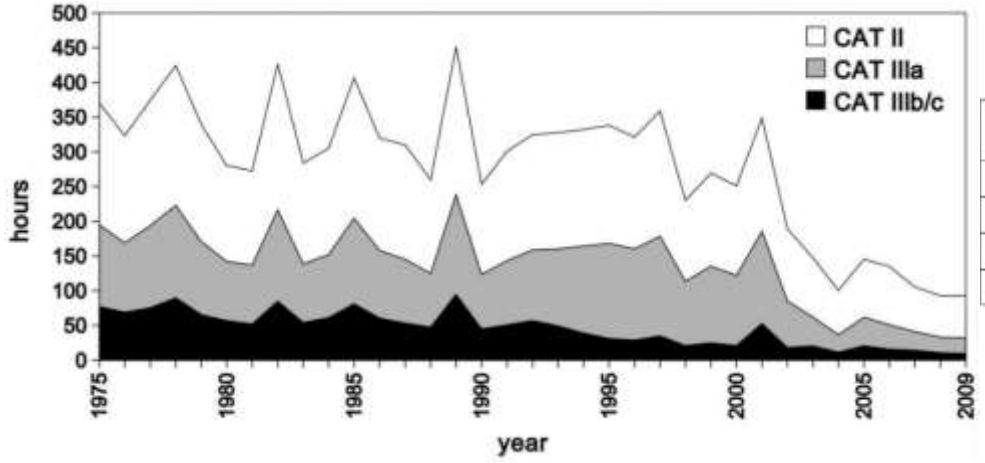

	horizontal visibility
CAT I	≥ 550 m
CAT II	≥ 300 m
CAT IIIa	≥ 200 m
CAT IIIb/c	< 200 m

Figure 33: Annual numbers of hours with particular visibility conditions averaged over the 24 analysed airports [157]

A comparable pattern can be observed in the data from measuring stations at airports. However, the authors note that although visibility below 200 meters only occurred for 10 hours in 2009 in Oslo, visibility between 200 and 500 meters was still present for 121 hours. A comparable situation can be observed at other airports that periods of low visibility have become rarer but do still occur [157]. Thus, on average, more than 100 hours with visibility of less than 550 m were observed in 2009, which equates to more than four complete days per year spent under such conditions.

4.4.1.2 In-depth analysis of German weather data

Since previous publications have not analysed fog data in the scope of automotive needs or have only used rough satellite data, an analysis of highly local fog data from numerous weather stations in Germany from the past 15 years is presented below. Due to the trend in the literature towards a sharp decrease in fog days between 1980 and 2000, this also ensures that the outcome of this study is up to date.
The same DWD database is used as in Chapter 3.5.3.3. Visibility measurements are available in this database in the smallest interval step every hour. Due to the large number of available measurement stations, a selection of 10 analysed stations is selected. It is the objective of this selection to ensure that it is as representative as possible and cover all geographical regions across the country. As far as possible, the same measuring stations are used as for analysing the precipitation events. If no measurement data on visibility was available from these stations or if a lot of data was missing in the period analysed, nearby measuring stations are selected as a substitute. Further details, including geographical information and a list of the analysed stations, can be found in Figure 34 and Table 27.

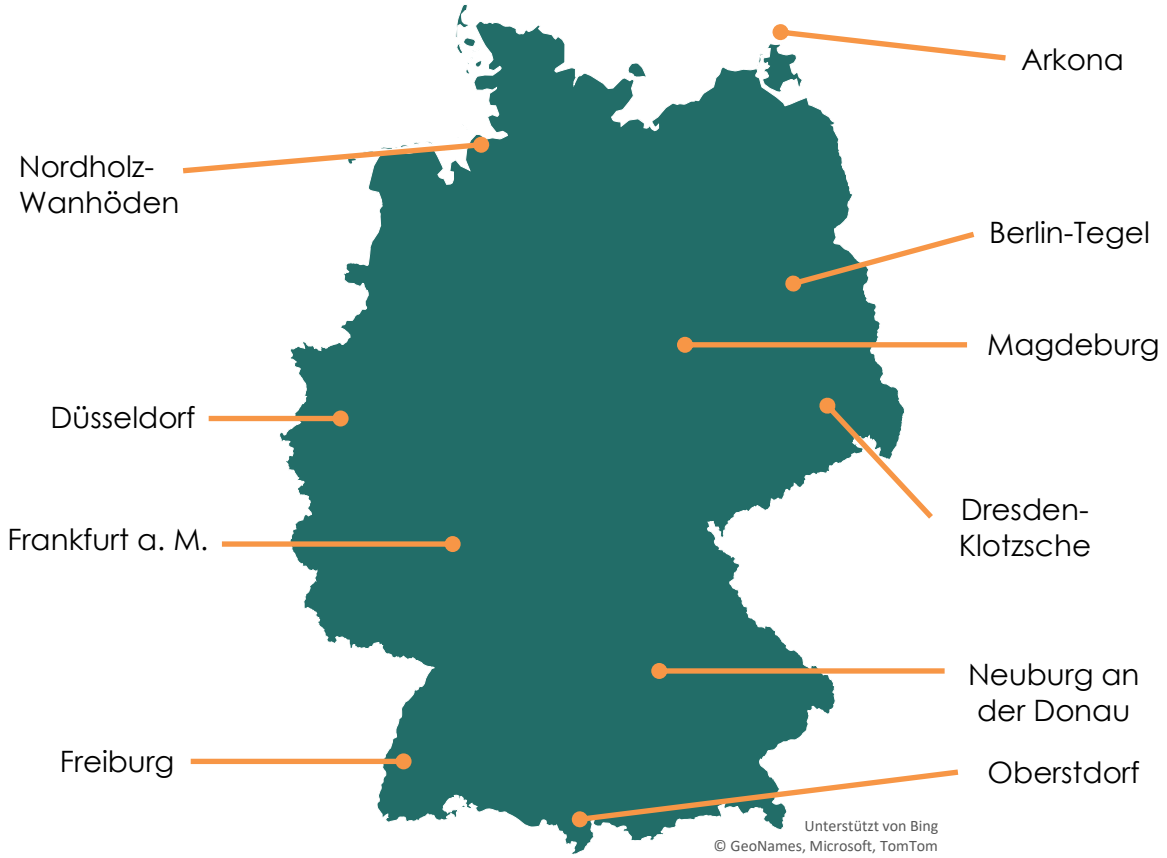

Figure 34: Selected weather stations

Table 27: Location data of the selected weather stations

Station name	Station ID	Station altitude	Latitude	Longitude
Arkona	00183	42 m	54.6791	13.4344
Berlin-Tegel	00430	36 m	52.5644	13.3088
Dresden-Klotzsche	01048	228 m	51.1278	13.7543
Düsseldorf	01078	37 m	51.2960	6.7686
Frankfurt a. M.	01420	100 m	50.0259	8.5213
Freiburg	01443	237 m	48.0232	7.8343
Magdeburg	03126	79 m	52.1029	11.5827
Neuburg an der Donau	03484	380 m	48.7085	11.2147
Nordholz-Wanhöden	03639	26 m	53.7647	8.6584
Oberstdorf	03730	806 m	47.3984	10.2759

The data set encompasses a 15-year period, from 1 January 2009 to 31 December 2023. Across all stations, the mean availability of visibility data is 97.4 % over the entire period.
A basic overview of the frequency of fog events (visibility <1 km) and turbid visibility (10 km > x > 1 km) is presented in Figure 35.

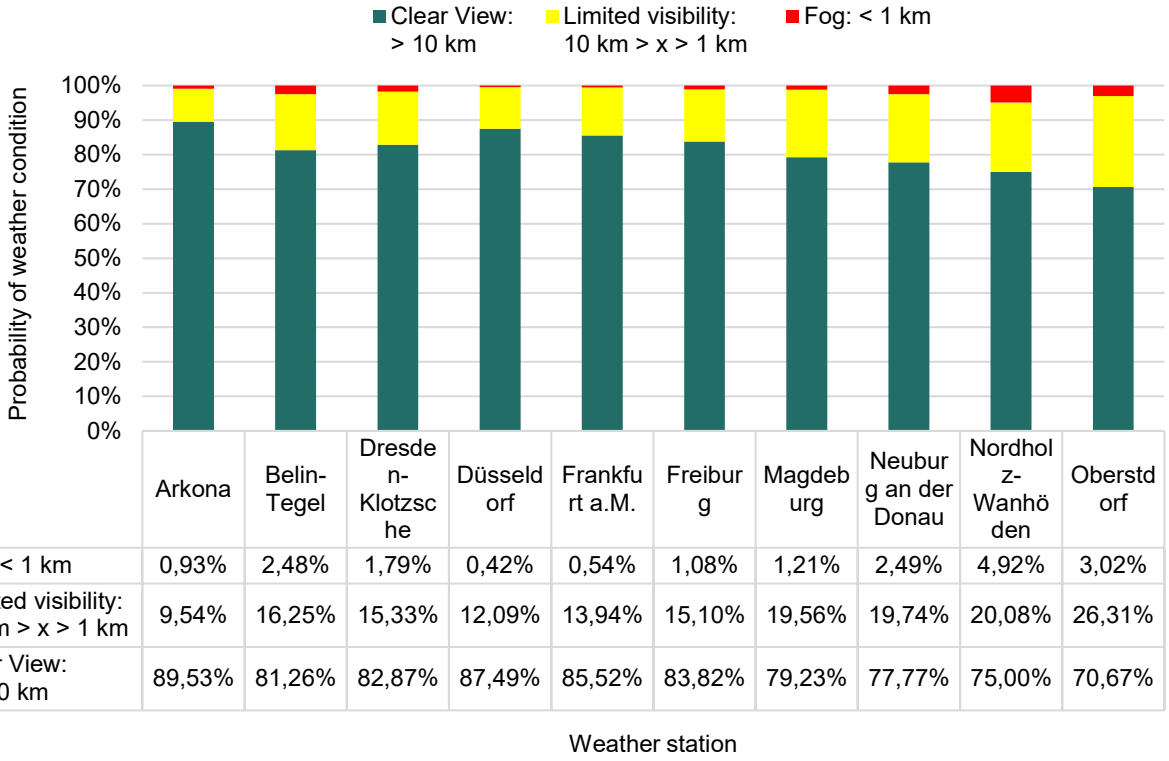

	Arkona	Belin-Tegel	Dresden-Klotzsche	Düsseldorf	Frankfurt a.M.	Freiburg	Magdeburg	Neuburg an der Donau	Nordholz-Wanhöden	Oberstdorf
Fog: < 1 km	0,93%	2,48%	1,79%	0,42%	0,54%	1,08%	1,21%	2,49%	4,92%	3,02%
Limited visibility: 10 km > x > 1 km	9,54%	16,25%	15,33%	12,09%	13,94%	15,10%	19,56%	19,74%	20,08%	26,31%
Clear View: > 10 km	89,53%	81,26%	82,87%	87,49%	85,52%	83,82%	79,23%	77,77%	75,00%	70,67%

Figure 35: Distribution of the measured visual ranges during the analysed period (2009-2023)

On the one hand, the limit level of 1 km was taken from the definition of fog. On the other hand, non-turbid / clear visibility is generally assumed above 10 km, hence this value was used for the second step. Figure 36 and Figure 37 shows the occurrence frequency of fog visibilities.

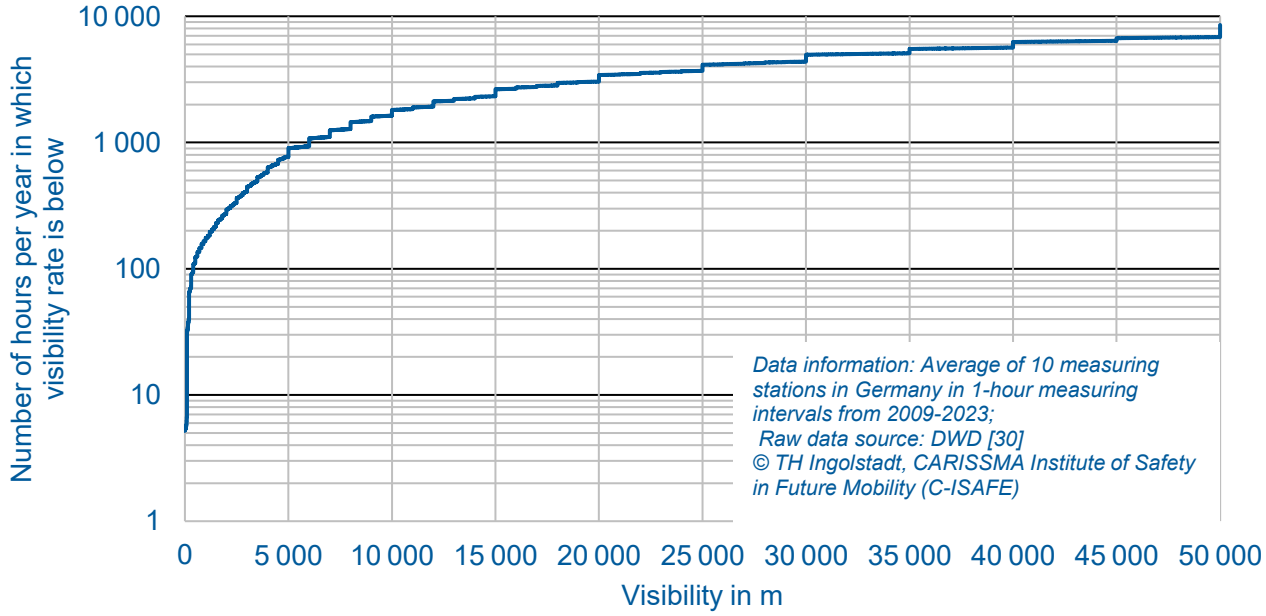

Figure 36: Occurrence frequency of fog events

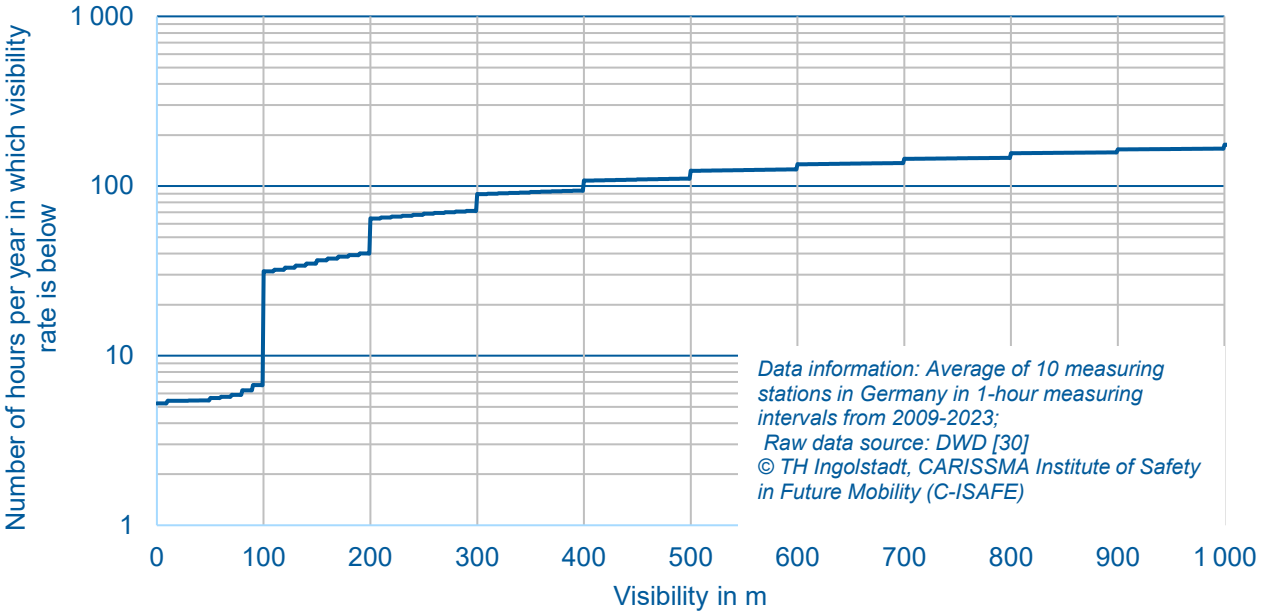

Figure 37: Occurrence frequency of fog events (cutted)

It can be seen that there is little data available for the visibility range below 100m, or that the instruments are often unable to resolve this sufficiently. For example, the device in Oberstdorf seems to only output visibility in 100 m increments, whereas Magdeburg, for example, outputs in 10 m increments. This results in larger jumps in the low visibility range, due to the logarithmic scale. The data indicates that low fog visibility is more dependent on local position than is the case with rain. Of the ten measurement stations analysed, fog is most prevalent on the north-west coast of Germany (Nordholz-Wanhöden), with the least occurrence in Frankfurt am Main and Düsseldorf. The presence of a river in the vicinity of a measurement station, such as the Danube in Neuburg, is associated with an elevated frequency of fog.

The frequency of fog events split by month is shown in Figure 38.

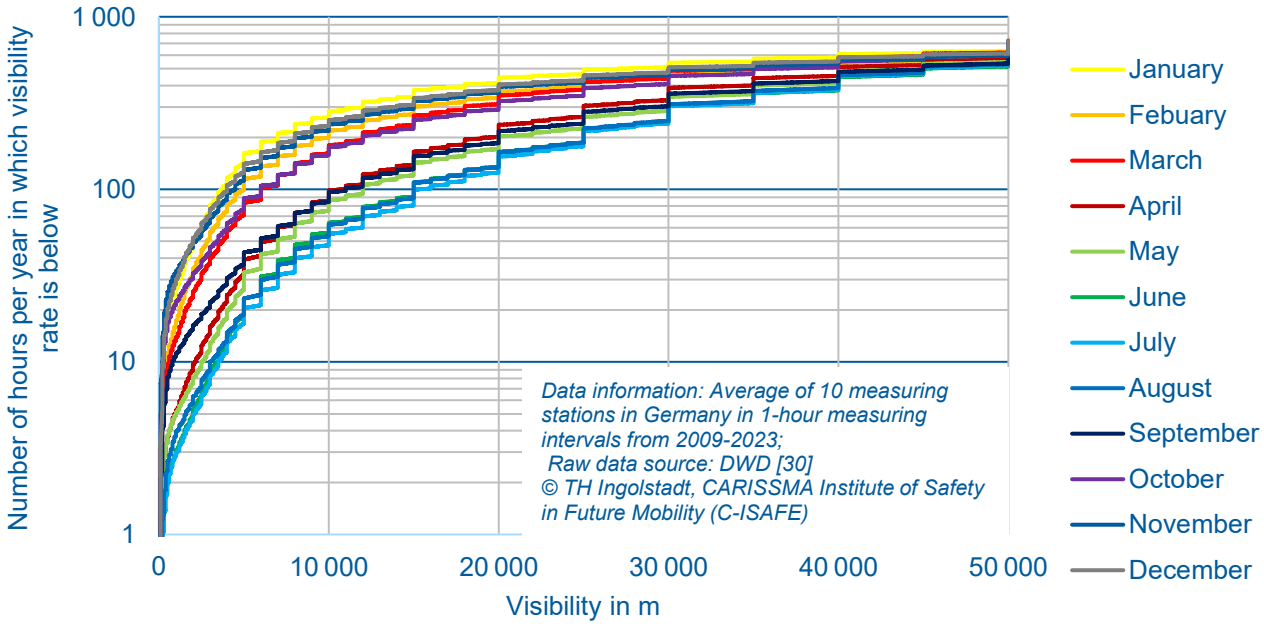

Figure 38: Monthly mean statistically occurrence frequency of fog events

The data indicates that fog and low visibility are most prevalent at the weather stations in Germany during the winter months (October to December). Conversely, fog is least frequent during the summer months. This trend is similar for all analysed stations. This result is corroborated by its resemblance to previous analyses of the annual distribution of fog occurrence.
An analysis of the influence of the time of day on the occurrence of fog is shown in Figure 39.

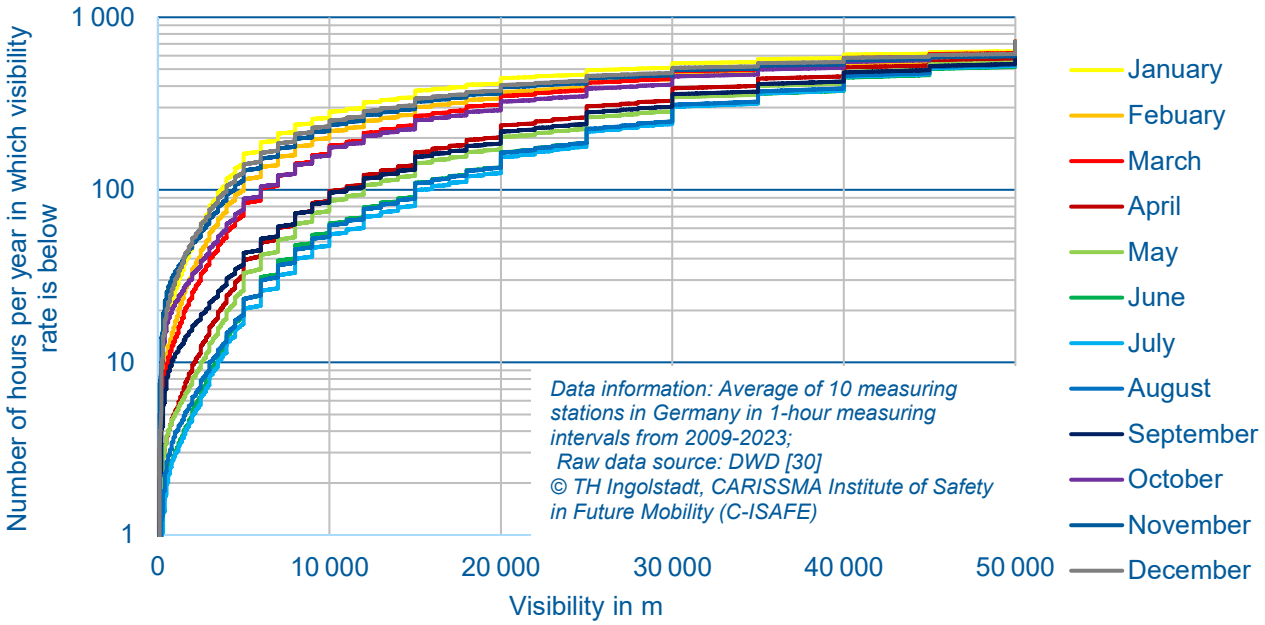

Figure 39: Mean statistically occurrence frequency of fog events categorized by time

Fog is observed most frequently at the analysed measuring stations at night and early in the morning. This is in accordance with theoretical findings on fog formation. The results agree very well with the analyses of fog from satellite data in Figure 30.

4.5 FOG CLASSIFICATION

In Europe, low visibility is typically attributed to moisture particles in the air. Solid suspended particles, such as sand dust or smoke, are less prevalent in Europe. Consequently, a test case should focus on moisture mist or fog. Therefore, fog events can be classified according to their visibility according to the following recommendation:

Table 28: Fog classification

Type	Range
Clear view	Visibility > 10 km
Mist	Visibility between 10 km and 1000 m
Moderate fog	Precipitation rate between 1000 m and 500 m
Dense fog	Visibility between 500 m and 100 m
Very dense fog	Visibility between 100 m and 10 m
Extreme fog	Visibility < 10 m

Due to the occurrence of fog in Europe, it is recommended that tests cover the range of moderate fog, dense fog and, if required , for critical applications very dense fog with a continental DSD.
In order to obtain an accurate measurement characterization, it is essential to determine the visibility with a sensor that measures based on the forward scatter or transmission concept. Furthermore, it is recommended that the droplet sizes be determined as well.

5. Glare

5.1 FUNDAMENTALS

For the sake of clarity, the relevant terms regarding glare are first defined and distinguished from one another below:

Luminous Flux Φ — *"How much light does the source emit in total?"*

- Definition: The luminous flux Φ describes the total visible light output emitted by a light source, regardless of direction, distance, or area.
- Unit: Φ [*lm*] *(Lumen)*
- Formula: $\Phi = \int_{\Omega} I\,(\theta, \varphi)\,\mathrm{d}\Omega$
  I… Luminous intensity in one direction
  Ω… solid angle
  Integration across all directions
- Example: Data sheet information for lamps: "How much light does the source generate in total?"

Light Intensity I — *"How much in one direction?"*

- Definition: Luminous intensity I is the luminous flux per solid angle in a specific direction.
- Unit: $I\ [cd] = \frac{lm}{sr}$
- Formula: $I = \frac{\mathrm{d}\Phi}{\mathrm{d}\Omega}$
- Example: Rated directivity (crucial for headlights, spotlights, or glare from point sources such as the sun)

Illuminance E — *"How much light reaches the target?"*

- Definition: Illuminance E describes how much light reaches a surface.
- Unit: $E\ [lx] \quad (Lux) \quad = \frac{lm}{m^2}$
- Formula (area-related): $E = \frac{\Phi}{A}$
- Physically correct (point source): $E = \frac{I}{r^2}\ \cos\theta$
  I… Luminous intensity of the source
  r… Distance to surface
  θ… Angle of incidence (oblique radiation → less light per surface area)
- Example: Workplace lighting, street lighting, sensor radiation (but not perception!)

Luminance L — *"How bright does it appear?"*

- Definition: Luminance L describes the perceived brightness of a luminous surface.
- Unit: $L\ [cd/m^2]$
- Formula: $L = \frac{\mathrm{d}I}{\mathrm{d}A\cos\theta}$
- Direction-dependent, but Distance-independent!
- Example: Light intensity per visible area

5.2 CHARACTERISTICS OF GLARE

Glare is a visual phenomenon caused by intense and uncontrolled light. The Illuminating Engineering Society (IES) defines glare as a phenomenon caused by either one or both of the following conditions [286]:

1. Excessive contrast
   a. The range of light in the field of view is too great.

   b. The difference between the background illumination and the light source is too great.
2. Excessive illumination
   a. The lumen count of the light source exceeds the observer's threshold.

A widely accepted method of measuring glare is to calculate the "Unified Glare Rating" (UGR). This unit has been used by the International Commission on Illimitation (CIE) since 1995 but was originally introduced by Sorensen in 1987 [287]. The unit UGR is as the name suggests a unit representing glare. The higher the value, the more intense the glare is. UGR sums up all the light sources in the observer's (eye, camera, lidar, etc) view.
The different light sources in the sake of WEATHERSAFE can be sun light, the beams of an oncoming vehicle and other lights sources. The UGR also considers the intensity of the light source, the angle to the observer as well as the background illumination (an important component in contrast) [288].

The UGR is calculated as followed [289]: $\mathrm{UGR} = 8log\frac{0,25}{L_b}\sum_n(L_n^2\frac{\omega_n}{p_n^2})$

Where log is the common logarithm (base 10), L_n is the luminance of each light source numbered n, ω_n is the solid angle of the light source seen form the observer and p_n is the Guth position index which is derived from the distance of the line of sight of the observer (in the automotive case, a sensor such as a camera or LiDAR).

5.3 DIFFERENT TYPES OF GLARES

Glare is a light-based phenomenon. Although, there are different types of glare created by different circumstances [290].

a) Direct Glare [291]

Source: Direct glare originates from direct and bright light sources such as the sun, vehicle headlights, streetlights or other artificial light sources like stadium lights.

Creation: When an intense light source is directly within the line of sight, it can overpower the observer (visual system, sensors or eye) leading to reduced visibility and discomfort. The intensity and angle of the light source are critical factors. This relates to the UGR (Unified Glare Rating) mentioned above.

b) Reflected Glare [291]

Source: Reflected glare occurs when light reflects off smooth, shiny surfaces such as water, glass, snow or metal.

Creation: Incident light hits a reflective surface and bounces back, with the possibility of concentrating the light and increasing its intensity. The nature of the reflective surface (its smoothness orientation) significantly influences the severity of the glare produced.

c) Diffuse Glare [292]

Source: Diffuse glare comes from light scattering in all directions due to interaction with particles or uneven surfaces.

Creation: This phenomenon occurs when light passes through or reflects off surfaces with irregular textures or with particles in the atmosphere like fog, rain or dust. The scattered light reduces contrast and clarity by creating a more uniformly bright environment.

d) Specular Glare [292]

Source: Originates from specular reflections, where light reflects off a surface at as single angle, like how light reflects of a mirror.

Creation: A close to perfect reflection from surfaces such as mirrors, water, or glossy car hoods can produce intense glare. The angle of incidence equals the angle of reflection, causing a focused and possibly blinding reflection both in terms of sensors and eyes.

5.4 EXTERNAL FACTORS INFLUENCING GLARE

a) Light source characteristics:

- **Intensity:** Brighter light sources are more likely to cause glare. High-intensity sources such as the sun or high-beam headlights may often be the reason for glare.
- **Color temperature:** Light sources with higher color temperatures (e.g., blue-wight light (like xenon headlights)) can be more glaring compared to warmer yellowish light (halogen headlights).

b) Surface properties:

- **Reflectivity:** Highly reflective surfaces, such as glass or polished metal, can create strong glare when light reflects off them.
- **Texture:** Smooth surfaces create specular reflections, while rough surfaces scatter light resulting in diffuse glare.

c) Environmental conditions:

- **Atmospheric/meteorological conditions:** Fog, mist, rain and dust in the air can scatter light, leading to diffuse glare.
- **Sun position:** The angle of the sun, especially during sunrise and sunset can create intense direct and reflected glare. Also worth noting is how the color temperature changes during the day. The more blue-wight light is more prevalent at midday compared to sunrise/sunset.

d) Geometry and angles:

- **Angle of incidence:** The angle at which light strikes a surface affects the intensity and direction of glare. Shallow angles often result in more pronounced reflections.
- **Observer's position:** While the focus here is on the source, the position of the observer relative to the light source and reflective surfaces can affect how glare is perceived and its intensity.

5.5 SUN GLARE

One of the most common sources of glare is from the sun. There are two main factors to consider: the brightness of the entire scene caused by the sunlight and the glare when looking directly towards the sun. The latter is particularly relevant when looking or driving eastwards at sunrise and westwards at sunset. The exposure of a whole scene to sunlight can be defined by illuminance (lx). Luminance (cd/m^2) can be used to describe the brightness of the sun's body itself. Figure 40 shows a typical sunlight spectrum with and without atmospheric effects.

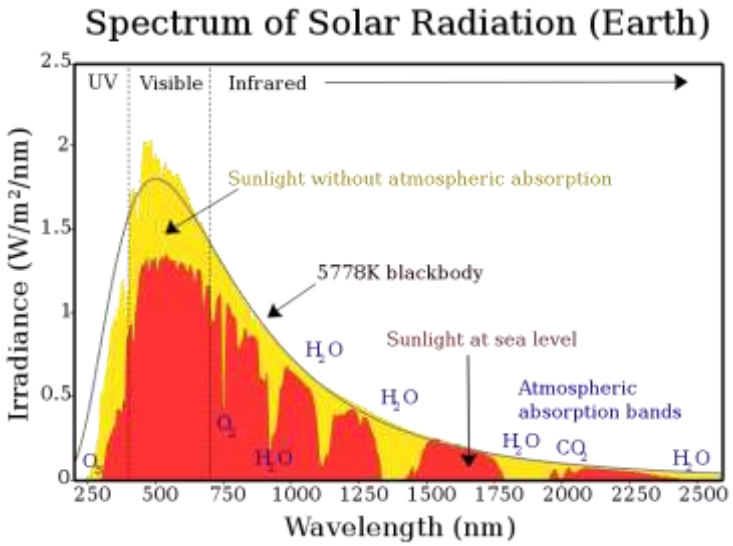

Figure 40: Solar radiation spectrum for direct light at both the top of the Earth's atmosphere (represented by the area in yellow) and at sea level (area in red) [293]

Depending on the time of day, both the spectrum and intensity of solar radiation reaching the Earth's surface change. Cloud cover also has an influence, as shown in Figure 41.

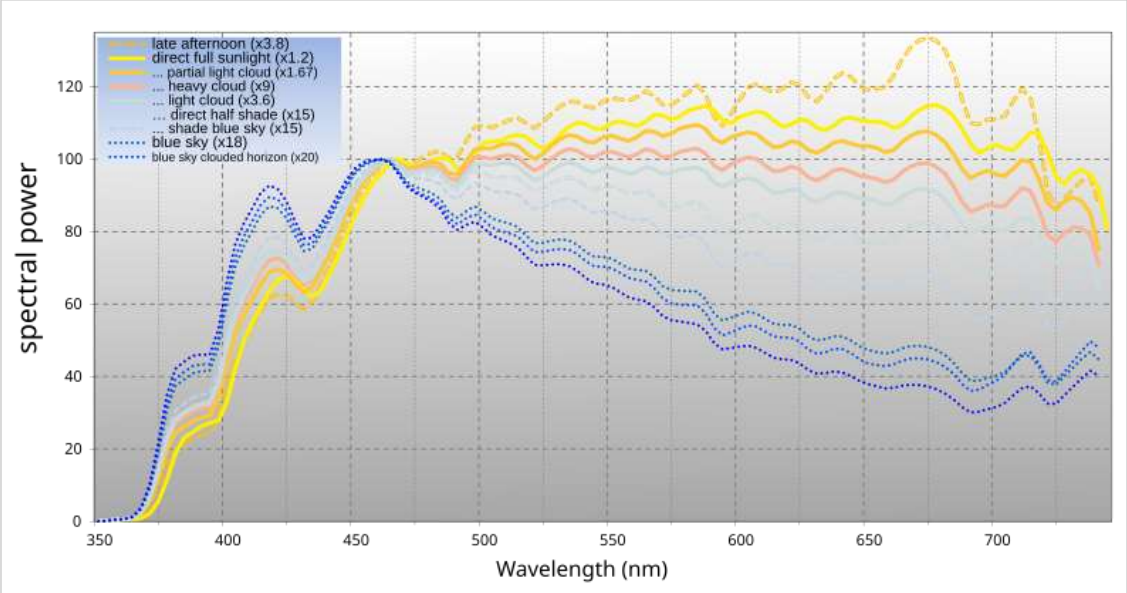

Figure 41: Spectrum of the visible wavelengths at approximately sea level. Illumination by direct sunlight compared with direct sunlight scattered by cloud cover and with indirect sunlight by varying degrees of cloud cover. The yellow line shows the power spectrum of direct sunlight under optimal conditions. To aid comparison, the other illumination conditions are scaled by the factor shown in the key so they match at about 470 nm (blue light) [294]

Furthermore, the distribution of the visible spectrum can be expressed in terms of correlated colour temperature (K). A summary of typical colour temperatures and horizontal illuminance can be found in Table 29.

Table 29: Typical values for colour temperature and horizontal illuminance depending on the time of day and sky conditions

	Correlated colour temperature (K) of the sun disk	Horizontal Illuminance on ground (lux)
Sunrise / Sunset	2,000 K – 3,000 K	400 – 900 lx
Morning / Afternoon	4,000 K – 5,000 K	25,000 – 80,000 lx
Noon Sun (clear sky)	5,500 K – 5,800 K	100,000 – 120,000 lx
Overcast Sky / Shade	6,500 K – 7,500 K	1,000 – 20,000 lx

A clear dependence of the correlated colour temperature and illuminance on the solar elevation angle can be observed. The global radiation reaching the Earth's surface is a composite of two primary sources: direct solar radiation and diffuse sky radiation (scattered by the atmosphere). These sources possess vastly different spectral characteristics. While the direct solar disk at low elevations exhibits a low correlated colour temperature (reddish-orange), the light scattered by the atmosphere maintains an extremely high correlated colour temperature ($> 10{,}000\ K$). This phenomenon is primarily driven by Rayleigh scattering whereby atmospheric molecules scatter shorter blue wavelengths much more efficiently than longer red ones. At very low solar angles, the direct radiation is so heavily attenuated that the diffuse blue light dominates the global mix. This results in a composite correlated colour temperature on the ground that is significantly higher than the temperature of the solar disk itself. Note, that given the average angular diameter of the solar disk is approximately $0.53°$ the sun's limb begins to break the horizon at an elevation of $-0.26°$ (accounting for geometric centre).
From a traffic safety perspective, the range of solar elevation between 3° and 10° is considered particularly critical. At these angles, the sun is usually below the cut-off angle of standard vehicle sun visors, yet high enough to bypass environmental obstructions such as buildings or vegetation. Consequently, drivers and sensors exposed to glare that is so bright it temporarily blinds them, with luminance values exceeding 10^7 cd/m², which significantly impairs visual contrast and thus reaction times.

5.6 DIFFERENT TYPES OF AUTOMOTIVE GLARE

Especially interesting from an automotive perspective, glare can be caused by the headlights of oncoming cars. There are multiple types of headlights used on the road which my interfere with different automotive sensors differently.
The most common headlight types out on the road are Xenon, Halogen and LED lights. Laser headlights might join the list of frequently used headlights later down the line.
Different headlights produce drastically different intensity wavelength outputs.

a) Xenon

Xenon headlights (also known as HID (High Intensity Discharge) lights work by emitting an electric current through a xenon-gas filled bulb which allows the bulb to emit light. A xenon bulb has an average output of about 3500 lumens. The following image illustrates the output profile of a xenon lightbulb.

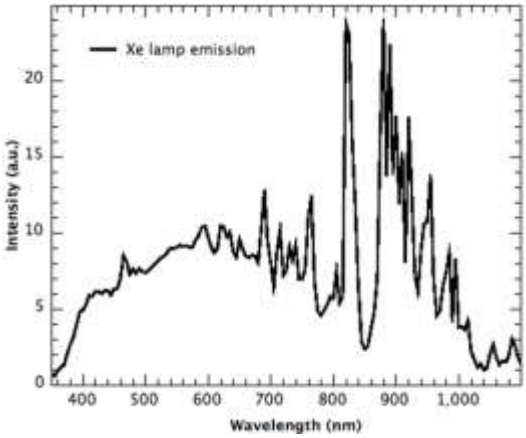

Figure 42: Xenon lamp spectrum [295]

b) Halogen

Halogen lights utilize a combination of gasses such as nitrogen, argon and tungsten filament in a glass tube. A halogen bulb produces around 700 lumens on the low beam, and 1200 on the high beam. The following image illustrates the output profile of a halogen lightbulb.

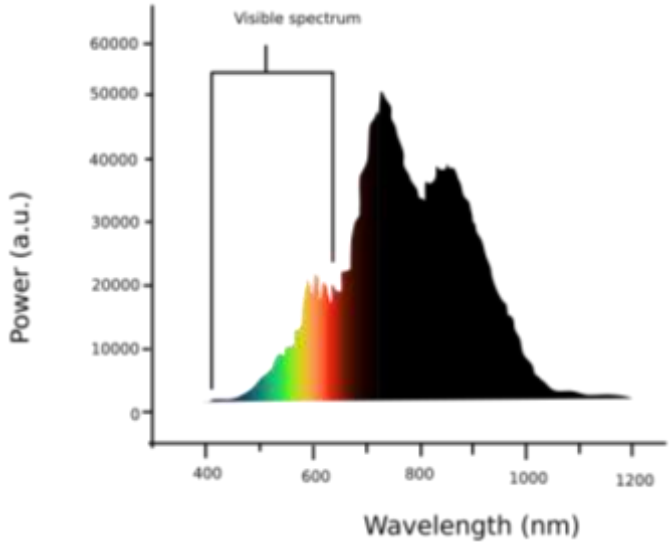

Figure 43: Halogen lamp spectrum [296]

c) LED

LED headlights produce light by converting electrical energy into light via diodes. This process is generally referred to electroluminescence and differs drastically to how light is produces in the previously mentioned headlights.
A LED headlight typically has a lumen counts within the range of 2000-4000. Although, there is models ranging lumens upwards to 6000.

6. Road conditions due to adverse weather conditions

Road conditions can change due to adverse weather conditions. The analysis from the "Deliverable 1 - Accident Data Study report" as well as further studies indicates that this can have a significant role in the occurrence of accidents [297]. In addition, adverse road conditions usually persist for an extended period of time during and after the actual adverse weather event, such as a snow-covered road that remains after the actual snowfall event.

The most common form of change is a reduction in the coefficient of friction of the road. Table 30 summarizes typical friction values for the most common weather scenarios.

Table 30: Common adverse road conditions with the corresponding friction values

Condition	Coefficient of Friction	Source
Rain	0.4 – 0.6	[298]
Wet (no rain)	0.4 – 0.6	[298, 299]
New snow	0.15 – 0.25	[300]
Old / packed snow	0.25 – 0.35	[298–301]
Refrozen snow	0.3 – 0.4	[300]
Shallow slush	0.3	[301]
(Wet) Ice	0.05 – 0.2	[298–300]

It should be noted that the exact friction coefficients are also influenced by the type of road surface (roughness, …), the water film thickness, the condition of the tires [302] and further factors [303–305]. In over 99.5% of wet road accidents, the water film height is between 0 and 1 mm [306]. While used tires provide increased friction on dry roads in comparison to new tires, they suffer a far more significant loss of grip in wet conditions [307]. A reduced friction can lead to an increased braking distance or hydroplaning [308, 309]. However, an analysis of GIDAS accident data indicates that complete aquaplaning, defined as the loss of contact between all four tires, occurs in only a very small percentage (0.6 %) of all cases with wet conditions [310]. On the other hand, 62 % of accidents on wet surfaces were caused by insufficient friction, while only approximately 37.4 % would have occurred regardless of the friction coefficient [306].
Furthermore, Wallmann [311] calculated the correlation of the friction coefficient and crash rates, as shown in Table 31.

Table 31: Accident rates) at different friction intervals [311]

Friction interval	Crash rate (personal injuries per million vehicle km)
< 0.15	0.8
0.15 – 0.24	0.55
0.25 – 0.34	0.25
0.35 – 0.44	0.20

A reduction in road friction can lead to an increase in the number of accidents. Research shows that in areas with normal friction, a reduction in friction by half can result in approximately twice the number of accidents. A summary of further studies on this topic can be found in [297]. It is noticeable, as shown in Figure 44, that the crash rate increases even though the crash impact speed is lower in wet road accidents. Since only a lower maximum deceleration is possible on wet roads, this indicates that people generally travel at lower speeds on wet surfaces. Nevertheless, the capability of the vehicle is often overestimated in these conditions, which leads to more accidents.

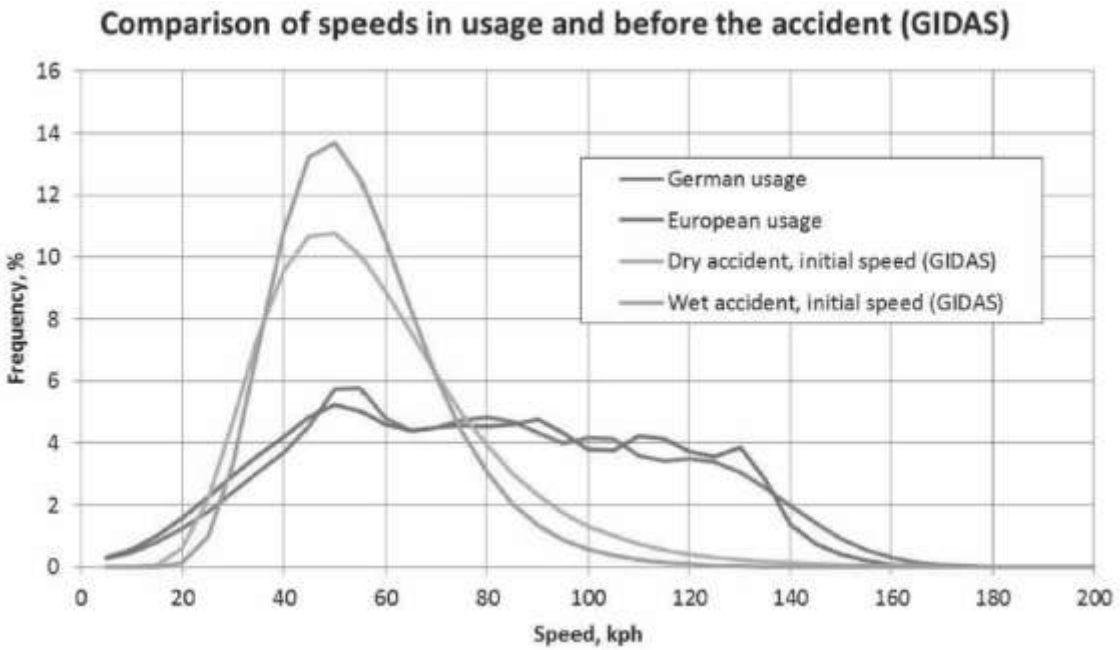

Figure 44: Comparison of speeds in usage (Michelin internal study) and initial speed before the accidents (GIDAS database)[306]

7. Conclusion

Adverse weather conditions can impact key parameters that affect safe driving, such as visibility and coefficient of friction. Each meteorological phenomenon can be described by a set of distinctive characteristic parameters. A comprehensive analysis of the accident data from D1 and the projected sensor degradation from D2.2 has led to the identification of the most relevant weather phenomena.

An analysis of the existing literature reveals the current state of knowledge regarding the formation process, types, and occurrence frequencies of rain and fog events. Precipitation intensity, droplet shape, rain drop size distribution and fall velocity for rain as well as meteorological optical range (MOR) and fog drop size distribution for fog were identified as the most relevant parameters to describe these phenomena. As detailed market research has shown, there are a variety of instruments on the market to measure these variables, based on different measurement principles. The most important parameters of rain, such as precipitation intensity, droplet size distribution, and velocity distribution, can be determined using a disdrometer. For fog, it is essential to determine visibility with a sensor that measures the MOR based on the forward scatter or transmission concept. Furthermore, it is recommended that fog droplet sizes are characterized which respective devices as well.

In terms of precipitation, Europe is in the moderate range. Precipitation intensities of more than 150 mm/h occur on average less than once a year. An analysis of the high-resolution precipitation data of the DWD over the last 15 years shows that precipitation of about 120 mm/h occurs on average every 6 months, with about 75 mm/h occurring monthly. An even greater accumulation of precipitation is observed especially in the Alps, on the west coast of Great Britain and in Scandinavia. Furthermore, in Europe in general, the strong convection typical over land creates clouds that produce particularly large drops during heavy rainfall.

The frequency of fog events decreased between 1980 and 2005 due to improvements in air quality and seems to have stagnated at a low level since then. Nevertheless, extremely low fog visibility (< 200 m) still occurs for a low two-digit number of hours per year. Visibility of up to 500 m occurs about 100 hours per year, which means that about four complete days can be observed.

Furthermore, glare has been identified as a frequent cause of accidents. Glare can be quantified with the help of the UGR index. There are several types of glare, ranging from direct sunlight to headlight glare. They differ in their characteristics and spectra.

Finally, most of the above-mentioned weather phenomena also change the road surface conditions. This can lead to a change in the coefficient of friction, as a result from various factors such as water film thickness, tire condition, vehicle dynamic state, weather conditions and so on. Although people drive more slowly on average on wet roads, the number of accidents is above average. The main reason seems to be that the reduced friction leads to an increase in braking distance, where systems or drivers do not intervene early enough.

Overall, the report enables the definition of concrete parameters and relevant use cases of different weather phenomena for later tests to increase the robustness of active safety and driver assistance systems.

8. Acknowledgements

The WeatherSafe consortium would like to acknowledge for their support and work all the Partners and Third Parties involved:



9. Table of illustrations

Table 1: Overview about environmental conditions with corresponding indicators [11] 5
Table 2: Overview over literature definition of drizzle intensity levels 14
Table 3: Overview over literature definition of shower intensity levels 14
Table 4: Overview over literature definition of rain types based on droplet diameter 15
Table 5: Specifications of selected tipping buckets commercially available 19
Table 6: Specifications of selected weighting sensor devices commercially available 19
Table 7: Specifications of selected optical disdrometer commercially available 21
Table 8: Specifications of selected Impact Disdrometer (Displacement) commercially available 21
Table 9: Specifications of selected Impact Disdrometer (Acoustic) commercially available 22
Table 10: Specifications of selected Video Disdrometer commercially available 22
Table 11: Specifications of selected forward scatter sensor commercially available 22
Table 12: Specifications of selected doppler radar sensor commercially available 23
Table 13: Requirements for precipitation measurement according to WMO [12] 23
Table 14: Projected precipitation trends for different climate change models [143] 26
Table 15: Rain records worldwide 27
Table 16: European Rain records in selected European countries 28
Table 17: Location data of the selected weather stations 35
Table 18: Rain classification 40
Table 19: Distinction between fog, mist and haze 41
Table 20: Types of fog formation according to [19] 42
Table 21: Modified gamma distribution parameterization by Shettle [230] 47
Table 22: Fog types and the values of coefficient b to estimate visibility range from LWC [244] 49
Table 23: Specifications of selected Transmissometer commercially available 51
Table 24: Ranking of different MOR measurement techniques. (1 = Best, 3 = Worst) [251] 51
Table 25: Specifications of selected Scatter Sensors commercially available 52
Table 26: Specifications of selected fog DSD measurement devices commercially available 53
Table 27: Location data of the selected weather stations 59
Table 28: Fog classification 62
Table 29: Typical values for colour temperature and horizontal illuminance depending on the time of day and sky conditions 68
Table 30: Common adverse road conditions with the corresponding friction values 70
Table 31: Accident rates) at different friction intervals [311] 70

10. References

[1] N. Becker, H. W. Rust, and U. Ulbrich, "Weather impacts on various types of road crashes: a quantitative analysis using generalized additive models," (in En;en), *Eur. Transp. Res. Rev.*, vol. 14, no. 1, pp. 1–18, 2022, doi: 10.1186/s12544-022-00561-2.

[2] A. Balint *et al.*, "SAFE-UP - D2. 6 Use Case Definitions and Initial Safety-Critical Scenarios. Project," 2021.

[3] U.S. Department of Transportation - Federal Highway Administration, *How Do Weather Events Impact Roads?: FHWA Road Weather Management Program.* [Online]. Available: https://ops.fhwa.dot.gov/weather/q1_roadimpact.htm (accessed: Nov. 7 2022).

[4] R. Al-Hindawi and T. Alhadidi, "Weather Conditions Using Bayesian Networks: A Scene-Based Approach with CARLA Simulator," in *Lecture Notes in Networks and Systems, Proceedings of Ninth International Congress on Information and Communication Technology*, X.-S. Yang, S. Sherratt, N. Dey, and A. Joshi, Eds., Singapore: Springer Nature Singapore, 2024, pp. 405–415.

[5] F. Ali, Z. H. Khan, K. S. Khattak, and T. A. Gulliver, "The effect of visibility on road traffic during foggy weather conditions," *IET Intelligent Trans Sys*, vol. 18, no. 1, pp. 47–57, 2024, doi: 10.1049/itr2.12432.

[6] D. Kokoris, *Incorporating Human Factors to Explain the Diving Behaviour under Adverse Weather Conditions*, 2021. [Online]. Available: https://repository.tudelft.nl/islandora/object/uuid:68bae084-b01d-4b4c-84f3-9e7cc09f1a71

[7] W. J. van Stralen, S. C. Calvert, and E. J. Molin, "The influence of adverse weather conditions on probability of congestion on Dutch motorways," *EJTIR*, vol. 15, no. 4, 2015, doi: 10.18757/ejtir.2015.15.4.3093.

[8] A. S. Mohammed, A. Amamou, F. K. Ayevide, S. Kelouwani, K. Agbossou, and N. Zioui, "The Perception System of Intelligent Ground Vehicles in All Weather Conditions: A Systematic Literature Review," *Sensors*, vol. 20, no. 22, p. 6532, 2020, doi: 10.3390/s20226532.

[9] Y. Zhang, A. Carballo, H. Yang, and K. Takeda, "Perception and sensing for autonomous vehicles under adverse weather conditions: A survey," *ISPRS Journal of Photogrammetry and Remote Sensing*, vol. 196, pp. 146–177, 2023, doi: 10.1016/j.isprsjprs.2022.12.021.

[10] S. Zang, M. Ding, D. Smith, P. Tyler, T. Rakotoarivelo, and M. A. Kaafar, "The Impact of Adverse Weather Conditions on Autonomous Vehicles: How Rain, Snow, Fog, and Hail Affect the Performance of a Self-Driving Car," *IEEE Veh. Technol. Mag.*, vol. 14, no. 2, pp. 103–111, 2019, doi: 10.1109/mvt.2019.2892497.

[11] Mitsubishi Heavy Industries Machinery Systems, Ltd., *Environmental Indicators*, 2023.

[12] World Meteorological Organization, *WMO-No. 8: Guide to instruments and methods of observation: Volume I – Measurement of Meteorological Variables*. Geneva: World Meteorological Organization, 2021.

[13] T. Dracos, *Hydrologie: Eine Einführung für Ingenieure*. Vienna: Springer Vienna, 1980.

[14] B. Klose, *Meteorologie: Eine interdisziplinäre Einführung in die Physik der Atmosphäre,* 3rd ed. Berlin, Heidelberg: Springer Berlin Heidelberg, 2016.

[15] MET Office, *Fact sheet No. 3 – Water in the atmosphere*. Exeter, 2023.

[16] J. Blüthgen and W. Weischet, Eds., *Allgemeine Klimageographie,* 3rd ed. Berlin, New York: Walter de Gruyter, 1980.

[17] R. A. Houze, "Orographic effects on precipitating clouds," *Reviews of Geophysics*, vol. 50, no. 1, 2012, doi: 10.1029/2011RG000365.

[18] DWD, *Wetter- und Klimalexikon.* [Online]. Available: https://www.dwd.de/lexikon (accessed: Jan. 15 2024).

[19] H. Häckel, *Meteorologie,* 8th ed. Stuttgart: Verlag Eugen Ulmer, 2016.

[20] T. Bergeron, "On the physics of clouds and precipitation," *Proc. 5th Assembly U.G.G.I., Lisbon, Portugal, 1935*, pp. 156–180, 1935. [Online]. Available: https://cir.nii.ac.jp/crid/1573105975504427392

[21] Pbroks13, *Raindrops sizes.* [Online]. Available: https://en.m.wikipedia.org/wiki/File:Raindrops_sizes.svg (accessed: Jan. 18 2024).
[22] H. R. Pruppacher and J. D. Klett, "Microstructure of Atmospheric Clouds and Precipitation," in *Microphysics of Clouds and Precipitation*: Springer, Dordrecht, 2010, pp. 10–73. [Online]. Available: https://link.springer.com/chapter/10.1007/978-0-306-48100-0_2
[23] D. C. Blanchard and A. T. Spencer, "Experiments on the Generation of Raindrop-Size Distributions by Drop Breakup," *J. Atmos. Sci.*, vol. 27, no. 1, pp. 101–108, 1970, doi: 10.1175/1520-0469(1970)027<0101:EOTGOR>2.0.CO;2.
[24] H. R. Pruppacher and R. L. Pitter, "A Semi-Empirical Determination of the Shape of Cloud and Rain Drops," *J. Atmos. Sci.*, vol. 28, no. 1, pp. 86–94, 1971, doi: 10.1175/1520-0469(1971)028<0086:ASEDOT>2.0.CO;2.
[25] A. W. Green, "An Approximation for the Shapes of Large Raindrops," *J. Appl. Meteor.*, vol. 14, no. 8, pp. 1578–1583, 1975, doi: 10.1175/1520-0450(1975)014<1578:AAFTSO>2.0.CO;2.
[26] K. V. Beard, R. J. Kubesh, and H. T. Ochs, "Laboratory Measurements of Small Raindrop Distortion. Part I: Axis Ratios and Fall Behavior," *J. Atmos. Sci.*, vol. 48, no. 5, pp. 698–710, 1991, doi: 10.1175/1520-0469(1991)048<0698:LMOSRD>2.0.CO;2.
[27] K. V. Beard, "Terminal Velocity and Shape of Cloud and Precipitation Drops Aloft," *J. Atmos. Sci.*, vol. 33, no. 5, pp. 851–864, 1976, doi: 10.1175/1520-0469(1976)033<0851:TVASOC>2.0.CO;2.
[28] L. W. Li, P. S. Kooi, M. S. Leong, and T. S. Yeo, "On the simplified expression of realistic raindrop shapes," *Microw. Opt. Technol. Lett.*, vol. 7, no. 4, pp. 201–205, 1994, doi: 10.1002/mop.4650070411.
[29] M. A. Serio, F. G. Carollo, and V. Ferro, "Raindrop size distribution and terminal velocity for rainfall erosivity studies. A review," *Journal of Hydrology*, vol. 576, pp. 210–228, 2019, doi: 10.1016/j.jhydrol.2019.06.040.
[30] R. Stull, "Precipitation Characteristics," 2020. [Online]. Available: www.geo.libretexts.org/Bookshelves/Meteorology_and_Climate_Science/Practical_Meteorology_%28Stull%29/07%3A_Precipitation_Processes/7.07%3A_Precipitation_Characteristics
[31] V. N. Bringi, V. Chandrasekar, J. Hubbert, E. Gorgucci, W. L. Randeu, and M. Schoenhuber, "Raindrop Size Distribution in Different Climatic Regimes from Disdrometer and Dual-Polarized Radar Analysis," *J. Atmos. Sci.*, vol. 60, no. 2, pp. 354–365, 2003, doi: 10.1175/1520-0469(2003)060<0354:RSDIDC>2.0.CO;2.
[32] E. S. Hong, S. Lane, D. Murrell, N. Tarasenko, C. Christodoulou, and J. Keeley, "Estimating Rain Attenuation at 72 and 84 GHz From Raindrop Size Distribution Measurements in Albuquerque, NM, USA," *IEEE Geosci. Remote Sensing Lett.*, vol. 16, no. 8, pp. 1175–1179, 2019, doi: 10.1109/lgrs.2019.2893906.
[33] B. Radhakrishna, "Raindrop size distribution (DSD) during the passage of tropical cyclone Nivar: effect of measuring principle and wind on DSDs and retrieved rain integral and polarimetric parameters from impact and laser disdrometers," *Atmos. Meas. Tech.*, vol. 15, no. 22, pp. 6705–6722, 2022, doi: 10.5194/amt-15-6705-2022.
[34] R. S. Tenorio, B.-H. Kwon, and Marcia Cristina da Silva, Moraes, *Raindrop size distribution over northeastern coast of brazil*, 2006. [Online]. Available: https://www.koreascience.or.kr/article/jako200622219285396.page
[35] J. C. Bezdek and K. H. Solomon, "Upper Limit Lognormal Distribution for Drop Size Data," *J. Irrig. Drain Eng.*, vol. 109, no. 1, pp. 72–88, 1983, doi: 10.1061/(ASCE)0733-9437(1983)109:1(72).
[36] S. G. Bradley and C. D. Stow, "The measurement of charge and size of raindrops: Part II. Results and analysis at ground level," *J. Appl. Meteorol.*, no. 13, pp. 13–147, 1962, doi: 10.1175/1520-0450(1974)013<0131:TMOCAS>2.0.CO;2.

[37] G. Feingold and Z. Levin, "The Lognormal Fit to Raindrop Spectra from Frontal Convective Clouds in Israel," *J. Climate Appl. Meteor.*, vol. 25, no. 10, pp. 1346–1363, 1986, doi: 10.1175/1520-0450(1986)025<1346:tlftrs>2.0.co;2.
[38] Z. Levin, "Charge Separation by Splashing of Naturally Falling Raindrops," *J. Atmos. Sci.*, vol. 28, no. 4, pp. 543–548, 1971, doi: 10.1175/1520-0469(1971)028<0543:CSBSON>2.0.CO;2.
[39] A. H. Markowitz, "Raindrop Size Distribution Expressions," *J. Appl. Meteor.*, vol. 15, no. 9, pp. 1029–1031, 1976, doi: 10.1175/1520-0450(1976)015<1029:rsde>2.0.co;2.
[40] A. D. Ochou, A. Nzeukou, and H. Sauvageot, "Parametrization of drop size distribution with rain rate," *Atmospheric Research*, vol. 84, no. 1, pp. 58–66, 2007, doi: 10.1016/j.atmosres.2006.05.003.
[41] S. Hasirlioglu, "A Novel Method for Simulation-based Testing and Validation of Automotive Surround Sensors under Adverse Weather Conditions," Dissertation, Institut für Pervasive Computing, Universität Linz, Linz, 2020. [Online]. Available: https://epub.jku.at/obvulihs/content/titleinfo/4837383
[42] I. Langmuir, "The Production of Rain by a Chain Reaction in Cumulus Clouds at Temperatures above Freezing," *J. Meteor.*, vol. 5, no. 5, pp. 175–192, 1948, doi: 10.1175/1520-0469(1948)005<0175:TPORBA>2.0.CO;2.
[43] W. Weibull, "A Statistical Distribution Function of Wide Applicability," *Journal of Applied Mechanics*, vol. 18, no. 3, pp. 293–297, 1951, doi: 10.1115/1.4010337.
[44] M. Sekine and G. Lind, "Rain Attenuation 0f Centimeter, Millimeter and Submillimeter Radio Waves," in *12th European Microwave Conference, 1982*, 1982.
[45] J. S. Marshall, "The distribution of raindrops with size," *J. Meteor.*, vol. 5, pp. 165–166, 1948, doi: 10.1175/1520-0469(1948)005<0165:TDORWS>2.0.CO;2.
[46] R. Uijlenhoet and J. Stricker, "Dependence of rainfall interception on drop size – a comment," *Journal of Hydrology*, vol. 217, 1-2, pp. 157–163, 1999, doi: 10.1016/S0022-1694(99)00004-9.
[47] J. Joss and A. Waldvogel, "Raindrop Size Distribution and Sampling Size Errors," *J. Atmos. Sci.*, vol. 26, no. 3, pp. 566–569, 1969, doi: 10.1175/1520-0469(1969)026<0566:RSDASS>2.0.CO;2.
[48] R. E. S. Gunn and J. S. Marshall, "The effect of wind shear on falling precipitation," *J. Meteor.*, vol. 12, no. 4, pp. 339–349, 1955, doi: 10.1175/1520-0469(1955)012<0339:TEOWSO>2.0.CO;2.
[49] A. Waldvogel, "The N0 Jump of Raindrop Spectra," *J. Atmos. Sci.*, vol. 31, no. 4, pp. 1067–1078, 1974, doi: 10.1175/1520-0469(1974)031<1067:TJORS>2.0.CO;2.
[50] D. S. Torres, J. M. Porrà, and J.-D. Creutin, "A General Formulation for Raindrop Size Distribution," *J. Appl. Meteor.*, vol. 33, no. 12, pp. 1494–1502, 1994, doi: 10.1175/1520-0450(1994)033<1494:AGFFRS>2.0.CO;2.
[51] J. Joss and E. G. Gori, "Shapes of Raindrop Size Distributions," *J. Appl. Meteor.*, vol. 17, no. 7, pp. 1054–1061, 1978, doi: 10.1175/1520-0450(1978)017<1054:sorsd>2.0.co;2.
[52] A. D. Ochou, A. Nzeukou, and H. Sauvageot, "Parametrization of drop size distribution with rain rate," *Atmospheric Research*, vol. 84, no. 1, pp. 58–66, 2007, doi: 10.1016/j.atmosres.2006.05.003.
[53] C. W. Ulbrich, "Natural Variations in the Analytical Form of the Raindrop Size Distribution," *J. Climate Appl. Meteor.*, vol. 22, no. 10, pp. 1764–1775, 1983, doi: 10.1175/1520-0450(1983)022<1764:nvitaf>2.0.co;2.
[54] D. C. Blanchard, *Raindrop size distribution and accicuated phenomena in hawaiian rains*. Fort Belvoir, VA: Defense Technical Information Center, 1952.
[55] A. N. Dingle and K. R. Hardy, "The description of rain by means of sequential raindrop-size distributions," *Quarterly Journal of the Royal Meteorological Society*, vol. 88, no. 377, pp. 301–314, 1962, doi: 10.1002/qj.49708837709.

[56] P. G. F. Caton, "A study of raindrop-size distributions in the free atmosphere," *Quarterly Journal of the Royal Meteorological Society*, vol. 92, no. 391, pp. 15–30, 1966, doi: 10.1002/qj.49709239103.
[57] F. G. Carollo and V. Ferro, "Modeling Rainfall Erosivity by Measured Drop-Size Distributions," *J. Hydrol. Eng.*, vol. 20, no. 6, C4014006, 2015, doi: 10.1061/(ASCE)HE.1943-5584.0001077.
[58] F. G. Carollo, V. Ferro, and M. A. Serio, "Estimating rainfall erosivity by aggregated drop size distributions," *Hydrological Processes*, vol. 30, no. 13, pp. 2119–2128, 2016, doi: 10.1002/hyp.10776.
[59] D. Brawn and G. Upton, "On the measurement of atmospheric gamma drop-size distributions," *Atmospheric Science Letters*, vol. 9, no. 4, pp. 245–247, 2008, doi: 10.1002/asl.198.
[60] D. Deirmendjian, *Electromagnetic scattering on spherical polydispersions*. The RAND Corporation. New York: American Elsevier Publishing Company, 1969. [Online]. Available: https://apps.dtic.mil/sti/citations/ad0689159
[61] H. Jiang, M. Sano, and M. Sekine, "Weibull raindrop-size distribution and its application to rain attenuation," *IEE Proc., Microw. Antennas Propag.*, vol. 144, no. 3, p. 197, 1997, doi: 10.1049/ip-map:19971193.
[62] M. Thurai, V. Bringi, P. Gatlin, and M. Wingo, "Raindrop fall velocity in turbulent flow: an observational study," in *Advances in Science and Research*, 2021, pp. 33–39. Accessed: Apr. 21 2021. [Online]. Available: https://asr.copernicus.org/articles/18/33/2021/
[63] Malvern Instruments Limited, "Basic principles of particle size analysis," 2014. [Online]. Available: https://www.atascientific.com.au/wp-content/uploads/2017/02/AN020710-Basic-Principles-Particle-Size-Analysis.pdf
[64] Hansa Engineering, *Which droplet size is most suitable for the spray process?* [Online]. Available: https://hansa-engineering.se/en/knowledge-base/which-droplet-size-is-most-suitable-for-the-spray-process/ (accessed: Sep. 18 2024).
[65] R. J. Schick, "Understanding Drop Size," 2008. [Online]. Available: https://www.spray.com/de-eu/-/media/dam/industrial/usa/sales-material/product-market-bulletin/b459c_understanding_drop_size.pdf
[66] T. Bassett, "Droplet Size Distribution," 2019.
[67] R. Gunn and G. D. Kinzer, "The terminal velocity of fall for water droplets in stagnant air," *J. Meteor.*, vol. 6, no. 4, pp. 243–248, 1949, doi: 10.1175/1520-0469(1949)006<0243:TTVOFF>2.0.CO;2.
[68] V. Bringi, M. Thurai, and D. Baumgardner, "Raindrop fall velocities from an optical array probe and 2-D video disdrometer," *Atmos. Meas. Tech.*, vol. 11, no. 3, pp. 1377–1384, 2018, doi: 10.5194/amt-11-1377-2018.
[69] S. A. Morsi and A. J. Alexander, "An investigation of particle trajectories in two-phase flow systems," *J. Fluid Mech.*, vol. 55, no. 02, p. 193, 1972, doi: 10.1017/s0022112072001806.
[70] G. B. Foote and P. S. Du Toit, "Terminal Velocity of Raindrops Aloft," *J. Appl. Meteor.*, vol. 8, no. 2, pp. 249–253, 1969, doi: 10.1175/1520-0450(1969)008<0249:tvora>2.0.co;2.
[71] E. A. Brandes, G. Zhang, and J. Vivekanandan, "Experiments in Rainfall Estimation with a Polarimetric Radar in a Subtropical Environment," *J. Appl. Meteor.*, vol. 41, no. 6, pp. 674–685, 2002, doi: 10.1175/1520-0450(2002)041<0674:EIREWA>2.0.CO;2.
[72] M. L. Larsen, A. B. Kostinski, and A. R. Jameson, "Further evidence for superterminal raindrops," *Geophysical Research Letters*, vol. 41, no. 19, pp. 6914–6918, 2014, doi: 10.1002/2014GL061397.
[73] G. Montero-Martínez and F. García-García, "On the behaviour of raindrop fall speed due to wind," *Quarterly Journal of the Royal Meteorological Society*, vol. 142, no. 698, pp. 2013–2020, 2016, doi: 10.1002/qj.2794.
[74] G. Montero-Martínez, A. B. Kostinski, R. A. Shaw, and F. García-García, "Do all raindrops fall at terminal speed?," *Geophysical Research Letters*, vol. 36, no. 11, 2009, doi: 10.1029/2008GL037111.

[75] M. Thurai, V. N. Bringi, W. A. Petersen, and P. N. Gatlin, "Drop Shapes and Fall Speeds in Rain: Two Contrasting Examples," *Journal of Applied Meteorology and Climatology*, vol. 52, no. 11, pp. 2567–2581, 2013, doi: 10.1175/JAMC-D-12-085.1.
[76] C.-K. Yu *et al.*, "Measuring droplet fall speed with a high-speed camera: indoor accuracy and potential outdoor applications," *Atmos. Meas. Tech.*, vol. 9, no. 4, pp. 1755–1766, 2016, doi: 10.5194/amt-9-1755-2016.
[77] G. M. McFarquhar, "The effect of raindrop clustering on collision-induced break-up of raindrops," *Quarterly Journal of the Royal Meteorological Society*, vol. 130, no. 601, pp. 2169–2190, 2004, doi: 10.1256/qj.03.98.
[78] *DIN 4049-3:1994-10, Hydrologie - Teil 3: Begriffe zur quantitativen Hydrologie,* Deutsches Institut für Normung e.V., Berlin.
[79] World Meteorological Organization, *WMO-No. 168: Guide to Hydrological Practice - Volume I: From Measurement to Hydrological,* 6th ed. Geneva: World Meteorological Organization, 2008.
[80] DWD, *Wetter und Klima - Deutscher Wetterdienst - Glossar - N - Niederschlagsintensität.* [Online]. Available: https://www.dwd.de/DE/service/lexikon/Functions/glossar.html?lv2=101812&lv3=101906 (accessed: Oct. 4 2021).
[81] *Road meteorology. Gathering of meteorological and road data. Terminology*, NF P99-320:1998-04-01, National standards and national normative documents.
[82] American Meteorological Society, *Rain - Glossary of Meteorology.* [Online]. Available: https://glossary.ametsoc.org/wiki/Rain (accessed: Apr. 30 2023).
[83] US Department of Commerce/National Oceanic and Atmospheric Administration, *Federal Meteoroligucal Handbook No. 1 - Surface Weather Observations and Reports*. Washington, D.C., 2019.
[84] MeteoSchweiz, *Niederschlag.* [Online]. Available: https://www.meteoschweiz.admin.ch/wetter/wetter-und-klima-von-a-bis-z/niederschlag.html (accessed: Dec. 12 2023).
[85] P. Koppe and A. Stozek, *Kommunales Abwasser: Seine Inhaltsstoffe nach Herkunft, Zusammensetzung und Reaktionen im Reinigungsprozeß einschließlich Klärschlämme,* 4th ed. Essen: Vulkan-Verl., 1999.
[86] UK Civil Aviaiton Authority, *Requirements for meteorological observations at aerodromes*. Crawley, 2023. Accessed: Apr. 2 2024. [Online]. Available: https://www.caa.co.uk/publication/download/12602
[87] *VDI 3786 Blatt 1, Umweltmeteorologie - meteorologische Messungen - Grundlagen: Environmental meteorology - meteorological measurements - Fundamentals*, 3786, Verein Deutscher Ingenieure, 2023.
[88] *VDI 3786 Blatt 7, Umweltmeteorologie - meteorologische Messungen - Niederschlag: Environmental meteorology - meteorological measurements - Precipitation*, 3786, Verein Deutscher Ingenieure, 2023.
[89] DWD, *Richtlinie: Automatische nebenamtliche Wetterstationen im DWD*. Offenbach am Main, 2020.
[90] Bayerisches Landesamt für Umwelt, *Niederschlagserfassung.* [Online]. Available: https://www.lfu.bayern.de/wasser/hydrometerologische_parameter/niederschlagserfassung/index.htm (accessed: Mar. 19 2024).
[91] World Meteorological Organization, *WMO-No. 39: Catalogue of national standard precipitation gauges*, 1989.
[92] M. Spreafico and R. Weingartner, "Hydrologie der Schweiz: Ausgewählte Aspekte und Resultate," Bundesamt für Wasser und Geologie BWG, Bern, 2005. [Online]. Available: https://boris.unibe.ch/134004/
[93] T. Foken, Ed., *Angewandte Meteorologie: Mikrometeorologische Methoden,* 3rd ed. Berlin, Heidelberg: Springer Spektrum, 2016.
[94] B. Sevruk and W. Kirchhofer, "Systematischer Niederschlagsmessfehler in der Schweiz," *Der Niederschlag in der Schweiz. Beitr. z. Geologie der Schweiz – Hydrologie*, no. 31, pp. 65–68, 1985.

[95] B. Sevruk, "Methodische Untersuchungen des systematischen Messfehlers der Hellmann-Regenmesser im Sommerhalbjahr in der Schweiz," Dissertation, TH Zürich, Zürich, 1981. [Online]. Available: https://www.research-collection.ethz.ch/bitstream/handle/20.500.11850/137067/eth-21882-01.pdf
[96] D. Richter, "Ergebnisse methodischer Untersuchungen zur Korrektur des systematischen Meßfehlers des Hellmann-Niederschlagmessers," *Berichte des Deutschen Wetterdienstes*, no. 194, 1995.
[97] L. G. Lanza and E. Vuerich, "The WMO Field Intercomparison of Rain Intensity Gauges," *Atmospheric Research*, vol. 94, no. 4, pp. 534–543, 2009, doi: 10.1016/j.atmosres.2009.06.012.
[98] J. Joss and E. Tognini, "Ein automatisch arbeitender Ombrograph mit grossem Auflsungsvermgen und mit fernbertragung der Messwerte," (in De;de), *PAGEOPH*, vol. 68, no. 1, pp. 229–239, 1967, doi: 10.1007/BF00874897.
[99] H. Löffler, *Meteorologische Bodenmesstechnik,* 3rd ed. Offenbach / Main: Selbstverl. des Dt. Wetterdienstes, 2012.
[100] Thies CLIMA, *Niederschlagsgeber Kippwaage.* [Online]. Available: https://www.thiesclima.com/de/Produkte/Niederschlag-Messtechnik-Elektrische-Geraete/?art=764 (accessed: Feb. 21 2024).
[101] ZATA, *Tipping Bucket Rain Gauge ZDR100.* [Online]. Available: https://www.zataiot.com/de/zdr100-tipping-bucket-rain-gauge/ (accessed: Feb. 29 2024).
[102] ACS Control-System, *Niederschlagssensor NR4M.* [Online]. Available: https://www.acs-controlsystem.de/produkt/niederschlagssensor-nr4m/#downloads_tab (accessed: Feb. 29 2024).
[103] Campbell Scientific, *RainVUE20 - SDI-12 Niederschlagssensor mit Aluminum - Auffangtrichter.* [Online]. Available: https://www.campbellsci.de/rainvue20 (accessed: Feb. 29 2024).
[104] LAMBRECHT meteo, "Niederschlagssensor nach Joss-Tognini-15189," [Online]. Available: https://www.lambrecht.net/scripts/pdf.php?id=49&lang=german
[105] VAISALA, *Rain Gauge RG13.* [Online]. Available: https://www.vaisala.com/en/products/weather-environmental-sensors/rain-gauge-rg13 (accessed: Mar. 25 2024).
[106] RIMCO, "RIM-7499-BOM," 2020. [Online]. Available: https://observator.com/wp-content/uploads/2019/07/Datasheet-RIM-7499-BOM-V20200210.pdf
[107] Thies CLIMA, "Niederschlagsgeber Wiegende Kippwaage," 2022. Accessed: Feb. 21 2024. [Online]. Available: https://www.thiesclima.com/db/dnl/5.4041.01.00x_Niederschlagsgeber_de.pdf
[108] OTT HydroMet, *OTT Pluvio² S.* [Online]. Available: https://www.ott.com/de-de/produkte/meteorologie-29/ott-pluvio2-s-regenmesser-niederschlagsmesser-850/productAction/outputAsPdf/ (accessed: Feb. 29 2024).
[109] OTT HydroMet, *OTT Pluvio² L.* [Online]. Available: https://www.ott.com/de-de/produkte/meteorologie-29/ott-pluvio2-l-regenmesser-niederschlagsmesser-1520/productAction/outputAsPdf/ (accessed: Feb. 29 2024).
[110] ZATA, *Weighing Rain Gauge ZWR.* [Online]. Available: https://www.zataiot.com/weighing-rain-gauge/ (accessed: Feb. 29 2024).
[111] LAMBRECHT meteo, *rain[e] - Wiegender Niederschlagssensor.* [Online]. Available: https://www.lambrecht.net/produkte/niederschlag/wiegender-niederschlagssensor-rain-e (accessed: Feb. 29 2024).
[112] H. I. Bloemink and L. Eckhard, "Precipitation type from the Thies disdrometer," in *WMO Technical Conference on Instruments and Methods of Observation*, pp. 4–7.
[113] OTT HydroMet, "Here comes the rain: High-precision measurement of hydrometeors," *Meteorological Technology International*, pp. 105–107, 2011. [Online]. Available: https://www.ott.com/download/meteorological-technology-international-article/

[114]H. Mahlke, "Niederschlagsmessung mit einem neuartigen optischen Distrometer (Flying Parsivel Sonde)," Diplomarbeit, Institut für Meteorologie und Klimaforschung, Karlsruher Institut für Technologie, Karlsruhe, 2007.
[115]G. Lempio, *Machbarkeitsstudie über die Messung festen Niederschlags mit dem optischen Disdrometer*, 2006. [Online]. Available: https://oceanrep.geomar.de/id/eprint/1131
[116]Thies CLIMA, *Funktionsprinzip - Optisches Distrometer* (accessed: Mar. 26 2024).
[117]Thies CLIMA, *Laser Niederschlags Monitor.* [Online]. Available: https://www.thiesclima.com/db/dnl/5.4110.xx.x00_LNM_deu.pdf (accessed: Feb. 21 2024).
[118]OTT HydroMet, *OTT Parsivel².* [Online]. Available: https://www.ott.com/de-de/produkte/meteorologie-29/ott-parsivel2-niederschlagsbestimmung-97/productAction/outputAsPdf/ (accessed: Feb. 29 2024).
[119]ZATA, *Disdrometer ZDM100.* [Online]. Available: https://www.zataiot.com/de/disdrometer-distrometer-zdm100/ (accessed: Feb. 29 2024).
[120]Eigenbrodt, *Optical Disdrometer ODM 470.* [Online]. Available: https://www.eigenbrodt.de/en/products/meteorologie/optical-disdrometer-odm-470/ (accessed: Feb. 29 2024).
[121]Droplet Measurement Technologies, *MPS Meteorological Particle Spectrometer.* [Online]. Available: https://www.dropletmeasurement.com/product/meteorological-particle-spectrometer/ (accessed: Feb. 21 2024).
[122]Distromet, *Disdrometer RD-80.* [Online]. Available: https://distromet.com/94 (accessed: Feb. 29 2024).
[123]G. Kathiravelu, T. Lucke, and P. Nichols, "Rain Drop Measurement Techniques: A Review," *Water*, vol. 8, no. 1, p. 29, 2016, doi: 10.3390/w8010029.
[124]VAISALA, *Weather Transmitter WXT530.* [Online]. Available: https://docs.vaisala.com/v/u/B211500EN-K/en-US (accessed: Feb. 29 2024).
[125]ISAW, "RainFlow RF4," [Online]. Available: https://www.isaw-products.com/wp-content/uploads/2023/08/03-RainFlow_RF4_Short_Product_Description_V4.3.pdf
[126]ZATA, *Piezoelectric Rain Sensor ZWS100.* [Online]. Available: https://www.zataiot.com/de/piezoelectric-rain-sensor/# (accessed: Feb. 29 2024).
[127]Thies CLIMA, *3D Stereo Disdrometer*.
[128]Joanneum Research, *2DVD.* [Online]. Available: https://www.distrometer.at/2dvd (accessed: Feb. 29 2024).
[129]Joanneum Research, *1DVD.* [Online]. Available: https://www.distrometer.at/1dvd (accessed: Feb. 29 2024).
[130]Campbell Scientific, *CS125 - Present Weather and Visibility Sensor.* [Online]. Available: https://www.campbellsci.de/cs125 (accessed: Feb. 29 2024).
[131]VAISALA, *Forward Scatter FD70.* [Online]. Available: https://docs.vaisala.com/v/u/B211744EN-G/en-US (accessed: Feb. 29 2024).
[132]VAISALA, *Present Weather and Visibility Sensors PWD10, PWD12, PWD20, and PWD22.* [Online]. Available: https://docs.vaisala.com/v/u/B210385EN-F/en-US (accessed: Feb. 29 2024).
[133]Thies CLIMA, *Clima Sensor US.* [Online]. Available: https://www.thiesclima.com/db/dnl/4.92xx.x0.xxx_ClimaSensor_US_d.pdf (accessed: Feb. 21 2024).
[134]OTT HydroMet, *Lufft WS100.* [Online]. Available: https://www.ott.com/de-de/produkte/meteorologie-29/lufft-ws100-radar-niederschlagssensor-intelligenter-disdrometer-2386/productAction/outputAsPdf/ (accessed: Feb. 29 2024).
[135]H. Walter, *Vegetation und Klimazonen: Grundriß der globalen Ökologie ; 1 Weltkarte der Zonobiome,* 6th ed. Stuttgart: Ulmer, 1990.
[136]Diercke, *Europa - Niederschläge im Jahr.* [Online]. Available: https://diercke.de/content/europa-niederschl%C3%A4ge-im-jahr-978-3-14-100803-6-95-3-1 (accessed: Apr. 3 2024).

[137]DWD, *Klimakarten Europa - Niederschlag.* [Online]. Available: https://www.dwd.de/DE/leistungen/rcccm/int/rcccm_month_rrr_ref.html?nn=781516 (accessed: Apr. 3 2024).
[138]DWD, *Nationaler Klimareport – Klima–Gestern, heute und in der Zukunft,* 6th ed., 2022.
[139]International Panel on climate change (IPCC), *IPCC AR6-WGI Atlas.* [Online]. Available: https://interactive-atlas.ipcc.ch/ (accessed: Apr. 3 2024).
[140]F. Kreienkamp *et al., Empfehlungen für die Charakterisierung ausgewählter Klimaszenarien*, 2022. [Online]. Available: https://pure.iiasa.ac.at/id/eprint/17944/1/szenariennamen-stand_20220315.pdf
[141]B. C. O'Neill *et al.,* "A new scenario framework for climate change research: the concept of shared socioeconomic pathways," (in En;en), *Climatic Change*, vol. 122, no. 3, pp. 387–400, 2014, doi: 10.1007/s10584-013-0905-2.
[142]D. P. van Vuuren *et al.,* "A new scenario framework for Climate Change Research: scenario matrix architecture," (in En;en), *Climatic Change*, vol. 122, no. 3, pp. 373–386, 2014, doi: 10.1007/s10584-013-0906-1.
[143]European Environment Agency, *European climate risk assessment — Executive summary*. Luxembourg: Publications Office of the European Union, 2024.
[144]World Meteorological Organization (WMO), *Guidelines for the WMO Evaluation of Records of Weather and Climate Extremes: WMO-No. 1317*. Geneva, Switzerland: World Meteorological Organization, 2023. Accessed: Jan. 3 2024. [Online]. Available: https://library.wmo.int/viewer/68658/download?file=1317_2023-edition_en.pdf&type=pdf&navigator=1
[145]DWD, *Wetterrekorde.* [Online]. Available: https://www.dwd.de/DE/service/lexikon/begriffe/W/Wetterrekorde.html (accessed: Jan. 18 2024).
[146]MeteoSchweiz, *Rekorde und Extreme.* [Online]. Available: https://www.meteoschweiz.admin.ch/klima/klima-der-schweiz/rekorde-und-extreme.html (accessed: Jan. 18 2024).
[147]MET Office, *UK climate extremes.* [Online]. Available: https://www.metoffice.gov.uk/research/climate/maps-and-data/uk-climate-extremes (accessed: Jan. 18 2024).
[148]Météo-France, *Records - 6 min à 12 h - Pluies extrêmes en France métropolitaine.* [Online]. Available: http://pluiesextremes.meteo.fr/france-metropole/Records-6-min-a-12-h.html (accessed: Jan. 18 2024).
[149]L. Emiliani, L. Luini, and C. Capsoni, *On the optimum estimation of 1-minute integrated rainfall statistics from data with longer integration time*, 2010.
[150]ITU Radiocommunication Bureau (BR), "Recommendation P.837-7 - Characteristics of precipitation for propagation modelling," 2017. [Online]. Available: https://www.itu.int/dms_pubrec/itu-r/rec/p/R-REC-P.837-7-201706-I!!PDF-E.pdf
[151]C. Capsoni and L. Luini, "A Physically Based Method for the Conversion of Rainfall Statistics From Long to Short Integration Time," *IEEE Trans. Antennas Propagat.*, vol. 57, no. 11, pp. 3692–3696, 2009, doi: 10.1109/tap.2009.2025189.
[152]L. Emiliani, C. Capsoni, and L. Luini, "Extension of ITU-R Method for conversion of rain rate statistics from various integration times to one minute," *Electron. Lett.*, vol. 44, no. 8, p. 557, 2008, doi: 10.1049/el:20080490.
[153]L. Emiliani, L. Luini, C. Capsoni, and C. Riva, "Performance evaluation of models for the conversion of rainfall statistics from long to short integration time," *ESA Workshop on Radiowave Propagation*, 2008. [Online]. Available: https://www.researchgate.net/profile/luis-emiliani-3/publication/271137708_performance_evaluation_of_models_for_the_conversion_of_the_rainfall_statistics_from_long_to_short_integration_time/links/561f569208aef097132d1ea0/performance-evaluation-of-models-for-the-conversion-of-the-rainfall-statistics-from-long-to-short-integration-time.pdf
[154]M.-W. Jung, I.-T. Han, M.-Y. Choi, J.-H. Lee, and J.-K. Pack, "Study on the Empirical Prediction of 1-min Rain Rate Distribution from Various Integration Time Data," in *2007 Korea-Japan Microwave Conference*, 2007.

[155]M.-W. Jung, I.-T. Han, M.-Y. Choi, J.-H. Lee, and J.-K. Pack, "Empirical Prediction Models of 1-min Rain Rate Distribution for Various Integration Time," *Journal of electromagnetic engineering and science*, vol. 8, no. 2, pp. 84–89, 2008, doi: 10.5515/jkiees.2008.8.2.084.
[156]ITU Radiocommunication Bureau (BR), "Recommendation P.837-1 - Characteristics of precipitation for propagation modelling," 1994. [Online]. Available: https://www.itu.int/dms_pubrec/itu-r/rec/p/R-REC-P.837-1-199408-S!!PDF-E.pdf
[157]A. Vajda *et al.*, "Probabilities of adverse weather affecting transport in Europe: climatology and scenarios up to the 2050s: Extreme weather impacts on European networks of transport (EWENT)," 2011:9, 2011.
[158]P. Groenemeijer *et al.*, "Present and future probability of meteorological and hydrological hazards in Europe: RAIN Project D 2.5," 2016. [Online]. Available: https://rain-project.eu/wp-content/uploads/2016/09/D2.5_REPORT_final.pdf
[159]J. Ryu, H.-J. Song, B.-J. Sohn, and C. Liu, "Global Distribution of Three Types of Drop Size Distribution Representing Heavy Rainfall From GPM/DPR Measurements," *Geophysical Research Letters*, vol. 48, no. 3, e2020GL090871, 2021, doi: 10.1029/2020GL090871.
[160]DWD, *Climate Data Center - German Weather Data.* [Online]. Available: https://cdc.dwd.de/portal/ (accessed: Feb. 8 2024).
[161]DWD, *Klimakarten Deutschland.* [Online]. Available: https://www.dwd.de/DE/leistungen/klimakartendeutschland/klimakartendeutschland.html (accessed: Apr. 8 2024).
[162]American Meteorological Society, *Fog - Glossary of Meteorology.* [Online]. Available: https://glossary.ametsoc.org/wiki/Fog (accessed: Apr. 27 2023).
[163]J. E. Oliver, *Encyclopedia of world climatology*. Dordrecht: Springer, 2008.
[164]WMO, *International Cloud Atlas - Fog.* [Online]. Available: https://cloudatlas.wmo.int/en/fog.html (accessed: Feb. 12 2024).
[165]National Oceanic and Atmospheric Administration, *Glossary - NOAA's National Weather Service.* [Online]. Available: https://w1.weather.gov/glossary/index.php?word=FOG (accessed: Feb. 15 2024).
[166]R. Nebuloni and C. Capsoni, "Effects of Adverse Weather on Free Space Optics," in *Optical Wireless Communications*: Springer, Cham, 2016, pp. 47–68. [Online]. Available: https://link.springer.com/chapter/10.1007/978-3-319-30201-0_3
[167]WMO, *International Cloud Atlas - Fog compared with Mist.* [Online]. Available: https://cloudatlas.wmo.int/en/fog-compared-with-mist.html (accessed: Apr. 18 2024).
[168]MET Office, *What is the difference between mist, fog and haze?* [Online]. Available: https://www.metoffice.gov.uk/weather/learn-about/weather/types-of-weather/fog/difference-mist-and-fog (accessed: Apr. 18 2024).
[169]K. Lakra and K. Avishek, "A review on factors influencing fog formation, classification, forecasting, detection and impacts," *Rend. Fis. Acc. Lincei*, vol. 33, no. 2, pp. 319–353, 2022, doi: 10.1007/s12210-022-01060-1.
[170]W. Seguin, *Glossary of Meteorology.* [Online]. Available: https://www.ametsoc.org/index.cfm/ams/publications/glossary-of-meteorology/
[171]W. Seguin, *Radiation fog - Glossary of Meteorology.* [Online]. Available: https://glossary.ametsoc.org/wiki/Radiation_fog (accessed: Feb. 12 2024).
[172]M. Haeffelin *et al.*, "A Comparative Study of Radiation Fog and Quasi-Fog Formation Processes During the ParisFog Field Experiment 2007," (in En;en), *Pure appl. geophys.*, vol. 170, no. 12, pp. 2283–2303, 2013, doi: 10.1007/s00024-013-0672-z.
[173]S. S. Muhammad, "Characterization of fog attenuation in terrestrial free space optical links," *Optical Engineering*, vol. 46, no. 6, p. 66001, 2007, doi: 10.1117/1.2749502.
[174]W. Seguin, *Advection fog - Glossary of Meteorology.* [Online]. Available: https://glossary.ametsoc.org/wiki/Advection_fog (accessed: Feb. 12 2024).
[175]J. M. Wallace and P. V. Hobbs, *Atmospheric Science: An introductory survey*. Burlington, Mass, San Diego, Calif., London: Academic Press Elsevier, 2006.

[176]W. Seguin, *Orographic fog - Glossary of Meteorology*. [Online]. Available: https://glossary.ametsoc.org/wiki/Orographic_fog (accessed: Feb. 12 2024).
[177]W. Seguin, *Frontal fog - Glossary of Meteorology*. [Online]. Available: https://glossary.ametsoc.org/wiki/Frontal_fog (accessed: Feb. 12 2024).
[178]I. Gultepe *et al.*, "Fog Research: A Review of Past Achievements and Future Perspectives," (in En;en), *Pure appl. geophys.*, vol. 164, 6-7, pp. 1121–1159, 2007, doi: 10.1007/s00024-007-0211-x.
[179]R. Tardif and R. M. Rasmussen, "Event-Based Climatology and Typology of Fog in the New York City Region," *Journal of Applied Meteorology and Climatology*, vol. 46, no. 8, pp. 1141–1168, 2007, doi: 10.1175/JAM2516.1.
[180]W. Seguin, *Steam fog - Glossary of Meteorology*. [Online]. Available: https://glossary.ametsoc.org/wiki/Steam_fog (accessed: Feb. 12 2024).
[181]W. Zheng, X. Li, J. Xie, L. Yin, and Y. Wang, "Impact of human activities on haze in Beijing based on grey relational analysis," (in En;en), *Rend. Fis. Acc. Lincei*, vol. 26, no. 2, pp. 187–192, 2015, doi: 10.1007/s12210-015-0402-9.
[182]C. Poku, A. N. Ross, A. M. Blyth, A. A. Hill, and J. D. Price, "How important are aerosol–fog interactions for the successful modelling of nocturnal radiation fog?," *Weather*, vol. 74, no. 7, pp. 237–243, 2019, doi: 10.1002/wea.3503.
[183]H. Cai and C. Wang, "Surviving With Smog and Smoke: Precision Interventions?," *Chest*, vol. 152, no. 5, pp. 925–929, 2017, doi: 10.1016/j.chest.2017.06.030.
[184]J. W. Hutchings, B. Ervens, D. Straub, and P. Herckes, "N-nitrosodimethylamine occurrence, formation and cycling in clouds and fogs," *Environmental science & technology*, vol. 44, no. 21, pp. 8128–8133, 2010, doi: 10.1021/es101698q.
[185]B. J. Polivka, "The Great London Smog of 1952," *The American journal of nursing*, vol. 118, no. 4, pp. 57–61, 2018, doi: 10.1097/01.NAJ.0000532078.72372.c3.
[186]S. N. Stolaki, S. A. Kazadzis, D. V. Foris, and T. S. Karacostas, "Fog characteristics at the airport of Thessaloniki, Greece," *Nat. Hazards Earth Syst. Sci.*, vol. 9, no. 5, pp. 1541–1549, 2009, doi: 10.5194/nhess-9-1541-2009.
[187]Y. Akimoto and H. Kusaka, "A climatological study of fog in Japan based on event data," *Atmospheric Research*, vol. 151, pp. 200–211, 2015, doi: 10.1016/j.atmosres.2014.04.003.
[188]D. Bari, T. Bergot, and M. El Khlifi, "Local Meteorological and Large-Scale Weather Characteristics of Fog over the Grand Casablanca Region, Morocco," *Journal of Applied Meteorology and Climatology*, vol. 55, no. 8, pp. 1731–1745, 2016, doi: 10.1175/JAMC-D-15-0314.1.
[189]M. Belorid, C. B. Lee, J.-C. Kim, and T.-H. Cheon, "Distribution and long-term trends in various fog types over South Korea," (in En;en), *Theor Appl Climatol*, vol. 122, 3-4, pp. 699–710, 2015, doi: 10.1007/s00704-014-1321-x.
[190]B. Roux, R. Potts, S. Siems, and M. Manton, "Towards a better understanding of fog at Perth Airport," *Journal of Hydrology*, vol. 600, p. 126516, 2021, doi: 10.1016/j.jhydrol.2021.126516.
[191]L. van Schalkwyk and L. L. Dyson, "Climatological Characteristics of Fog at Cape Town International Airport," *Weather and Forecasting*, vol. 28, no. 3, pp. 631–646, 2013, doi: 10.1175/WAF-D-12-00028.1.
[192]D. Lin *et al.*, "Fog type classification using a modified Richardson number for Christchurch, New Zealand," *Intl Journal of Climatology*, vol. 43, no. 1, pp. 314–330, 2023, doi: 10.1002/joc.7761.
[193]Y. Xue, L.-P. Wang, and W. W. Grabowski, "Growth of Cloud Droplets by Turbulent Collision–Coalescence," *J. Atmos. Sci.*, vol. 65, no. 2, pp. 331–356, 2008, doi: 10.1175/2007JAS2406.1.
[194]L. Zhao, S. Niu, Y. Zhang, and F. Xu, "Microphysical characteristics of sea fog over the east coast of Leizhou Peninsula, China," (in En;en), *Adv. Atmos. Sci.*, vol. 30, no. 4, pp. 1154–1172, 2013, doi: 10.1007/s00376-012-1266-x.

[195]F. Yang, P. Kollias, R. A. Shaw, and A. M. Vogelmann, "Cloud droplet size distribution broadening during diffusional growth: ripening amplified by deactivation and reactivation," *Atmos. Chem. Phys.*, vol. 18, no. 10, pp. 7313–7328, 2018, doi: 10.5194/acp-18-7313-2018.
[196]Q. Liu, B. Wu, Z. Wang, and T. Hao, "Fog Droplet Size Distribution and the Interaction between Fog Droplets and Fine Particles during Dense Fog in Tianjin, China," *Atmosphere*, vol. 11, no. 3, p. 258, 2020, doi: 10.3390/atmos11030258.
[197]C. Lu, Y. Liu, S. Niu, L. Zhao, H. Yu, and M. Cheng, "Examination of microphysical relationships and corresponding microphysical processes in warm fogs," (in En;en), *Acta Meteorol Sin*, vol. 27, no. 6, pp. 832–848, 2013, doi: 10.1007/s13351-013-0610-0.
[198]J. Price, "Radiation Fog. Part I: Observations of Stability and Drop Size Distributions," (in En;en), *Boundary-Layer Meteorol*, vol. 139, no. 2, pp. 167–191, 2011, doi: 10.1007/s10546-010-9580-2.
[199]M. Mazoyer, F. Burnet, and C. Denjean, "Experimental study on the evolution of droplet size distribution during the fog life cycle," *Atmos. Chem. Phys.*, vol. 22, no. 17, pp. 11305–11321, 2022, doi: 10.5194/acp-22-11305-2022.
[200]T. W. Choularton, G. Fullarton, J. Latham, C. S. Mill, M. H. Smith, and I. M. Stromberg, "A field study of radiation fog in meppen, West Germany," *Quarterly Journal of the Royal Meteorological Society*, vol. 107, no. 452, pp. 381–394, 1981, doi: 10.1002/qj.49710745209.
[201]R. J. Pilié, E. J. Mack, W. C. Kocmond, C. W. Rogers, and W. J. Eadie, "The Life Cycle of Valley Fog. Part I: Micrometeorological Characteristics," *J. Appl. Meteor.*, vol. 14, no. 3, pp. 347–363, 1975, doi: 10.1175/1520-0450(1975)014<0347:TLCOVF>2.0.CO;2.
[202]H. J. S. Fernando *et al.*, "C-FOG: Life of Coastal Fog," no. 2, E244-E272, 2021. [Online]. Available: https://journals.ametsoc.org/view/journals/bams/102/2/bams-d-19-0070.1.xml
[203]M. Haeffelin *et al.*, "Parisfog," *Bulletin of the American Meteorological Society*, vol. 91, no. 6, pp. 767–783, 2010, doi: 10.1175/2009BAMS2671.1.
[204]T. Bergot, "Large-eddy simulation study of the dissipation of radiation fog," *Quarterly Journal of the Royal Meteorological Society*, vol. 142, no. 695, pp. 1029–1040, 2016, doi: 10.1002/qj.2706.
[205]A. Bott, "On the influence of the physico-chemical properties of aerosols on the life cycle of radiation fogs," (in En;en), *Boundary-Layer Meteorol*, vol. 56, 1-2, pp. 1–31, 1991, doi: 10.1007/BF00119960.
[206]D. T. Degefie *et al.*, "Microphysics and energy and water fluxes of various fog types at SIRTA, France," *Atmospheric Research*, vol. 151, pp. 162–175, 2015, doi: 10.1016/j.atmosres.2014.03.016.
[207]J. Tav *et al.*, "Determination of Fog-Droplet Deposition Velocity from a Simple Weighing Method," *Aerosol Air Qual. Res.*, vol. 18, no. 1, pp. 103–113, 2018, doi: 10.4209/aaqr.2016.11.0519.
[208]M. Nakanishi, "Large-Eddy Simulation Of Radiation Fog," (in En;en), *Boundary-Layer Meteorology*, vol. 94, no. 3, pp. 461–493, 2000, doi: 10.1023/A:1002490423389.
[209]D. F. Leipper, *Fog development at San Diego*, 1948. [Online]. Available: https:// elischolar.library.yale.edu/journal_of_marine_research/673/
[210]World Meteorological Organization, *International meteorological vocabulary - No. 182*, 1992.
[211]H. Israël, *Die Sichtweite Im Nebel und Die Möglichkeiten Ihrer Künstlichen Beeinflussung*. Wiesbaden: VS Verlag fur Sozialwissenschaften GmbH, 1959.
[212]P. Bouguer, *Essai d'optique sur la gradation de la lumière*: Claude Jombert, 1729.
[213]J. H. Lambert, *Photometria sive de mensura et gradibus luminis, colorum et umbrae*: sumptibus vidvae E. Klett, typis C.P. Detleffsen, 1760.
[214]A. Beer, "Bestimmung der Absorption des rothen Lichts in farbigen Flüssigkeiten," *Annalen der Physik*, vol. 162, no. 5, pp. 78–88, 1852, doi: 10.1002/andp.18521620505.
[215]H. Koschmieder, "Theorie der horizontalen Sichtweite," *Beitrage zur Physik der freien Atmosphare*, pp. 33–53, 1924.

[216]International Commission on Illumination, *ILV: International Lighting Vocabulary*. [Online]. Available: https://cie.co.at/eilv/772 (accessed: Feb. 19 2024).
[217]K. W. Kim, "The comparison of visibility measurement between image-based visual range, human eye-based visual range, and meteorological optical range," *Atmospheric Environment*, vol. 190, pp. 74–86, 2018, doi: 10.1016/j.atmosenv.2018.07.020.
[218]F. Carretas, F. Wagner, and F. M. Janeiro, "Atmospheric visibility and Angström exponent measurements through digital photography," *Measurement*, vol. 64, pp. 147–156, 2015, doi: 10.1016/j.measurement.2014.12.041.
[219]N. Graves and S. Newsam, "Camera-based visibility estimation: Incorporating multiple regions and unlabeled observations," *1574-9541*, vol. 23, pp. 62–68, 2014, doi: 10.1016/j.ecoinf.2013.08.005.
[220]R. G. Hallowell and M. P. Matthews, *An automated visibility detection algorithm utilizing camera imagery*, 2007. [Online]. Available: https://citeseerx.ist.psu.edu/document?repid=rep1&type=pdf&doi=454642225fb85686379addf1d375c133d9879bef
[221]J.-J. Liaw, S.-B. Lian, Y.-F. Huang, and R.-C. Chen, "Using Sharpness Image with Haar Function for Urban Atmospheric Visibility Measurement," *Aerosol Air Qual. Res.*, vol. 10, no. 4, pp. 323–330, 2010, doi: 10.4209/aaqr.2009.11.0074.
[222]Y. Nagata, T. Hagiwara, K. Araki, Y. Kaneda, and H. Sasaki, "Application of Road Visibility Information System to Winter Maintenance," *Transportation Research Record*, vol. 2055, no. 1, pp. 128–138, 2008, doi: 10.3141/2055-15.
[223]K. Dahmane, P. Duthon, F. Bernardin, M. Colomb, F. Chausse, and C. Blanc, "WeatherEye-Proposal of an Algorithm Able to Classify Weather Conditions from Traffic Camera Images," *Atmosphere*, vol. 12, no. 6, p. 717, 2021, doi: 10.3390/atmos12060717.
[224]World Meteorological Organization, "The first WMO intercomparison of visibility measurements: TD-No. 401," *Instruments and Observing Methods (IOM) Report No. 41*, 1990.
[225]J. Liang *et al.*, "Influence of transmissometers' light source spectral distribution in measuring visibility," *Optics Communications*, vol. 499, p. 127294, 2021, doi: 10.1016/j.optcom.2021.127294.
[226]H. Vasseur and C. J. Gibbins, "Inference of fog characteristics from attenuation measurements at millimeter and optical wavelengths," *Radio Science*, vol. 31, no. 5, pp. 1089–1097, 1996, doi: 10.1029/96RS01725.
[227]T. Elias *et al.*, "Enhanced extinction of visible radiation due to hydrated aerosols in mist and fog," *Atmos. Chem. Phys.*, vol. 15, no. 12, pp. 6605–6623, 2015, doi: 10.5194/acp-15-6605-2015.
[228]P. Duthon, M. Colomb, and F. Bernardin, "Fog Classification by Their Droplet Size Distributions: Application to the Characterization of Cerema's Platform," *Atmosphere*, vol. 11, no. 6, p. 596, 2020, doi: 10.3390/atmos11060596.
[229]M. Colomb, P. Duthon, and S. Laukkanen, *Characteristics of Adverse Weather Conditions - DENSE D2.1*, 2017.
[230]E. P. Shettle and R. W. Fenn, *Models for the Aerosols of the Lower Atmosphere and the Effects of Humidity Variations on Their Optical Properties*: Optical Physics Division, Air Force Geophysics Laboratory, 1979.
[231]L. M. Levin, "Distribution functions of cloud droplets," *Izvestiya AN SSSR*, no. 10, p. 1211, 1958.
[232]A. K. Khrgian and I. P. Mazin, "The size distribution of droplets in clouds," *Trudy TsAo*, vol. 7., 1952.
[233]J. A. Garland, "Some fog droplet size distributions obtained by an impaction method," *Quarterly Journal of the Royal Meteorological Society*, vol. 97, no. 414, pp. 483–494, 1971, doi: 10.1002/qj.49709741408.
[234]F. Tampieri and C. Tomasi, "Size distribution models of fog and cloud droplets in terms of the modified gamma function," *Tellus A: Dynamic Meteorology and Oceanography*, vol. 28, no. 4, p. 333, 1975, doi: 10.3402/tellusa.v28i4.10300.

[235]D. Harris, "The attenuation of electromagnetic waves due to atmospheric fog," (in En;en), *International Journal of Infrared and Millimeter Waves*, vol. 16, no. 6, pp. 1091–1108, 1995, doi: 10.1007/BF02068279.
[236]F. Bernardin, M. Colomb, F. Egal, P. Morange, and J. J. Boreux, "Droplet distribution models for visibility calculation," Münster, Jul. 25 2010.
[237]L. M. Levin, "Size distribution functions of cloud and rain drops," *Doklady AN SSSR*, 1954.
[238]A. N. Kolmogorov, "Über das logarithmisch normale verteilungsgesetz der dimensionen der teilchen bei zerstückelung," *Dokl. Akad. Nauk SSSR*, vol. 31, p. 99, 1941. [Online]. Available: https://cir.nii.ac.jp/crid/1370285709899182208
[239]A. C. Best, "Drop-size distribution in cloud and fog," *Q.J Royal Met. Soc.*, vol. 77, no. 333, pp. 418–426, 1951, doi: 10.1002/qj.49707733307.
[240]S. Egli, F. Maier, J. Bendix, and B. Thies, "Vertical distribution of microphysical properties in radiation fogs — A case study," *Atmospheric Research*, vol. 151, pp. 130–145, 2015, doi: 10.1016/j.atmosres.2014.05.027.
[241]R. G. Eldridge, "Haze and Fog Aerosol Distributions," *J. Atmos. Sci.*, vol. 23, no. 5, pp. 605–613, 1966, doi: 10.1175/1520-0469(1966)023<0605:HAFAD>2.0.CO;2.
[242]R. G. Eldridge, "The Relationship Between Visibility and Liquid Water Content in Fog," *J. Atmos. Sci.*, vol. 28, no. 7, pp. 1183–1186, 1971, doi: 10.1175/1520-0469(1971)028<1183:TRBVAL>2.0.CO;2.
[243]Q. Long, B. Wu, X. Mi, S. Liu, X. Fei, and T. Ju, "Review on Parameterization Schemes of Visibility in Fog and Brief Discussion of Applications Performance," *Atmosphere*, vol. 12, no. 12, p. 1666, 2021, doi: 10.3390/atmos12121666.
[244]S. S. Muhammad, M. S. Awan, and A. Rehman, "PDF Estimation and Liquid Water Content Based Attenuation Modeling for Fog in Terrestrial FSO Links," *Radioengineering*, 2010. [Online]. Available: https://www.researchgate.net/profile/sajid-muhammad-3/publication/44247434_pdf_estimation_and_liquid_water_content_based_attenuation_modeling_for_fog_in_terrestrial_fso_links/links/540d6fd20cf2f2b29a3849ef/pdf-estimation-and-liquid-water-content-based-attenuation-modeling-for-fog-in-terrestrial-fso-links.pdf
[245]K. L. Koester and L. H. Kosowsky, "Attenuation of millimeter waves in fog," *Fourteenth Radar Meteorology Conference*, 1970.
[246]I. Gultepe and G. A. Isaac, "A natural fog dissipation process in a marine fog event during FRAM," *9th WMO Scientific Conference on Weather Modification*, 2007. [Online]. Available: https://scholar.google.de/citations?user=qjtlemuaaaaj&hl=de&oi=sra
[247]B. A. Kunkel, "Parameterization of Droplet Terminal Velocity and Extinction Coefficient in Fog Models," *J. Climate Appl. Meteor.*, vol. 23, no. 1, pp. 34–41, 1984, doi: 10.1175/1520-0450(1984)023<0034:PODTVA>2.0.CO;2.
[248]I. Gultepe, M. D. Müller, and Z. Boybeyi, "A New Visibility Parameterization for Warm-Fog Applications in Numerical Weather Prediction Models," *Journal of Applied Meteorology and Climatology*, vol. 45, no. 11, pp. 1469–1480, 2006, doi: 10.1175/JAM2423.1.
[249]I. Gultepe *et al.,* "The Fog Remote Sensing and Modeling (FRAM) field project: visibility analysis and remote sensing of fog," pp. 32–43, doi: 10.1117/12.793281.
[250]S. G. Gonser, O. Klemm, F. Griessbaum, S.-C. Chang, H.-S. Chu, and Y.-J. Hsia, "The Relation Between Humidity and Liquid Water Content in Fog: An Experimental Approach," (in En;en), *Pure appl. geophys.*, vol. 169, 5-6, pp. 821–833, 2012, doi: 10.1007/s00024-011-0270-x.
[251]Optical Sensors, *Methods for detecting fog and measuring visibility.* [Online]. Available: https://www.opticalsensors.se/measuringvisibility.html (accessed: Mar. 28 2024).
[252]*DIN CEN/TS 15518-4:2013-06, Winterdienstausrüstung - Straßenzustands- und Wetterinformationssysteme - Teil 4: Prüfverfahren bei stationären Einrichtungen; Deutsche Fassung CEN/TS 15518-4:2013*, 15518, Deutsches Institut für Normung e.V., Berlin.
[253]Degreane Horizon, "TR30LED," Accessed: Feb. 21 2024. [Online]. Available: https://www.degreane-horizon.com/app/uploads/sites/96/2023/02/T311050I-TR30LED-GB-3.pdf
[254]VAISALA, "Transmissometer LT31," 2024.

[255]International Civil Aviation Organization (ICAO), *Annex 3 to the Convention on International Civil Aviation – Meteorological Service for International Air Navigation,* 17th ed., 2010.
[256]Z. Zhuang, J. Li, P. W. Chan, and H. Tai, "Substitutability research for forward-scatter meters in indoor low-visibility environments," *Meteorological Applications*, vol. 29, no. 2, e2050, 2022, doi: 10.1002/met.2050.
[257]International Civil Aviation Organization (ICAO), "Manual of runway visual range observing and reporting practices," 2005. [Online]. Available: https://camd.imd.gov.in/icao/pdf/ICAO-Doc%209328%20Manual%20of%20Runway%20Visual%20Range%20Observing%20and%20Reporting%20Practices.pdf
[258]Degreane Horizon, "DF320," [Online]. Available: https://www.degreane-horizon.com/app/uploads/sites/96/2023/02/T311034C-DF320-GB.pdf
[259]Degreane Horizon, *TP320.* [Online]. Available: https://www.degreane-horizon.com/app/uploads/sites/96/2023/02/T311048C-TP320-GB-1.pdf (accessed: Feb. 21 2024).
[260]Eigenbrodt, *Fog Sensor ONED 250 (OFS).* [Online]. Available: https://www.eigenbrodt.de/en/products/meteorologie/fog-sensor-oned-250-ofs/ (accessed: Apr. 2 2024).
[261]Optical Sensors, *Fog Sensor (OFS Mini)* (accessed: May 1 2023).
[262]Sabik Offshore, "SWSxxx-N-AC Visibility meter," 2019. [Online]. Available: https://productssabik-offshore.b-cdn.net/wp-content/uploads/2021/05/SWS-XXX-Datasheet.pdf
[263]SICK, *Sichtweitemessgeräte VISIC620.* [Online]. Available: https://www.sick.com/de/de/verkehrssensoren/sichtweitemessgeraete/visic620/c/g57494 (accessed: May 1 2023).
[264]VAISALA, "Visibility Sensor FS11," 2024. [Online]. Available: https://www.vaisala.com/sites/default/files/documents/FS11-Datasheet-B210244EN-F.pdf
[265]Palas GmbH, "AEROSOLSENSOR WELAS 2100," 2024. Accessed: Feb. 21 2024. [Online]. Available: https://www.palas.de/product/download/aerosolsensorwelas2100/datasheet/pdf
[266]Droplet Measurement Technologies, *FM-120 Fog Monitor.* [Online]. Available: https://www.dropletmeasurement.com/product/fog-monitor/ (accessed: Feb. 21 2024).
[267]R. Vautard, P. Yiou, and G. J. van Oldenborgh, "Decline of fog, mist and haze in Europe over the past 30 years," (in En;en), *Nature Geosci*, vol. 2, no. 2, pp. 115–119, 2009, doi: 10.1038/ngeo414.
[268]G. J. van Oldenborgh, P. Yiou, and R. Vautard, "On the roles of circulation and aerosols in the decline of mist and dense fog in Europe over the last 30 years," *Atmos. Chem. Phys.*, vol. 10, no. 10, pp. 4597–4609, 2010, doi: 10.5194/acp-10-4597-2010.
[269]A. Skomorowski and P. Piotrowski, "The Occurrence of Fog at Meteorological Stations Located on the Airport in Poland in the Years 2005-2015," (in English;en), *Przegląd Geofizyczny*, Z. 4, 315--327, 2018. [Online]. Available: https://www.infona.pl/resource/bwmeta1.element.baztech-b98d44a9-04e5-421f-abc4-1b20c8c4401f
[270]Z. Avotniece, M. Klavins, and L. Lizuma, "Fog climatology in Latvia," (in En;en), *Theor Appl Climatol*, vol. 122, 1-2, pp. 97–109, 2015, doi: 10.1007/s00704-014-1270-4.
[271]M. Błaś, M. Sobik, F. Quiel, and P. Netzel, "Temporal and spatial variations of fog in the Western Sudety Mts., Poland," *Atmospheric Research*, vol. 64, 1-4, pp. 19–28, 2002, doi: 10.1016/S0169-8095(02)00076-5.
[272]A. Cséplő, N. Sarkadi, Á. Horváth, G. Schmeller, and T. Lemler, "Fog climatology in Hungary," *IDŐJÁRÁS / QUARTERLY JOURNAL OF THE HUNGARIAN METEOROLOGICAL SERVICE*, vol. 123, no. 2, pp. 241–264, 2019. [Online]. Available: https://real.mtak.hu/105258/
[273]S. Egli, B. Thies, J. Drönner, J. Cermak, and J. Bendix, "A 10 year fog and low stratus climatology for Europe based on Meteosat Second Generation data," *Quarterly Journal of the Royal Meteorological Society*, vol. 143, no. 702, pp. 530–541, 2017, doi: 10.1002/qj.2941.

[274]L. Giulianelli *et al.,* "Fog occurrence and chemical composition in the Po valley over the last twenty years," *Atmospheric Environment*, vol. 98, pp. 394–401, 2014, doi: 10.1016/j.atmosenv.2014.08.080.
[275]P. M. P. Guerreiro, P. M. M. Soares, R. M. Cardoso, and A. M. Ramos, "An Analysis of Fog in the Mainland Portuguese International Airports," *Atmosphere*, vol. 11, no. 11, p. 1239, 2020, doi: 10.3390/atmos11111239.
[276]I. Hůnová, M. Brabec, M. Malý, and A. Valeriánová, "Long-term trends in fog occurrence in the Czech Republic, Central Europe," *The Science of the total environment*, vol. 711, p. 135018, 2020, doi: 10.1016/j.scitotenv.2019.135018.
[277]J. G. Izett, B. J. H. van de Wiel, P. Baas, J. A. van Hooft, and R. B. Schulte, "Dutch fog: On the observed spatio-temporal variability of fog in the Netherlands," *Q.J Royal Met. Soc.*, vol. 145, no. 723, pp. 2817–2834, 2019, doi: 10.1002/qj.3597.
[278]E. Łupikasza and T. Niedźwiedź, "Synoptic climatology of fog in selected locations of southern Poland (1966–2015)," *Bulletin of Geography. Physical Geography Series*, vol. 11, no. 1, pp. 5–15, 2016, doi: 10.1515/bgeo-2016-0010.
[279]S. C. Scherrer and C. Appenzeller, "Fog and low stratus over the Swiss Plateau − a climatological study," *Int. J. Climatol.*, vol. 34, no. 3, pp. 678–686, 2014, doi: 10.1002/joc.3714.
[280]K. Veljović and D. Vujović, "Climatology of fog occurrence over a wide flat area in Serbia based on visibility observations," *Int. J. Climatol.*, vol. 39, no. 3, pp. 1331–1344, 2019, doi: 10.1002/joc.5883.
[281]S. Egli, B. Thies, and J. Bendix, "A spatially explicit and temporally highly resolved analysis of variations in fog occurrence over Europe," *Quarterly Journal of the Royal Meteorological Society*, vol. 145, no. 721, pp. 1721–1740, 2019, doi: 10.1002/qj.3522.
[282]M. Sachweh and P. Koepke, "Radiation fog and urban climate," *Geophysical Research Letters*, vol. 22, no. 9, pp. 1073–1076, 1995, doi: 10.1029/95GL00907.
[283]I. Hůnová, M. Brabec, J. Geletič, M. Malý, and A. Dumitrescu, "Local fresh- and sea-water effects on fog occurrence," *The Science of the total environment*, vol. 807, Pt 2, p. 150799, 2022, doi: 10.1016/j.scitotenv.2021.150799.
[284]I. Hunova, M. Brabec, M. Malý, A. Dumitrescu, and J. Geletič, "Environmental and geographical effects on fog occurrence," *EGU General Assembly Conference Abstracts*, EGU21-5810, 2021, doi: 10.5194/egusphere-egu21-5810.
[285]I. Hůnová, M. Brabec, M. Malý, A. Dumitrescu, and J. Geletič, "Terrain and its effects on fog occurrence," *The Science of the total environment*, vol. 768, p. 144359, 2021, doi: 10.1016/j.scitotenv.2020.144359.
[286]Illuminating Engineering Society, *Glare.* [Online]. Available: https://www.ies.org/definitions/glare/ (accessed: Aug. 13 2024).
[287]P. R. Boyce, *Human Factors in Lighting*: CRC Press, 2003. [Online]. Available: https://www.taylorfrancis.com/books/mono/10.1201/9780203426340/human-factors-lighting-peter-robert-boyce
[288]Y. Akashi, R. Muramatsu, and S. Kanaya, "Unified Glare Rating (UGR) and subjective appraisal of discomfort glare," *Lighting Research and Technology*, vol. 28, no. 4, pp. 199–206, 1996, doi: 10.1177/14771535960280040501.
[289]M. L. Eble-Hankins and C. E. Waters, "VCP and UGR Glare Evaluation Systems: A Look Back and a Way Forward," *LEUKOS*, vol. 1, no. 2, pp. 7–38, 2005, doi: 10.1582/leukos.2004.01.02.001.
[290]BYJU'S, *Specular & Diffuse Reflection.* [Online]. Available: https://byjus.com/physics/specular-diffuse-reflection/ (accessed: Aug. 13 2024).
[291]Erco, *Glare – types and definition.* [Online]. Available: https://www.erco.com/en/designing-with-light/lighting-knowledge/visual-perception/glare-7462/#Whattypesofglarecanoccur? (accessed: Aug. 13 2024).

[292]the Physics Classroom, *Physics Tutorial: Specular vs. Diffuse Reflection.* [Online]. Available: https://www.physicsclassroom.com/class/refln/Lesson-1/Specular-vs-Diffuse-Reflection (accessed: Aug. 13 2024).
[293]Wikipedia, *Solar spectrum.* [Online]. Available: https://commons.wikimedia.org/wiki/File:Solar_spectrum_en.svg (accessed: Aug. 13 2024).
[294]Wikipedia, *Spectrum of Sunlight.* [Online]. Available: https://commons.wikimedia.org/wiki/File:Spectrum_of_Sunlight_en.svg (accessed: Aug. 13 2024).
[295]A. Presciutti, F. Asdrubali, A. Marrocchi, A. Broggi, G. Pizzoli, and A. Damiani, "Sun Simulators: Development of an Innovative Low Cost Film Filter," *Sustainability*, vol. 6, no. 10, pp. 6830–6846, 2014, doi: 10.3390/su6106830.
[296]Wikipedia, *Halogen spectrum.* [Online]. Available: https://commons.wikimedia.org/wiki/File:Halogen_spectrum.svg (accessed: Aug. 13 2024).
[297]J. W. Hall, K. L. Smith, L. Titus-Glover, J. C. Wambold, T. J. Yager, and Z. Rado, *Guide for pavement friction*, 2009. [Online]. Available: http://rhvpi.ca/od/documents/ham/ham0028606_0001.pdf
[298]C. Tong and T. Li, *Car Driving Safety Analysis in Rainy and Snowy Weather Based on ADAMS/Car*: American Society of Civil Engineers, 2015.
[299]M. Hippi, I. Juga, and P. Nurmi, *A statistical forecast model for road surface friction*, 2010. [Online]. Available: https://www.researchgate.net/profile/marjo-hippi/publication/271133153_a_statistical_forecast_model_for_road_surface_friction/links/54be4fa20cf218d4a16a5986/a-statistical-forecast-model-for-road-surface-friction.pdf
[300]K. Ichihara and M. Mizoguchi, "Skid resistance of snow- or ice-coverd roads," *Highway Research Board Special Report*, no. 115, 1970. [Online]. Available: https://trid.trb.org/view/105097
[301]K. Maruyama, K. Fuse, and M. Kumagai, *Skid Resistance of Porous Asphalt Pavement under Winter Conditions*, 2010. [Online]. Available: https://proceedings-quebec2010.piarc.org/en/programme/en/ip4-0083-maruyama-e.pdf
[302]R. Pečeliūnas, V. Žuraulis, P. Droździel, and S. Pukalskas, "Prediction of Road Accident Risk for Vehicle Fleet Based on Statistically Processed Tire Wear Model," *Promet - Traffic&Transportation*, vol. 34, no. 4, pp. 619–630, 2022, doi: 10.7307/ptt.v34i4.3997.
[303]J. Ling, F. Yang, J. Zhang, P. Li, M. I. Uddin, and T. Cao, "Water-film depth assessment for pavements of roads and airport runways: A review," *Construction and Building Materials*, vol. 392, p. 132054, 2023, doi: 10.1016/j.conbuildmat.2023.132054.
[304]P. Staufer, M. Siekmann, S. Loos, and J. Pinnekamp, "Numerical Modeling of Water Levels on Pavements under Extreme Rainfall," *J. Transp. Eng.*, vol. 138, no. 6, pp. 732–740, 2012, doi: 10.1061/(ASCE)TE.1943-5436.0000373.
[305]M. H. Dehnad and A. Yazdi, "A review of numerical and experimental studies on hydroplaning of vehicles in motion on road surfaces," *2590-1230*, vol. 23, p. 102438, 2024, doi: 10.1016/j.rineng.2024.102438.
[306]F. Biesse, "Analysis of wet road usage with a driving safety concern," *VDA Technischer Konress*, pp. 74–91, 2019.
[307]F. Biesse and V. Todoroff, "Analysis of tire wet grip mechanisms and their respective weightings in a wet braking test," *11th International Munich Chassis Symposium 2020*, pp. 161–176, 2021, doi: 10.1007/978-3-662-63193-5_12.
[308]H. Edmar Schulz, J. Edgar Curry, and A. L. Andrade Simões, "Water Films and Hydroplaning on Highways: Hydrodynamic Aspects," *J. Transp. Eng., Part B: Pavements*, vol. 147, no. 4, p. 4021053, 2021, doi: 10.1061/JPEODX.0000309.
[309]A. Abdi Kordani, O. Rahmani, A. S. Abdollahzadeh Nasiri, and S. M. Boroomandrad, "Effect of Adverse Weather Conditions on Vehicle Braking Distance of Highways," *CivileJournal*, vol. 4, no. 1, p. 46, 2018, doi: 10.28991/cej-030967.
[310]F. Spitzhüttl, F. Goizet, T. Unger, and F. Biesse, "The real impact of full hydroplaning on driving safety," *Accident Analysis and Prevention*, vol. 138, p. 105458, 2020, doi: 10.1016/j.aap.2020.105458.

[311]C.-G. Wallman and H. Aström, "Friction measurement methods and the correlation between road friction and traffic safety," *VTI meddelande*, no. 911, 2001.